STRUCTURAL MULTI-MECHANISM MODEL WITH ANISOTROPIC DAMAGE FOR CEREBRAL ARTERIAL TISSUES AND ITS FINITE ELEMENT MODELING

by

Dalong Li

B.E., Xi'an Jiaotong University, 1998

M.S., Shanghai Jiaotong University, 2003

Submitted to the Graduate Faculty of

the Swanson School of Engineering in partial fulfillment

of the requirements for the degree of

Doctor of Philosophy

University of Pittsburgh

2009

UNIVERSITY OF PITTSBURGH

SWANSON SCHOOL OF ENGINEERING

This dissertation was presented

by

Dalong Li

It was defended on

November 13th 2009

and approved by

Anne M. Robertson, Associate Professor, Mechanical Engineering Dept.

William S. Slaughter, Associate Professor, Mechanical Engineering Dept.

Patrick Smolinski, Associate Professor, Mechanical Engineering Dept.

David A. Vorp, Professor, Surgery and Bioengineering Dept.

Dissertation Director: Anne M. Robertson, Associate Professor, Mechanical Engineering Dept.

STRUCTURAL MULTI-MECHANISM MODEL WITH ANISOTROPIC DAMAGE FOR CEREBRAL ARTERIAL TISSUES AND ITS FINITE ELEMENT MODELING

Dalong Li, PhD

University of Pittsburgh, 2009

A structural multi-mechanism constitutive equation is proposed to describe the anisotropic and damage behavior of cerebral arterial tissue. The arterial tissue is modeled as a non-linear, incompressible and inelastic material. In this model, new deformation criteria are proposed for the recruitment of collagen fibers and degradation of internal elastic lamina (IEL), two important features of early stage aneurysm formation.

This structural anisotropic model is formulated by modifying a previous multi-mechanism model to include the fibrous nature of collagen fibers and incorporates morphological information such as fiber orientation and dispersion. An anisotropic damage model is included to characterize tissue weakening and softening before failure of the IEL, ground matrix or collagen fibers. Two possible damage mechanisms are formulated in this model: mechanical damage dependent on material strains and enzymatic damage induced by hemodynamic stresses.

The elastin/ground matrix and collagen fibers are treated as separate components of arteries. The elastin and ground matrix, which are represented by an isotropic response, bear loads at low strain level, and degrade gradually due to damage or disrupt due to eventual failure. The collagen fibers are recruited into load-bearing and subfailure damage at higher strain levels. Two approaches are considered for modeling their anisotropic behavior. In the first, they are characterized by the anisotropic behavior of N fibers. In the second, the collagen fibers are arranged in two helically oriented families with dispersion in their orien-

tation. The fiber distribution is modeled by an orientation density function or distribution parameter. The fiber orientation and dispersion can be prescribed from arterial histology studies, or identified from stress-strain response as structural parameters.

Pressure inflation test data for cerebral arteries are used to evaluate the constitutive model. It is found to fit the mechanical response of uniaxial test well. There is a need for additional experimental data to further evaluate and develop this model. The constitutive model is implemented in commercial finite element analysis package for numerical computation. The numerical implementation is validated by analytical solutions. The numerical model is used for the study of arterial microstructural behavior in complex biomechanical procedure of angioplasty surgery.

TABLE OF CONTENTS

LIST OF TABLES

LIST OF FIGURES

PREFACE

I would like to thank my advisor, Dr. Anne M. Robertson, sincerely for her guidance and supervision. Her constant encouragement has been a driving force in the course of my Ph.D. study and this research work. I would like to express my appreciation to Dr. William S. Slaughter, Dr. Patrick Smolinski, and Dr. David A. Vorp for serving on my dissertation committee and their invaluable suggestions and comments. I want to thank Dr. Michael R. Lovell, Dr. Guoyu Lin and Dr. Sergey Sidorov for the discussion over their research work.

I am very thankful to the Department of Mechanical Engineering and Materials Science for supporting me with teaching scholarship over the past four years. I also thank ANSYS Inc. for providing development internship as part of my professional training.

I must thank my colleague students in our research group: Dr. Rachmadian Wulandana, Michael Hill, Christen Hydrean, Zijing Zeng, Michael Durka, Hasballah Zakaria and Mahzad Bastani Nejad for spending time together in the valuable discussions and collaborations.

I would like to sincerely thank Glinda Harvey and Brittany Guthrie for providing crucial administration and help essential to my studies and work.

I am indebted and grateful to my family. My deeply thanks to my father Yingtian Li, my mother Yanling Yu, and my sisters Xiaohong Li and Xiaojun Li for their love, support, and encouragement. My sincere thanks to my wife Jenny Yue Cui, also my best friend, for exploring the world with me, and for giving me a handsome son Jonathan Haoyang Li, whose brilliant smile is always shining our life.

1.0 INTRODUCTION

1.1 MOTIVATION

The motivation of the current work is the study of the biomechanics of the formation of human intracranial aneurysms. The initiation and development of arterial aneurysms are complex biological and mechanical processes. At this point in time, most theories regarding the formation mechanisms are hypotheses, which need further exploration and validation.

Our long-term objective is to understand the biomechanical mechanisms of aneurysms and vascular injuries. A theoretical approach is taken in this dissertation by developing constitutive models for arterial walls and robust numerical implementation of these models. The constitutive models are motivated by current experimental studies, and can be used to analyze the mechanical response of cerebral arteries. Numerical simulations can help us to explore the micromechanical behavior of tissue components due to realistic biomechanical factors.

1.2 CEREBRAL ARTERIES AND INTRACRANIAL CEREBRAL ANEURYSMS

Intracranial cerebral aneurysms (ICA) are local dilatations of cerebral arterial walls. Most ICA are saccular and 2 mm or more in diameter. ICA are commonly found at the bifurcation or curved area of cerebral arteries in or near the Circle of Willis (Camarata *et al.*, 1992), and often show a clear neck region.

Saccular aneurysms are very common in US populations. An angiography study revealed a 1% incidence of anterior circulation aneurysms in the U.S. general population (Atkinson *et al.*, 1989). Other autopsy studies reported 0.8-8.1% incidence of saccular aneurysms in the U.S. population (McCormick and Acosta-Rua , 1970; Inagawa and Hirano, 1990).

Rupture of cerebral aneurysms is very dangerous for the patient. When aneurysms rupture, the blood will flood into the subarachnoid space and cause a subarachnoid hemorrhage (SAH). The highest reported incidence of ruptured aneurysms in autopsy studies is 3% among the population of the United States (McCormick and Acosta-Rua , 1970). The incidence of patient death following aneurysm rupture is over 50% (Ingall *et al.*, 1989; Broderick *et al.*, 1994), while 14-20% of the patients are disabled moderately or severely (Broderick *et al.*, 1994; Longstreth *et al.*, 1993).

1.3 HISTOLOGY OF CEREBRAL ARTERIAL TISSUES AND ANEURYSMS

Cerebral arteries are muscular arteries with a distinct three-layer structure: the intima, media and adventitia (Rhodin, 1979), Fig. 1. The intima is the innermost layer of the artery, and is composed of a single layer of endothelial cells resting on a thin basal membrane. In a healthy young person, the intima is usually very thin and ignored for the mechanical properties of the artery. The media is in the middle of the artery, and primarily consists of smooth muscle cells and collagen fibrils between them. The adventitia is the most outer layer of the artery. It consists mainly of thick bundles of collagen fibers plus ground substances (Rhodin, 1979; Stehbens *et al.*, 1972). In typical muscular arteries, the media is separated from the intima and adventitia by an internal elastic lamina (IEL) and external elastin lamina (EEL), both composed of fenestrated sheets of elastin (Stehbens *et al.*, 1972). Cerebral arteries have a thicker IEL, thinner media and no EEL compared with other arteries. Elastin and collagen fibers are the two significant contributors to the passive mechanical properties of arteries. The elastin of cerebral arteries is concentrated in the IEL but more broadly distributed

throughout the arterial wall in extracranial arteries. Histological studies of human arteries have shown the collagen fibers are in a wavy state in unloaded arteries and progressively straighten with loading (Samila and Carter, 1981).

The arterial tissue of cerebral aneurysm walls is structurally different from healthy arteries, Fig. 2. At the orifice of the sack, the media terminates, and the IEL is fragmented, or slightly extends into the aneurysm neck region. In the aneurysm wall away from the orifice, the media is completely absent and the IEL is totally disrupted (Crawford, 1959; Cajander and Hassler, 1976).

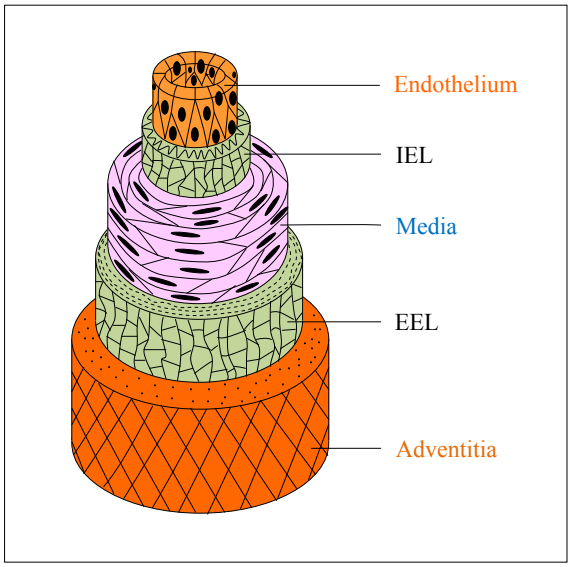

Figure 1: Muscular arterial wall.

The three-dimensional organization of collagen fibers and muscle cells in cerebral arteries has been investigated experimentally. Peters *et al.* (1983) showed that cerebral arteries have highly oriented medial muscle cells, aligned circumferentially with very small variation in angle. Finlay *et al.* (1995) found that collagen and smooth muscle cells in the media are consistently circumferentially and coherently aligned, while the collagen fibers in the adventitia are highly varied in coherence and mean direction with a substantial component of longitudinal fibers. At increasing pressures, the collagen fibers in all layers become increasingly coherent and more circumferential in direction (Finlay *et al.*, 1995).

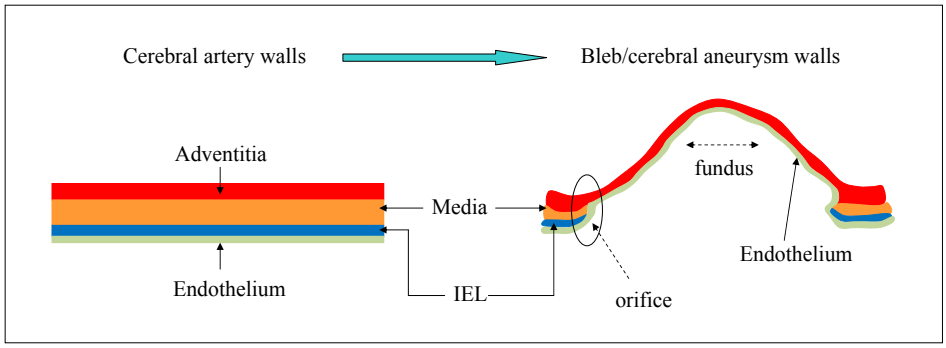

Figure 2: Components of cerebral arterial and aneurysm walls.

1.4 MECHANICAL BEHAVIOR OF CEREBRAL ARTERIAL AND ANEURYSM TISSUES

The mechanical properties of cerebral arteries is very important for the understanding of tissue behavior in aneurysm initiation, development and rupture, which are complex biomechanical processes. In-vitro and in-vivo tests of human cerebral arterial tissue is still a challenging task. To date, there is still limited experimental data available for the nonlinear and inelastic response of cerebral arteries to test hypotheses on aneurysm etiology. Monson (2001) studied the failure properties of human cerebral arteries, and reported the uniaxial and biaxial mechanical response (Monson *et al.*, 2003, 2006).

In their pioneering work, Scott *et al.* (1972) explored the hypothesis that the main difference in mechanical properties between cerebral arterial and aneurysm tissue is due to elastin degradation during the aneurysm formation process. As part of their work, they inflated segments of cerebral arterial tissue in-vitro to obtain pressure-volume data. Significantly, they found that after three runs to 200 mmHg, the mechanical properties of the tissue changed abruptly and the unloaded radius of the vessel increased, Fig. 3.

The tension-stretch curve for the later loading cycles had no toe region, but was repeatable. Scott *et al.* (1972) found similar results for all three cerebral arteries loaded to this level. No shift was seen in control experiments of cyclic loading to a maximum pressure of

100 mm Hg. They hypothesized the qualitative change in the curve was due to the disruption of the elastin membrane caused by mechanical loading beyond the breaking strength of elastin. Their conjecture was based on (i) the lack of toe region in the second runs, and (ii) the qualitative similarity in the curves for the second runs and those of arterial tissue in which elastin had been chemically removed as a load bearing component (Roach & Burton, 1957). This is also consistent with the histological study (Nystrom *et al.*, 1963) showing that the aneurysm tissue has decreased and fragmented elastin.

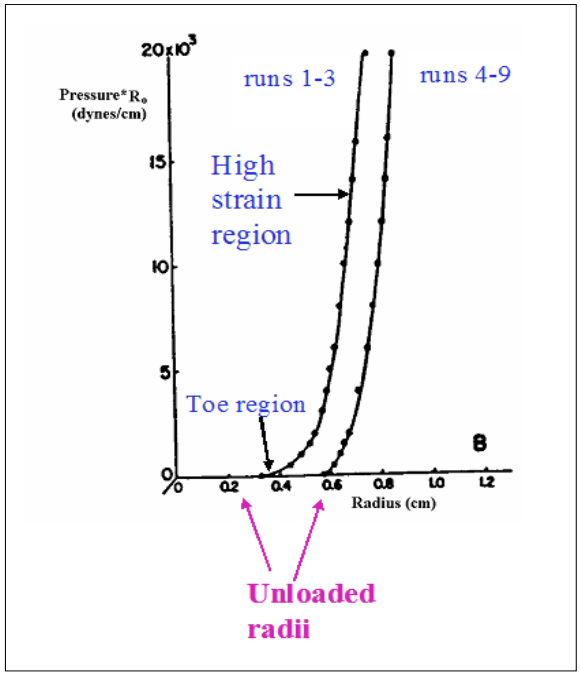

Figure 3: Tension-radius data of an anterior cerebral artery (Scott *et al.*, 1972).

1.5 MODEL FOR CEREBRAL ANEURYSM FORMATION

To better understand the mechanisms of aneurysm formation, instead of modeling arteries and aneurysms as distinct entities with independent reference configurations (Canham and Ferguson, 1985; Hademenos *et al.*, 1994; Hung and Botwin, 1975; Ryan and Humphrey, 1999), Wulandana and Robertson (2005) developed a multi-mechanism, inelastic constitutive

equation to model the initiation and early development stages of cerebral aneurysm from a segment of arterial wall. In that work, elastin and collagen fibers were modeled as two distinct mechanisms with different mechanical properties and unloaded configurations. The recruitment of collagen fibers and degradation of the internal elastic lamina are initiated based on the deformation state in the arterial wall. To our knowledge, this is the first attempt at modeling early stage aneurysm formation including these two important characteristics. Isotropic material responses were used for both elastin and collagen, and exponential strain energy functions were found to have the best fit with the pressure inflation experimental data of Scott *et al.* (1972). While this model is structurally motivated, it is phenomenological in nature.

2.0 A STRUCTURAL MULTI-MECHANISM MODEL FOR CEREBRAL ARTERIES

2.1 INTRODUCTION

Anisotropic structural constitutive models have been developed for a variety of soft tissues. Although phenomenological models are successfully used to fit biaxial experimental data, the material constants do not reflect the structural properties. By comparison, structural constitutive models integrate more information on tissue composition, structure, and the load carrying mechanisms of individual parts, so provide more insight into the function and mechanics of tissue components (Lanir, 1983). A more detailed review of structural models for arterial tissue can be found in Gasser *et al.* (2006). The most complete approach has been presented by Lanir (1983) and Lanir *et al.* (1996). In his model for fibrous connective tissues, the total strain energy of tissue is assumed to be the sum of individual fibers, and the fiber strain is related to the global strain by a tensor transformation between global coordinates and fiber coordinates. Lanir included fiber orientation in the model through prescribed statistical distributions and obtained the distribution parameters from experimental data. Sacks (2000); Billar & Sacks (2000) and Sacks (2003) developed an experimental method for measuring the distribution of collagen fiber angles in some tissues using small angle light scattering (SALS) and developed a structural model based on Lanir′s work. This was the first structural model with parameters derived directly from experimental measures of fiber orientation. Holzapfel *et al.* (2000) proposed a fiber-reinforced structural model for arteries, in which two families of collagen fibers are assumed to be embedded in an isotropic ground matrix. In accordance with arterial histology, this model seems to represent the media architecture better than the intima and adventitia architecture (Gasser *et al.*,

2006). Motivated further by the study of arterial tissue morphology (Canham *et al.*, 1989; Finlay *et al.*, 1995), Gasser *et al.* (2006) generalized Holzapfel′s model to include a large range of fiber orientations. They introduced an orientation density function to characterize collagen fiber distribution with respect to a reference orientation in the unloaded reference configuration. A scalar structure parameter is obtained from the integration of the density function and represents the degree of anisotropy. This model was used to describe the fiber dispersion characteristics of the intima and adventitia in arterial tissue. Lanir′s and Holzapfel′s structural models have been used successfully in some recent fibrous tissue models (De Vita and Slaughter, 2006; Natali *et al.*, 2004, 2005; Gasser and Holzapfel, 2002).

In this study, an anisotropic, structural, multi-mechanism constitutive model is developed to describe the mechanical behavior of cerebral arteries. The material anisotropy arising from the collagen fiber orientation in cerebral vessels is modeled using the approach of Holzapfel *et al.* (2000) and Gasser *et al.* (2006). The fiber orientation is modeled using two approaches (i) a finite number of fiber families and (ii) a fiber distribution function. A new parameter for collagen recruitment based on local collagen stretch is used. Published inelastic pressure inflation data (Scott *et al.*, 1972) are used to select the specific form of the strain energy function. There is a pressing need for multi-axial experiments to further refine this model.

2.2 STRUCTURAL MULTI-MECHANISM MODEL FOR CEREBRAL ARTERIAL TISSUE

2.2.1 Qualitative features of the multi-mechanism model in cylindrical inflation

To elaborate fundamental roles of different mechanisms, we first discuss the qualitative features of quasi-static inflation of an arterial segment which is idealized as a transversely isotropic, multi-mechanism material. Here, the artery wall is idealized as a homogeneous, single-layer, cylindrical membrane in which case the inflation deformation is also homogeneous. In sections 2.2.2, 2.2.3 and 2.2.4, we will discuss the general 3-D case and rigorous continuum formulation. In order to clarify the separate and changing roles of the elastin

and collagen mechanisms during loading, we subdivide the deformation into seven possible stages, Fig. 4. Cylindrical coordinates (r, θ, z) with z-axis aligned with the artery centerline and corresponding basis $(\underline{e}_r, \underline{e}_\theta, \underline{e}_z)$ will be used to discuss the idealized deformation. Elastin is shown as red color before disruption, and white after disruption. Collagen fibers are shown as black lines.

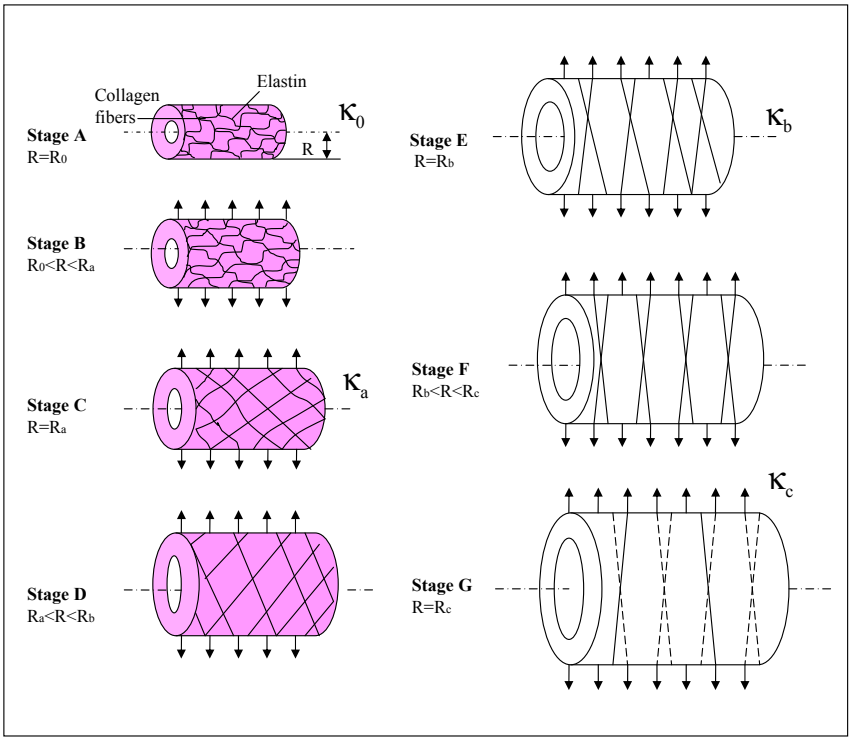

Figure 4: Schematic of stages during inflation of a cylindrical membrane composed of the transversely isotropic, multi-mechanism model. Stage A: Stress-free tissue, Stage B: Only elastin load bearing, Stage C: Initiation of collagen load bearing, Stage D: Elastin and collagen load bearing, Stage E: Elastin disruption, Stage F: Only collagen load bearing, Stage G: Partial disruption of collagen.

Stage A denotes the stress-free configuration, κ_o of the cylindrical membrane with surface $R = R_0$. This is also the unloaded configuration. Motivated by the morphology of arteries (Rhodin, 1979; Stehbens *et al.*, 1972), we extend the model of Wulandana and Robertson (2005) and treat the unloaded state as composed of separate mechanisms: an isotropic mech-

anism largely controlled by the response of elastin and the surrounding matrix as well as an anisotropic response arising from a helical network of crimped collagen fibers. These crimped fibers require a finite deformation to bear load. The contribution of fibers in the radial direction are neglected but can be included if their inclusion is supported by experimental data. By way of illustration, in this section we consider one pair of fibers with angles $\beta_1 = \beta$, $\beta_2 = -\beta$, without dispersion in the plane of the membrane, Fig 5.

As the artery is pressurized, the lateral surface of the membrane moves to radial position R. During Stage B, the deformation is sufficiently small that the collagen fibers show diminishing waviness and change their orientation without contributing significantly to load bearing. The stress generation is dominated by elastin, corresponding to the toe region in a typical stress/stretch curve (Busby and Burton, 1965). In further discussions, we denote the circumferential stretch of the membrane as λ. For example, during Stage B, $\lambda = R/R_0$. In this work, the symmetry of unloaded fiber orientation and symmetric form of the deformation are such that the two families of fibers undergo the same fiber stretch for all times, which we denote as λ_f. The subscript f is used to emphasize that, in general, the fiber and circumferential stretch are different.

At Stage C, a critical level of λ_f is reached, denoted as λ_{fa} when the waviness has diminished to the point that under further stretch, the fibers will bear load. Hence, the quantity λ_{fa} reflects the degree of waviness of the collagen fibers in the unloaded material. The corresponding radius of the artery in this configuration is denoted as R_a, the circumferential stretch as $\lambda = \lambda_a$ and the configuration as κ_a. The subscript a is used to emphasize the *activation* of the collagen mechanism in this configuration. It follows that $\lambda_a = R_a/R_0$. The fiber stretch λ_{fa} can be computed from the tensorial transformation of the global membrane stretch λ_a referenced to fiber coordinates, assuming the deformation is affine.

Upon further loading, Stage D, both the collagen and elastin mechanisms contribute to load bearing. The contribution of the elastin mechanism continues to depend on the deformation relative to κ_0, while the stress within the collagen fibers is a function of the fiber stretch relative to stretch λ_{fa}. The addition of the stiffer collagen fibers leads to the steep increase in stiffness in the stress/stretch curve in Stage D, ending the shallow toe region of Stage B (Busby and Burton, 1965; Hoffman *et al.*, 1977; Samila and Carter, 1981).

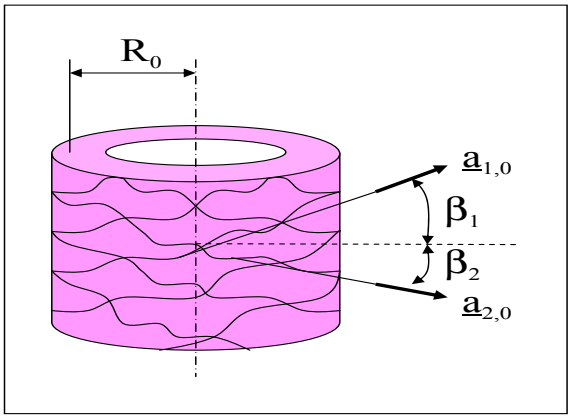

Figure 5: Schematic of the collagen fiber structure in the arterial wall in the unloaded configuration.

Upon further loading, Stage E, a critical radius is reached R_b where the elastin mechanism is disrupted to the point of ceasing to contribute to load bearing. The corresponding circumferential stretch of the membrane is denoted as $\lambda_b = R_b/R_0$ and the configuration as κ_b. In a purely mechanical theory, this disruption is entirely due to an increase in mechanical loading and the criterion for disruption is purely a function of a kinematic measure of the deformation. We conjecture that in some cerebral arteries, for example during early stages of aneurysm formation, this critical level of stretch may be reached even under fixed pressure due to a degradation of the IEL arising from a combination of factors such as fatigue, extended periods of exposure to elevated hemodynamic loading such as wall shear stress and wall shear stress gradient (Robertson *et al.*, 2007), damage due to environment factors, and aging (Busby and Burton, 1965; Samila and Carter, 1981). Disruption of the IEL is a feature common to all cerebral aneurysm walls and has been hypothesized to be associated with the inelastic behavior of cerebral arteries and with the initiation of an ICA (Scott *et al.*, 1972).

Upon further loading (or unloading), Stage F, only collagen will contribute to load bearing. Unloading during this stage, will return the fibers to stretch λ_{fa}. As a result, the unloaded radius will increase. If the arterial segment without a functioning IEL is considered as a second material, it will appear stiffer than the original artery, and will not display

a toe region. This behavior of our model is consistent with mechanical data from Scott *et al.* (1972) and Roach & Burton (1957).

We expect that an additional stage, Stage G, will be associated with partial collagen disruption and potentially the generation of new collagen in an altered reference configuration as part of a longer time scale process, involving growth and remodeling (Wulandana and Robertson, 2005; Humphrey, 2002).

2.2.2 Elastic mechanical response of elastin and surrounding matrix

This discussion of the kinematics for the elastin mechanism follows that in Wulandana and Robertson (2005). A section of cerebral artery will be represented by a three-dimensional body $\mathfrak{B}$ which initially, say at time $t = t_1$, is stress free and occupies a region that will be referred to as the undeformed reference configuration κ_0. A typical material particle, labeled Y, in the body $\mathfrak{B}$ will be identified by vector position $\underline{X}_0$ in κ_0 relative to a chosen coordinate system, Fig. 6. Using this notation, the motion of an arbitrary material particle Y can be described through the relationship

$$\underline{x} = \boldsymbol{\chi}_{\kappa_0}(\underline{X}_0, t), \tag{2.1}$$

where the vector function $\boldsymbol{\chi}_{\kappa_0}(\underline{X}_0, t)$ is single-valued, invertible and continuously differentiable with respect to its arguments as many times as required in the subsequent analysis. The configuration at arbitrary time $t > t_1$ will be denoted by $\kappa(t)$. The deformation gradient $\underline{F}_0$ at time t for an arbitrary material particle Y in reference configuration κ_0 is given by

$$\underline{F}_0 = \underline{F}_{\kappa_0}(\underline{X}_0, t) \;=\; \frac{\partial \boldsymbol{\chi}_{\kappa_0}(\underline{X}_0, t)}{\partial \underline{X}_0}. \tag{2.2}$$

The associated left and right Cauchy Green tensors for κ_0 are then,

$$\underline{B}_0 \;=\; \underline{F}_0 \cdot \underline{F}_0^T, \qquad \underline{C}_0 \;=\; \underline{F}_0^T \cdot \underline{F}_0. \tag{2.3}$$

As in Wulandana and Robertson (2005), we model the mechanical response of the first mechanism using a hyperelastic strain energy function per unit volume in reference configuration κ_0 as $\psi_0 = \psi_0(\underline{F}_0)$. Based on invariance requirements and assuming the material is isotropic

with respect to configuration κ_0, the strain energy function reduces to $\psi_0 = \psi_0(I_0, II_0)$ where I_0 and II_0 are the first and second invariants of $\underline{C}_0$,

$$I_0 \;=\; \hat{I}(\underline{C}_0) \;=\; \mathrm{tr}\,\underline{C}_0, \qquad II_0 \;=\; \hat{II}(\underline{C}_0) \;=\; \frac{1}{2}\left[(\mathrm{tr}\,\underline{C}_0)^2 \;-\; \mathrm{tr}\,\underline{C}_0^2\right]. \tag{2.4}$$

Furthermore, as in Wulandana and Robertson (2005), we will assume the isotropic mech-

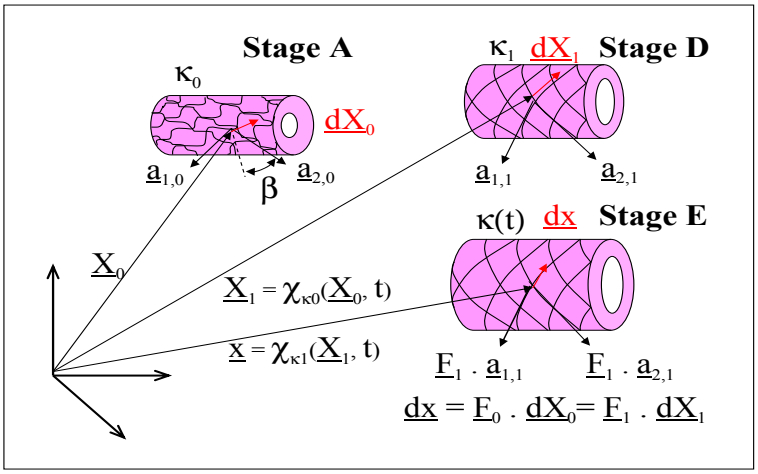

Figure 6: Schematic of reference configurations for the dual mechanism constitutive model with relevant kinematic variables drawn.

anism ψ_0 is dominated by the dependence on I_0 and the effect of II_0 is comparatively negligible.

$$\psi_0 = \psi_0(I_0). \tag{2.5}$$

2.2.2.1 Deactivation criterion for elastin As in Wulandana and Robertson (2005), we assume there exists a critical level of deformation when the first mechanism is disrupted and ceases to contribute to load bearing. We introduce a metric of loading for the elastin mechanism, called the deformation state parameter, which is chosen to be a monotonically increasing function of I_0,

$$s_0 = \hat{s}_0(I_0). \tag{2.6}$$

Without loss in generality, we choose a linear function,

$$s_0 = \max(I_0 - 3), \tag{2.7}$$

normalized so that s_0 is zero when there is no deformation. The criterion for deactivation of the first mechanism will then be defined through a deactivation criterion of the form $s_0 = s_{0b}$. Once $s_0 \geq s_{0b}$ for some deformation, elastin no longer contributes to load bearing in all further deformations, even when s_0 develops below s_{0b}.

In Section 3.2.3, we will generalize the constitutive response to include progressive damage of this isotropic mechanism. As discussed below, we can extend the functional dependence of ψ_0 to include the effect of changes in mechanical response of elastin arising due to aging, fatigue related factors, and deleterious hemodynamic loads (Robertson *et al.*, 2007).

2.2.3 Mechanical response of multi-mechanism material with collagen mechanism composed of N fiber families

In this section, the fiber orientation is modeled using a finite number of fiber families. The mechanical model for the contribution of the collagenous fibers builds on that introduced by Lanir (1983), Lanir *et al.* (1996) and Holzapfel *et al.* (e.g. Holzapfel *et al.*, 2000; Holzapfel, 2000, Section 6.7). While in these works, a single zero stress state reference configuration was employed for all material constituents, here we introduce an additional reference configuration κ_i for each fiber with an associated activation criterion. This additional constitutive structure makes it possible to capture the change in unloaded configuration when the first mechanism is disrupted.

2.2.3.1 Constitutive response of N collagen fiber families We assume any anisotropic response of the material arises from the contribution of collagenous fibers in the wall. At each point in space, the collagen contribution is represented by N fibers. The direction of an arbitrary fiber i in κ_0 is characterized by a unit vector $\underline{a}_{i,0}$ which makes an angle β_i relative to a reference direction in κ_0, Fig. 5. The first subscript on $\underline{a}$ is the fiber number and the second is the configuration. For example, using $\underline{e}_\theta$ as the reference angle, $\underline{a}_{i,0} = \cos\beta_i \underline{e}_\theta + \sin\beta_i \underline{e}_z$

is the direction of fiber i in configuration κ_0. We further assume the fibers move affinely with the underlying material during the deformation. Therefore, an infinitesimal material element of fiber i, denoted as $\underline{dX_0} = dS_0\,\underline{a}_{i,0}$ at point $\underline{X}_0$ in configuration κ_0, will be mapped to $\underline{dx} = \underline{F}_0 \cdot \underline{a}_{i,0}\,dS_0$ at $\underline{x}$ in configuration $\kappa(t)$, Fig. 6. The stretch of this infinitesimal fiber material element relative to its length in κ_0 is therefore,

$$\lambda_{i,0}^2 \;=\; \frac{|\underline{dx}|^2}{|\underline{dX_0}|^2} \;=\; \underline{C}_0 : \underline{a}_{i,0} \otimes \underline{a}_{i,0}. \tag{2.8}$$

The unit vector $\underline{a}_{i,0}$ represents the direction of fiber i in κ_0 is mapped to $\underline{F}_0 \cdot \underline{a}_{i,0}$ in κ_i. This new fiber direction can be normalized as a unit vector $\underline{a}_{i,i}$,

$$\underline{a}_{i,i} \;=\; \frac{1}{\lambda_{i,0}}\,\underline{F}_0 \cdot \underline{a}_{i,0}. \tag{2.9}$$

In the qualitative discussion in Section 2.2.1, when the fibers reached a critical stretch λ_{fa}, they became load bearing and this critical stretch was fiber independent. More generally, λ_{fa} will be different for different fibers and we will denote the critical stretch for fiber i as λ_{ia} and the corresponding configuration as κ_{ia},

$$\lambda_{ia}^2 \;=\; \lambda_{i,0}^2|_{\kappa_{ia}}, \tag{2.10}$$

where $|\kappa_{ia}$ after a quantity is used to denote that the quantity takes the value it held in configuration κ_{ia}.

The mechanical response of collagen fiber i will depend on the stretch beyond λ_{ia} and we therefore turn attention to kinematic quantities defined relative κ_{ia}. The motion of a particle at time t (configuration κ), which has position $\underline{X}_i$ in configuration κ_{ia} is,

$$\underline{x} = \boldsymbol{\chi}_{\kappa_{ia}}(\underline{X}_i, t), \tag{2.11}$$

and the corresponding deformation gradient relative to κ_{ia} is,

$$\underline{F}_i = \underline{F}_i(\underline{X}_i, t) \;=\; \frac{\partial \boldsymbol{\chi}_{\kappa_{ia}}(\underline{X}_i, t)}{\partial \underline{X}_i}. \tag{2.12}$$

The associated left and right Cauchy Green tensors are,

$$\underline{B}_i \;=\; \underline{F}_i \cdot \underline{F}_i^T, \qquad \underline{C}_i \;=\; \underline{F}_i^T \cdot \underline{F}_i \qquad \text{i = 1,2,...,N.} \tag{2.13}$$

In configuration κ, the deformation gradient $\underline{F}_i$ is related to $\underline{F}_0$ (the deformation gradient relative to κ_0) through,

$$\underline{F}_i \;=\; \underline{F}_0 \cdot \underline{F}_0{}^{-1}|_{\kappa_{ia}}, \tag{2.14}$$

and therefore

$$\underline{C}_i \;=\; \underline{F}_0{}^{-T}|_{\kappa_{ia}} \cdot \underline{C}_0 \cdot \underline{F}_0{}^{-1}|_{\kappa_{ia}}. \tag{2.15}$$

As in Holzapfel *et al.* (2000), we assume the collagen mechanism can be modeled as the collective response of N fibers, each of which behaves as a hyperelastic, transversely isotropic material. The total strain energy function for the collagen mechanism is then,

$$\psi_{aniso} \;=\; \sum_{i=1}^{N} \psi_i(\underline{C}_i, \underline{a}_{i,i} \otimes \underline{a}_{i,i}). \tag{2.16}$$

Note, the form (2.16) implicitly assumes the response of the fibers are decoupled. Since the material response should not depend on the sign of $\underline{a}_{i,i}$, it has been included in the strain energy function (2.16) as a tensor product,

$$\underline{A}_{i,i} = \underline{a}_{i,i} \otimes \underline{a}_{i,i}, \tag{2.17}$$

which is sometimes referred to as the *structure tensor* (Holzapfel *et al.*, 2000; Gasser *et al.*, 2006).

The integrity basis for the symmetric second order tensors $\underline{C}_i, \underline{A}_{i,i}$ (i=1,2,...,N) is composed of the following invariants (e.g. Holzapfel *et al.*, 2000),

$$\begin{aligned} I_i \;&=\; \mathrm{tr}\,\underline{C}_i, \quad II_i \;=\; \frac{1}{2}\left[(\mathrm{tr}\,\underline{C}_i)^2 \;-\; \mathrm{tr}\,\underline{C}_i^2\right], \quad III_i \;=\; 1, \\ IV_{i,i} \;&=\; \underline{C}_i : \underline{A}_{i,i}, \quad V_{i,i} \;=\; \underline{C}_i^2 : \underline{A}_{i,i}. \end{aligned} \tag{2.18}$$

A strain energy function of the form (2.16) which is transversely isotropic can therefore be written as (Holzapfel *et al.*, 2000),

$$\psi_{aniso} \;=\; \sum_{i=1}^{N} \psi_i(I_i, II_i, IV_{i,i}, V_{i,i}). \tag{2.19}$$

For lack of extensive data for the anisotropic behavior of cerebral arteries, we reduce the dependence of ψ_{aniso} to the simplest form that is consistent with the expected mechanism

of collagen load bearing. In particular, we assume the response of the collagen fibers is dominated by the stretch of individual collagen fibers relative to the stretch in reference configuration κ_{ia}, which is denoted by, $\lambda_{i,i}$. Noting that an infinitesimal fiber element $\underline{dX_i} = dS_i\,\underline{a}_{i,i}$ in configuration κ_{ia} will be mapped to $\underline{dx} = \underline{F}_i \cdot \underline{a}_{i,i}\,dS_i$ in κ, it follows that,

$$\lambda_{i,i}^2 \;=\; \frac{|\underline{dx}|^2}{|\underline{dX_i}|^2} \;=\; \underline{C}_i : \underline{a}_{i,i} \otimes \underline{a}_{i,i} \;=\; IV_{i,i}. \tag{2.20}$$

We therefore, simplify Eq. (2.19) to

$$\psi_{aniso} \;=\; \sum_{i=1}^{N} \psi_i(IV_{i,i}). \tag{2.21}$$

Note that $\lambda_{i,i}$ is related to $\lambda_{i,0}$ through,

$$\lambda_{i,i} \;=\; \frac{\lambda_{i,0}}{\lambda_{ia}}. \tag{2.22}$$

2.2.3.2 Activation criterion for recruitment of N-fiber families We introduced λ_{ia} as a material parameter defining the stretch at which fiber i is load bearing. Here, we restate this condition in terms of kinematic invariants. As in Wulandana and Robertson (2005), we introduce a deformation state parameter which serves as a metric of the relevant aspects of the deformation. In that work, the collagen mechanism was modeled as isotropic and the metric was chosen to be a function of I_0. The same metric was used for both collagen and elastin. Here, we consider the role of collagen fibers and use the collagen stretch $\lambda_{i,0}$ defined in (2.8) as a measure of this deformation from the strain free state in κ_0. We define the deformation state parameter for collagen as a monotonically increasing scalar function for fiber i

$$s_i \;=\; \hat{s}_i(IV_{i,0}), \tag{2.23}$$

where

$$\lambda_{i,0}^2 \;=\; IV_{i,0} \;=\; \underline{C}_0 : \underline{a}_{i,0} \otimes \underline{a}_{i,0}. \tag{2.24}$$

As shown in (2.23), the state parameter for the fibers depends only on one variable. Without loss in generality, we choose a linear function,

$$s_i \;=\; IV_{i,0} - 1, \tag{2.25}$$

normalized so that s_i is zero when the body is unloaded, κ_0. Fiber i will be considered uncrimped when s_i reaches a critical value, $s_i = s_{ia}$. Denoting $IV_{ia,0}$ as the corresponding critical value of the $IV_{i,0}$,

$$s_{ia} \;=\; \hat{s}_i(IV_{ia,0}). \tag{2.26}$$

It follows from (2.8) and (2.10) that $IV_{ia,0}$ is related to λ_{ia} through,

$$IV_{ia,0} \;=\; {\lambda_{ia}}^2. \tag{2.27}$$

In the case of homogeneous deformations, with homogeneous fiber distribution, $IV_{i,0}$ will be constant throughout the material and hence the criterion (2.27) will be met simultaneously at all points in the body. However, more generally, activation of the collagen fiber i can occur at different times t for different points in the body if, for example, λ_{ia} takes the same value throughout the material (material is homogeneous with respect to this parameter), but the deformation is inhomogeneous. In addition, the activation criterion will be met at different times at points in the body, if the deformation is homogeneous but the value of λ_{ia} varies in the body.

2.2.3.3 Total constitutive response for structural, multi-mechanism model with collagen mechanism composed of N fiber families At arbitrary time and material point, the strain energy function of anisotropic cerebral arterial tissue can be expressed as:

$$\psi \;=\; (1-d_0)\psi_0(I_0) \;+\; \sum_{i=1}^{N}(1-d_i)\psi_i(IV_{i,i}) \tag{2.28}$$

where d_0 and d_i are weighting functions for elastin deactivation and collagen activation, respectively,

$$d_0 \;=\; \begin{cases} 0 & s_0 < s_{0b} \\ 1 & s_0 \geq s_{0b}, \end{cases} \tag{2.29}$$

$$d_i \;=\; \begin{cases} 1 & s_i < s_{ia}, \quad i \in [1,N] \\ 0 & s_i \geq s_{ia}, \quad i \in [1,N]. \end{cases} \tag{2.30}$$

It is assumed that once the elastin mechanism has been deactivated, it cannot be activated again.

The corresponding Cauchy stress tensor is (Holzapfel, 2000),

$$\underline{T} \;=\; -p\underline{I} \;+\; 2(1-d_0)\frac{\partial \psi_0}{\partial I_0}\,\underline{B}_0 \;+\; \sum_{i=1}^{N}(1-d_i)\left[2\frac{\partial \psi_i}{\partial IV_{i,i}}\underline{F}_i\cdot\underline{a}_{i,i}\otimes\underline{F}_i\cdot\underline{a}_{i,i}\right] \tag{2.31}$$

2.2.4 Mechanical response of multi-mechanism material with distribution model for collagen fibers

2.2.4.1 Distribution model for collagen fibers In the previous discussion, the contribution of N fibers are modeled independently. In this section, we simplify the constitutive equation by replacing the N fiber response with a collective response of dispersed fibers (Gasser *et al.*, 2006). By way of example, here the artery wall is characterized by two families of dispersed fibers with mean directions β_1, β_2 in κ_0,

$$\underline{a}_{\alpha,0} \;=\; \cos\beta_\alpha\underline{e}_\theta \;+\; \sin\beta_\alpha\underline{e}_z, \quad \alpha=1,2. \tag{2.32}$$

Furthermore, it is assumed the fibers are distributed with rotational symmetry such that $\beta_1 = -\beta_2$. In the arterial model, this symmetry will correspond to transverse isotropy of the material. It should be emphasized that previously β_i represented the direction of fiber i (i=1,2,...,N). Here, β_1, β_2 are the mean directions of dispersed families of fibers.

As in Gasser *et al.* (2006), the three-dimensional distribution of fiber angles is modeled using an orientation density function $\rho(\underline{M}(\Theta,\Phi))$ which characterizes the three-dimensional distribution of fiber angles in the reference configuration κ_0 with respect to a *reference orientation* $\underline{M}$, Fig. 7. In the most general case, $\underline{M}$ is an arbitrary unit vector which is characterized by two Euler angles $\Theta\in[0,\pi]$ and $\Phi\in[0,2\pi]$ in a three-dimensional Cartesian coordinate system with basis $\{\underline{e}_1,\underline{e}_2,\underline{e}_3\}$,

$$\underline{M}(\Theta,\Phi) = \sin\Theta\cos\Phi\underline{e}_1 + \sin\Theta\sin\Phi\underline{e}_2 + \cos\Theta\underline{e}_3. \tag{2.33}$$

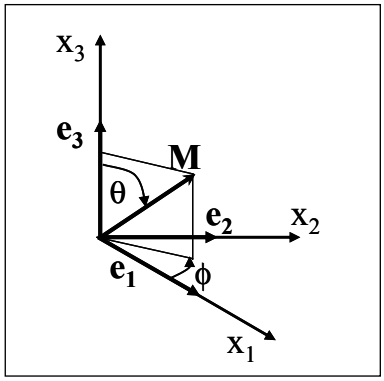

Figure 7: Schematic of geometric variables used in dispersion model for collagen fiber distribution

A non-negative density function is defined such that $\rho(\underline{M}(\Theta,\Phi))d\omega$ represents the normalized number of fibers with orientations in the range $[(\Theta,\Theta+d\Theta),(\Phi,\Phi+d\Phi)]$, where $d\omega = \sin\Theta d\Theta d\Phi$. Furthermore, ρ is symmetric with respect to $\underline{M}$ and normalized,

$$\rho(\underline{M}) = \rho(-\underline{M}) \qquad \text{and} \qquad \frac{1}{4\pi}\int_{\omega}\rho(\underline{M}(\Theta,\Phi))\,d\omega \;=\; 1. \tag{2.34}$$

While the fiber orientation is, in general, characterized by ρ, for the special case of the artery model where the fibers have rotational symmetry about some mean referential direction $\underline{a}_{\alpha,0}$, it is convenient to characterize this orientation in terms of a generalized symmetric second order tensor $\underline{H}$,

$$\underline{H} = \frac{1}{4\pi}\int \rho(\underline{M}(\Theta,\Phi))\underline{M}(\Theta,\Phi)\otimes\underline{M}(\Theta,\Phi)\,\sin\,\Theta\,d\Theta\,d\Phi, \tag{2.35}$$

and referred to as the *structure tensor*, (Gasser *et al.*, 2006), which accounts for the collective contribution of dispersed fibers in all directions. Choosing Cartesian coordinates, such that $\underline{a}_{\alpha,0}$ is equal to $\underline{e}_3$, it follows that the density function ρ is independent of Φ. It can then be shown, (Gasser *et al.*, 2006), that for each family of fibers the structure tensor can be written with respect to a single dispersion parameter, k, in κ_0,

$$\underline{H}_{\alpha,0} = k\underline{I} + (1-3k)\underline{a}_{\alpha,0}\otimes\underline{a}_{\alpha,0}, \tag{2.36}$$

where $\underline{I}$ is the identity tensor, and k is defined as a structure parameter that represents the fiber distribution in an integral sense, describing the degree of anisotropy,

$$k = \frac{1}{4}\int_0^{\pi} \rho(\Theta)\sin^3(\Theta)\, d\Theta. \tag{2.37}$$

The parameter k can either be thought of as a material parameter, determined directly from the experimental data, or calculated, from experimental knowledge of $\rho(\Theta)$. When there is an isotropic distribution of collagen fibers, ρ equals one, so $k = 1/3$ and the structure tensor $\underline{H}$ is proportional to the identity tensor. Furthermore, if ρ is chosen to be proportional to a Dirac delta function, namely, $\rho = K\delta(\Theta_0)$ where K is a constant and $\delta(\Theta_0)$ is the Dirac delta function then for $\Theta_0 \in (0, \pi)$, $k = 1/2sin^2(\Theta_0)$.

The anisotropic strain energy function for the dispersed collagen mechanism based on the generalized structure tensor $\underline{H}$ is,

$$\psi_{aniso} \;=\; \sum_{\alpha=1}^{2} \psi_\alpha(\underline{C}_\alpha, \underline{H}_{\alpha,\alpha}), \tag{2.38}$$

which is analogous to Eq. (2.16). Here, $\underline{H}_{\alpha,\alpha}$ is the structure tensor of αth fiber family in its reference configuration κ_α associated with an activation criterion, and $\underline{C}_\alpha$ is the right Cauchy Green tensor defined by the deformation gradient $\underline{F}_\alpha$ relative to κ_α,

$$\underline{C}_\alpha \;=\; \underline{F}_\alpha^T \cdot \underline{F}_\alpha. \tag{2.39}$$

We now assume the only anisotropy in the material is due to families of dispersed fibers and therefore require,

$$\hat{\psi}_\alpha(\underline{C}_\alpha, \underline{H}_{\alpha,\alpha}) = \hat{\psi}_\alpha(\underline{Q} \cdot \underline{C}_\alpha \cdot \underline{Q}^T, \underline{Q} \cdot \underline{H}_{\alpha,\alpha} \cdot \underline{Q}^T), \tag{2.40}$$

for all proper orthogonal $\underline{Q}$. Therefore, without loss in generality, the strain energy for fiber family i can be written with respect to its integrity basis for $(\underline{C}_\alpha, \underline{H}_{\alpha,\alpha})$ (Spencer , 1984). For lack of extensive data for the anisotropic behavior of cerebral arteries, we reduce the dependence of ψ_α on these invariants to the simplest form that is consistent with the expected mechanism of collagen load bearing for incompressible materials.

In particular, we assume the response of the collagen fibers is dominated by $E_{\alpha,\alpha}$, the strain in the mean direction of a fiber family relative to κ_α,

$$E_{\alpha,\alpha} = kI_\alpha + (1-3k)IV_{\alpha,\alpha} - 1, \tag{2.41}$$

so that $\psi_\alpha = \psi_\alpha(I_\alpha, IV_{\alpha,\alpha})$. The anisotropic strain energy function then can be written in terms of two tensor invariants (Gasser *et al.*, 2006),

$$\psi_{aniso} = \sum_{\alpha=1}^{2} \psi_\alpha(I_\alpha, IV_{\alpha,\alpha}), \qquad I_\alpha = tr\underline{C}_\alpha, \qquad IV_{\alpha,\alpha} = \underline{C}_\alpha : \underline{a}_{\alpha,\alpha} \otimes \underline{a}_{\alpha,\alpha}. \tag{2.42}$$

Compared to Eq. (2.21), the strain energy function (2.42) depends on both I_α and $IV_{\alpha,\alpha}$, which shows that the mechanical response of dispersed collagen fiber family is determined by the collective and averaged effect of the distributed collagen fibers.

2.2.4.2 Activation criterion for recruitment of collagen fibers in distribution model While in Gasser *et al.* (2006), a single reference configuration was used for all components of the arterial wall. Here, the recruitment of the αth family of crimped collagen fibers with representative orientation $a_{\alpha,0}$ in κ_0 initiates in a configuration denoted as $\kappa_{\alpha a}$.

To identify $\kappa_{\alpha a}$ and define the constitutive framework for the commencement of load bearing, we introduce a metric of deformation for each of the fiber families, denoted as, s_α. For the case of N discrete fibers in Section 2.2.3.2, this metric was assumed to depend on the strain of the specific fiber family under consideration. For a dispersed family of fibers, this identification is less clear. We assume s_α is a function of the following scalar measure of strain of the αth family of fibers relative to κ_0,

$$s_\alpha = s_\alpha(E_{\alpha,0}) \qquad where \qquad E_{\alpha,0} = \underline{H}_{\alpha,0} : \underline{C}_0 - 1. \tag{2.43}$$

This is the GreenLagrange-like strain previously used in Gasser *et al.* (2006) to characterize the strain in the mean direction of a fiber family. Using (2.36), it is clear that for materials with transverse isotropy, $E_{\alpha,0}$ simplifies to

$$E_{\alpha,0} = kI_0 + (1-3k)IV_{\alpha,0} - 1, \qquad with \qquad IV_{\alpha,0} = \underline{C}_0 : \underline{a}_{\alpha,0} \otimes \underline{a}_{\alpha,0}, \tag{2.44}$$

for $\alpha = 1, 2$.

Without loss in generality, we set $s_\alpha(E_{\alpha,0})$ equal to $E_{\alpha,0}$,

$$s_\alpha = E_{\alpha,0} = kI_0 + (1-3k)IV_{\alpha,0} - 1, \qquad \alpha = 1,2. \tag{2.45}$$

We then introduce a material parameter, $s_{\alpha a}$, such that the αth fiber family will be activated when s_α reaches the critical value $s_{\alpha a}$. The corresponding configuration is denoted as $\kappa_{\alpha a}$. In writing (2.45), we assume the fibers in each family are activated simultaneously. We can relax this assumption by introducing a gradual recruitment function. Note that when $k = 1/3$, (2.45) is similar in form to (2.7) for an isotropic material and to (2.25) for two fibers when $k = 0$.

2.2.4.3 Total constitutive response for structural, multi-mechanism model with collagen mechanism composed of a distribution of fibers

Using weighting functions d_0 from (2.29) for elastin activation and d_α for collagen deactivation,

$$d_\alpha \;=\; \begin{cases} 1 & s_\alpha < s_{\alpha a}, \quad \alpha = 1,2, \\ 0 & s_\alpha \geq s_{\alpha a}, \quad \alpha = 1,2, \end{cases} \tag{2.46}$$

the strain energy function at arbitrary time and material point can be expressed by,

$$\psi \;=\; (1-d_0)\psi_0(I_0) \;+\; \sum_{\alpha=1}^{2}(1-d_\alpha)\psi_\alpha(I_\alpha, IV_{\alpha,\alpha}). \tag{2.47}$$

The corresponding Cauchy stress tensor is,

$$\underline{T} \;=\; -p\underline{I} \;+\; 2(1-d_0)\frac{\partial\psi_0}{\partial I_0}\underline{B}_0 \;+\; \sum_{\alpha=1}^{2}(1-d_\alpha)\left[2\frac{\partial\psi_\alpha}{\partial I_\alpha}\underline{B}_\alpha \;+\; 2\frac{\partial\psi_\alpha}{\partial IV_{\alpha,\alpha}}\underline{F}_\alpha\cdot\underline{a}_{\alpha,\alpha}\otimes\underline{F}_\alpha\cdot\underline{a}_{\alpha,\alpha}\right]. \tag{2.48}$$

2.3 APPLICATION OF THE STRUCTURAL MULTI-MECHANISM MODEL TO CYLINDRICAL INFLATION

Motivated by the work of Scott, Fergusen and Roach (Scott *et al.*, 1972), we consider the behavior of the structural multi-mechanism model under cylindrical inflation in this section. In their pioneering work, Scott *et al.* (1972) explored the hypothesis that the main difference in mechanical properties between cerebral arterial and aneurysm tissue is due to elastin degradation during the aneurysm formation process. As part of their work, they inflated segments of cerebral arterial tissue *in-vitro* to obtain pressure-volume data. Significantly, they found that after three runs to 200 mmHg, the mechanical properties of the tissue changed abruptly and the unloaded radius of the vessel increased, Fig. 8. The tension-stretch curve for further loading cycles had no toe region, but was repeatable. Scott *et al.* (1972) found similar results for all three cerebral arteries loaded to this level. No shift was seen in control experiments of cyclic loading to a maximum pressure of 100 mm Hg. They hypothesized the qualitative change in the curve was due to the disruption of the elastin membrane caused by mechanical loading beyond the breaking strength of elastin. Their conjecture was based on (i) the lack of toe region in the second runs, and (ii) the qualitative similarity in the curves for the second runs and those of arterial tissue in which elastin had been chemically removed as a load bearing component (Roach & Burton, 1957).

In Section 2.3.1, we present analytical solutions for quasi-static cylindrical inflation of an artery segment modeled as the structural multi-mechanism equation with N fibers given in 2.2.3.1 and fiber distribution given in 2.2.4.1. In Section 2.3.2, we use the inflation test data from Scott *et al.* (1972) for cerebral arteries and the analytic solutions to select the form of the strain energy functions for the elastin and collagen mechanisms, and identify the material constants and deformation state parameters. This deformation corresponds to Stages A-F of Fig. 4.

2.3.1 Analytic solution for inflation of a cylindrical membrane composed of the structural multi-mechanism material

For lack of necessary details in the experimental work of Scott *et al.*, in this analysis we neglect the effect of residual stress. The unloaded artery wall is modeled as a homogeneous cylindrical membrane of constant thickness composed of the structural multi-mechanism model with fiber families. The fibers are assumed to have rotational symmetry about the direction $\underline{e}_\theta$. In the remainder of this section, we model the collagen mechanism as (i) N independent fibers, in which for every fiber with angle β_i relative to $\underline{e}_\theta$, there exists a second fiber with similar mechanical properties oriented at angle $-\beta_i$. (ii) a distributed fiber model, in which the fibers are taken as symmetrically arranged around $\underline{e}_\theta$ in κ_0, so we consider only one dispersion direction $\underline{a}_{1,0} = \underline{e}_\theta$ and set $\beta = 0$. The direction of material elements oriented parallel to $\underline{a}_{1,0}$ are unchanged during this axisymmetric deformation, so $\underline{a}_{1,1} = \underline{e}_\theta$.

The deformation is assumed to be a purely radial, axisymmetric deformation so that a material point located at $\underline{X}_0 = R_0\underline{e}_r + Z_0\underline{e}_z$, in the unloaded configuration with respect to cylindrical basis $\underline{e}_r, \underline{e}_\theta, \underline{e}_z$, is mapped to position $\underline{x} = R(R_0)\underline{e}_r + Z_0\underline{e}_z$ and the circumferential stretch is $\lambda = R/R_0$. The cylindrical components of the left and right Cauchy strain tensors relative to the reference configurations κ_0 is,

$$[\underline{B}_0] \;=\; [\underline{C}_0] \;=\; \begin{bmatrix} \dfrac{1}{\lambda^2} & 0 & 0 \\ 0 & \lambda^2 & 0 \\ 0 & 0 & 1 \end{bmatrix}, \tag{2.49}$$

so that from (2.4), (2.24) and (2.44),

$$I_0 \;=\; \frac{1}{\lambda^2} \;+\; \lambda^2 \;+\; 1, \quad IV_{i,0} \;=\; \lambda^2 \cos^2\beta_i \;+\; \sin^2\beta_i, \quad IV_{1,0} \;=\; \lambda^2. \tag{2.50}$$

It then follows from (2.7), (2.25) and (2.45),

$$s_0 \;=\; \max(\frac{1}{\lambda^2} + \lambda^2 - 2), \tag{2.51}$$

$$s_i \;=\; \lambda^2 \cos^2\beta_i \;+\; \sin^2\beta_i - 1, \tag{2.52}$$

$$s_1 \;=\; k(\frac{1}{\lambda^2}+\lambda^2+1)+(1-3k)\lambda^2-1. \tag{2.53}$$

We denote λ_{ia} and λ_{1a} as the circumferential stretches in κ_{ia}, and κ_{1a}, respectively, so that with Eq. (2.50),

$$IV_{ia,0} \;=\; \lambda_{fia}^2 \;=\; \lambda_{ia}^2\cos^2\beta_i \;+\; \sin^2\beta_i, \quad IV_{1a,0} \;=\; \lambda_{1a}^2, \tag{2.54}$$

where λ_{ia} will in general be different from λ_{fia}. In cases where the critical fiber stretch λ_{fia} is known a priori, λ_{ia} can be determined from (2.54),

$$\lambda_{ia}^2 = (\lambda_{fia}^2 - \sin^2\beta_i)/\cos^2\beta_i. \tag{2.55}$$

The relevant kinematic variables with respect to κ_i (i= 1,2,...,N) and κ_α can then be calculated from (2.49),

$$[\underline{B}_i] \;=\; [\underline{C}_i] \;=\; \begin{bmatrix} \frac{\lambda_{ia}^2}{\lambda^2} & 0 & 0 \\ 0 & \frac{\lambda^2}{\lambda_{ia}^2} & 0 \\ 0 & 0 & 1 \end{bmatrix}, \qquad [\underline{B}_1] \;=\; [\underline{C}_1] \;=\; \begin{bmatrix} \frac{\lambda_{1a}^2}{\lambda^2} & 0 & 0 \\ 0 & \frac{\lambda^2}{\lambda_{1a}^2} & 0 \\ 0 & 0 & 1 \end{bmatrix}, \tag{2.56}$$

In addition, it follows from Equations (2.50) and (2.54),

$$IV_{i,i} \;=\; \frac{\lambda^2\cos^2\beta_i \;+\; \sin^2\beta_i}{\lambda_{ia}^2\cos^2\beta_i \;+\; \sin^2\beta_i}, \quad I_1 \;=\; \frac{\lambda_{1a}^2}{\lambda^2}+\frac{\lambda^2}{\lambda_{1a}^2}+1, \quad IV_{1,1} \;=\; \frac{\lambda^2}{\lambda_{1a}^2}. \tag{2.57}$$

Following Wulandana and Robertson (2005), we can obtain the membrane equations for the tension $\mathcal{T} = r\,\Delta P$. For the N fiber model,

$$\mathcal{T} = \frac{4H_1}{\lambda}[(1-d_0)(\lambda^2-\frac{1}{\lambda^2})\frac{\partial\psi_0}{\partial I_0} \;+\; \sum_{i=1}^{N}(1-d_i)\frac{\partial\psi_i}{\partial IV_{i,i}}\frac{\lambda^2\cos^2\beta_i}{IV_{ia,0}}], \tag{2.58}$$

where H_1 is the half thickness of the membrane in configuration κ_0, and

$$d_0 \;=\; \begin{cases} 0 & for\;\; \lambda<\lambda_b \\ 1 & for\;\; \lambda\geq\lambda_b, \end{cases} \qquad d_i \;=\; \begin{cases} 1 & for\;\; \lambda<\lambda_{ia},\;\; i\in[1,N] \\ 0 & for\;\; \lambda\geq\lambda_{ia},\;\; i\in[1,N], \end{cases} \tag{2.59}$$

where λ_b is the stretch corresponding to $s_0 = s_{0b}$.

If the material parameter s_{0b} is known, then λ_b is the root of the equation,

$$\lambda_b^2 + 1/\lambda_b^2 - 2 = s_{0b}. \tag{2.60}$$

For the distributed collagen model, the membrane solution for wall tension is,

$$\mathcal{T} = \frac{4H_1}{\lambda}[(1-d_0)(\lambda^2 - \frac{1}{\lambda^2})\frac{\partial \psi_0}{\partial I_0} \; + \; (1-d_1)\frac{\partial \psi_1}{\partial E_{1,1}}[(1-3k)\frac{\lambda^2}{IV_{1a,0}} \; + \; k(\frac{\lambda^2}{\lambda_{1a}^2} - \frac{\lambda_{1a}^2}{\lambda^2})]], \tag{2.61}$$

where d_0 has the same definition given in (2.59),

$$d_1 \; = \; \begin{cases} 1 & for \;\; \lambda < \lambda_{1a}, \\ 0 & for \;\; \lambda \geq \lambda_{1a}, \end{cases} \tag{2.62}$$

and

$$E_{1,1} = kI_1 + (1-3k)IV_{1,1} - 1. \tag{2.63}$$

If the material parameter s_{1a} is known, then λ_{1a} can be determined using (2.53) with the condition $s_1 = s_{1a}$. Namely, λ_{1a} is the root of the equation,

$$s_{1a} \; = \; k(\frac{1}{\lambda_{1a}^2} + \lambda_{1a}^2 + 1) + (1-3k)\lambda_{1a}^2 - 1. \tag{2.64}$$

2.3.2 Application of structural multi-mechanism model to the data of Scott, Fergusen and Roach

We now turn attention to the selection of the material functions for the multi-mechanism models using the data from Scott *et al.* (1972) and the analytical solutions given above. For the elastin mechanism, the functional form of ψ_0 and s_{0b} must be determined. Motivated by the results of Wulandana and Robertson (2005), exponential and Neo-Hookean forms for the isotropic strain energy function were considered for $\psi_0(I_0)$, Table 1. For simplicity, only two fibers are considered in the N-fiber model for collagen. As mentioned above, we assume fiber symmetry such that $\beta_2 = -\beta_1 = -\beta$ and assume these fibers have identical material properties so that $s_{2a} = s_{1a}$ and $\psi_2(IV_{2,2}) = \psi_1(IV_{1,1})$. Due to the symmetry of the loading, this implies that $\lambda_{2a} = \lambda_{1a}$. In this case, only the function $\psi_1(IV_{1,1})$ and material parameters s_{1a} or λ_{f1a}, and β_1 must be determined. Using similar arguments, only the function $\bar{\psi}_1(E_{1,1})$

and the material parameters $\bar{s}_{1b}$ and need to be determined for the dispersion model. Second order exponential functions are considered for the strain energy functions for both anisotropic collagen mechanisms, Table 1. Exponential strain energy functions with second order terms for arterial tissue have been proposed by Fung (Fung *et al.*, 1979) and Holzapfel (Holzapfel *et al.*, 2000) et al., and widely used the literature (Humphrey, 1995; Sacks, 2000; Gasser and Holzapfel, 2002; Gasser *et al.*, 2006).

Table 1: Strain energy functions considered for the elastin and collagen mechanisms.

Elastin Mechanism	
Neo-Hookean (NH):	$\psi_0 = \frac{\eta_0}{2}(I_0 - 3),$
First Order Exponential (E-EXP1):	$\psi_0 = \frac{\eta_0}{2\gamma_0}\left(e^{\gamma_0(I_0-3)} - 1\right),$
Second Order Exponential (E-EXP2):	$\psi_0 = \frac{\eta_0}{2\gamma_0}\left(e^{\gamma_0(I_0-3)^2} - 1\right),$
Collagen Mechanism	
Isotropic Model	
Exponential (C-EXP-iso):	$\psi_1 = \frac{\eta}{2\gamma}\left(e^{\gamma(I_1-3)} - 1\right),$
Anisotropic 2 Fiber Model	
Exponential (C-EXP2-2-fiber):	$\psi_\alpha = \frac{\eta}{2\gamma}\left(e^{\gamma(IV_{\alpha,\alpha}-1)^2} - 1\right), \quad \alpha = 1, 2,$
Anisotropic Dispersion Model	
Exponential (C-EXP2-disp):	$\psi_\alpha = \frac{\eta}{2\gamma}\left(e^{\gamma(kI_\alpha+(1-3k)IV_{\alpha,\alpha}-1)^2} - 1\right), \quad \alpha = 1, 2.$

As in Wulandana and Robertson (2005), it is assumed that only the elastin mechanism is active for $\lambda \in [1, \lambda_{1a})$ of Runs 1-3, both mechanisms are active for $\lambda \in [\lambda_{1a}, \lambda_b)$ of Runs 1-3, and only the collagen mechanism is active during Runs 4-9. An arterial thickness of 125 μm was used. Following the approach taken in Wulandana and Robertson (2005), the values for the critical circumferential stretches are $\lambda_{1a} = 1.76$ and $\lambda_b = 2.3$. Using these values, a nonlinear regression analysis was performed using a modified Levenberg-Marquardt method. All data from the two curves (Runs 1-3 and Runs 4-9) were fit simultaneously using the

solutions for tension given in (2.58) and (2.61). The quality of the fit was quantified using a modified pseudo R^2 value defined by

$$R^2 = 1 - \frac{\sum_{i=1}^{n}(\mathcal{T}_i - \mathcal{T}(\lambda_i))^2}{\sum_{i=1}^{n}(\mathcal{T}_i - \overline{\mathcal{T}_k})^2}, \tag{2.65}$$

where n is the number of data points, $\mathcal{T}_i$ is a tension data and $\overline{\mathcal{T}_k}$ is the average value of the tension data. $\mathcal{T}(\lambda_i)$ is the tension calculated for stretch ratio λ_i using (2.58) and (2.61).

2.3.2.1 Results of nonlinear regression analysis To select a strain energy for the elastin mechanism, we compared the results of the regression analysis for the three choices of elastin mechanism given in Table 1 for a 2-fiber collagen model. As will be discussed below, the results for all three collagen models were able to fit the data well. For this reason, when comparing the choices of elastin strain energy functions, we only considered one of the models (the 2-fiber model). Results of the nonlinear regression analysis are shown in Table 2 and Fig. 8. The exponential models were clearly better than the Neo-Hookean model and the second order exponential model was slightly better than the first order exponential model.

Table 2: Results of nonlinear regression analysis for three choices of strain energy function for elastin mechanism.

ψ	η_0(KPa)	γ_0	η(KPa)	γ	β	R^2
E-NH,C-EXP2-2-fiber	27.6	NA	27.0	0.0981	0.0	0.8618
E-EXP1,C-EXP2-2-fiber	6.82	0.582	18.5	0.340	0.0	0.9922
E-EXP2,C-EXP2-2-fiber	5.09	0.0293	18.4	0.346	0.0	0.9944

Results for the 2-fiber and disperse fiber collagen models are shown in Table 3 and Fig. 9. In both cases the second order exponential model for elastin is used. There is a tremendous need for both additional structural data on fiber orientation and biaxial loading data for the cerebral vessels. All material parameters in Table 3 including fiber orientation variable β

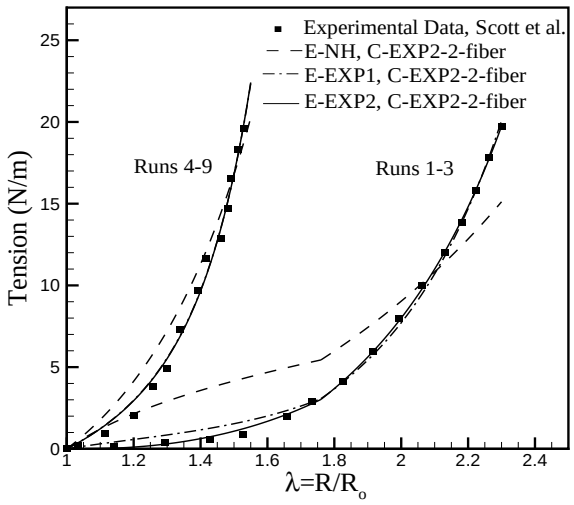

Figure 8: Comparison of Neo-Hookean (NH), first order exponential (E-EXP1) and second order exponential (E-EXP2) strain energy functions for the elastin mechanism of dual-mechanism model, with second order exponential function (C-EXP2) used for the collagen mechanism for all cases.

and were determined from the regression analysis. Also shown for comparison are results for the isotropic dual-mechanism model introduced in Wulandana and Robertson (2005). A first order exponential strain energy function was used for both elastin and collagen mechanisms. Due to a typographical error in Wulandana and Robertson (2005), the values reported in Table 3 for η, η_0 differ from those in Wulandana and Robertson (2005) (variables α_1, α_2 in that work). While the anisotropic collagen models introduced here give slightly better fits than the isotropic model, more experimental data is needed to fully appreciate and develop the anisotropic models.

From the results of the regression analysis, it is useful to calculate the material parameters related to the activation of collagen and deactivation of elastin so that these models can be considered for other deformations.From (2.51) with $\lambda_b = 2.3$, it follows that $s_{0b} = 3.48$. Evaluating (2.53) with $\beta = 48^o$, $k = 0$ and $\lambda_{1a} = 1.76$, it follows that $s_{1a} = 0.94$. Using (2.53) with $k = 0.298$ and $\beta = 0^o$, $s_{1a} = 0.65$. We emphasize that the value of β and hence s_{1a} needs to be further explored when inelastic biaxial data becomes available.

Table 3: Results of regression analysis for 2-fiber, dispersion and isotropic collagen models.

ψ	η_0(KPa)	γ_0	η(KPa)	γ	$\beta_1 = -\beta_2$		R^2
E-EXP2, C-EXP2-2-fiber	5.09	0.0293	35.9	0.677	48^o		0.9944
ψ	η_0(KPa)	γ_0	η(KPa)	γ	β	k	R^2
E-EXP2, C-EXP2-disp	5.67	0.0213	380.2	1.83	0^o	0.298	0.9959
ψ	η_0(KPa)	γ_0	η(KPa)	γ			R^2
E-EXP1, C-EXP1-iso	6.45	0.599	54.7	1.84			0.9917

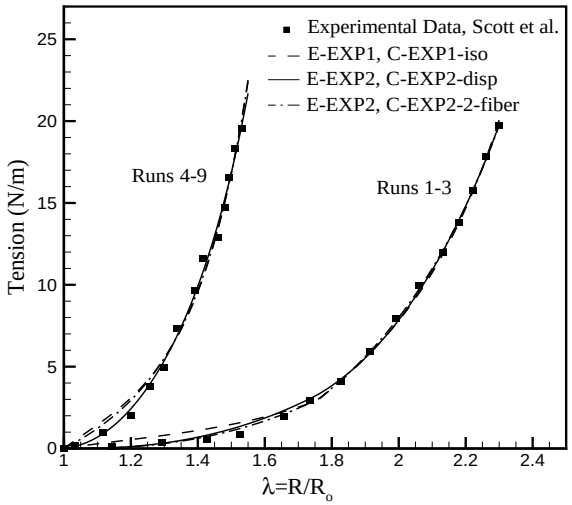

Figure 9: Comparison of three choices of the collagen mechanism with an exponential elastin mechanism (i) 2-fiber model (E-EXP2, C-EXP2-2-fiber),(ii) dispersion model (E-EXP2, C-EXP2-disp), a(ii) isotropic model (E-EXP1, C-EXP1-iso) used in Wulandana and Robertson (2005).

3.0 A DAMAGE MODEL FOR CEREBRAL ARTERIES

3.1 INTRODUCTION

Early stage cerebral aneurysms are characterized by the fragmentation and disruption of the internal elastic lamina (IEL), which was observed both in human cerebral aneurysms (Nystrom *et al.*, 1963; Scanarini et al., 1978; Stehbens , 1963) and experimentally induced animal cerebral aneurysms (Hazama *et al.*, 1986; Hashimoto *et al.*, 1987; Kondo et al., 1997; Morimoto *et al.*, 2002). The weaker or absent elastin and arterial wall can be distended more easily and give way to under elevated blood pressure, which can lead to enlargement of the walls (Nystrom *et al.*, 1963). The cause of this breakdown and degeneration, congenital or postnatal origin, is still not understood, but it has been conjectured to be caused by overstretch, fatigue failure or alternatively by a breakdown in homeostatic mechanisms in the wall arising from some aspect of the local hemodynamic stress and wall tension, e.g. (Robertson *et al.*, 2007; Meng *et al.*, 2006; Humphrey, 2002).

Elastin, an insoluble polymer composed of several tropoelastin molecules covalently bound to each other by cross links, is considered extremely stable, so that it turns over so slowly that it lasts for the lifetime of the organism (Debelle and Tamburro, 1999). Davis (1995) cites several references supporting this claim (Keeley, 1979; Lefevre and Rucker, 1980; Mariencheck *et al.*, 1995) and, by using tritium-labeled valine, has shown that no elastin turnover or growth occurs in the mouse aorta during adulthood (Davis, 1993). Therefore, the detrimental effects of the degradation will not, in general, be repaired.

Experimental studies of cerebral aneurysms have revealed that the degradation of IEL is progressive. Currently only animal models are available for experimental studies, in which aneurysms are induced artificially by hemodynamic change and diet control. Hazama *et al.*

(1986) and Morimoto *et al.* (2002) examined various stages of the cerebral aneurysms in mice by electron microscopy. The mouse birfurcation model (Morimoto *et al.*, 2002) shows initial IEL fragmentation and slight media thinning in the early stage of artificially induced ICA. The IEL degeneration and media damage are more progressive at the proximal portion of the aneurysmal wall than at the distal portion in the early stage of ICA development

Studies of aneurysm formation in animal models have shown that elastin degradation associated with aneurysm initiation can be induced by exposing bifurcations to altered hemodynamic loads. In particular, it appears that some combination of elevated (WSS), wall shear stress gradient (WSSG) and hemodynamic pressure will lead to elastin degradation in native and non-native bifurcations (Fukuda *et al.*, 2000; Morimoto *et al.*, 2002; Meng *et al.*, 2006).

The degradation and loss of IEL and media can cause severe and irreversible biomechanical changes in the arterial wall (Scott *et al.*, 1972; Fonck, 2007). Fonck (2007) studied the effect of elastin degradation on arterial wall mechanics. In their studies, the biomechanical properties of carotid arterial wall were analyzed before and after enzymatic degradation of the elastin. It was shown that the incremental elastic modulus of the elastase-treated arteries decreased compared with the control arteries at low to medium stretch region, which means that arteries become softer and weaker due to lack of elastin. Constitutive models which can capture the dependence of elastin damage on both mechanical and biomechanical events will be necessary to model the initiation of ICA.

Humphrey (2002) proposed a constrained mixture model to characterize soft tissue growth and remodeling - the homeostatic adaptation of tissues in response to altered mechanical stimulus. In this theory, growth is interpreted as the mass increase due to constituent turnover (production and removal), and remodeling is material property change due to constituent microstructure evolution, such as the reorganization of existing material or the synthesization of new material. The constrained mixture model provides a general framework for the stress response analysis of soft tissue based on continual constituent turnover and microstructure evolution. The specification of evolution functions is still a challenging work with competing hypothesis. This model does not accommodate damage to the wall constituents.

The experimental studies of human intracranial arteries from Scott *et al.* (1972); Monson (2001) suggested that the cyclic and creep damage of tissue are closely related to elastin degradation for cerebral arteries. Scott *et al.* (1972) found that under a cyclic inflation test with 200 mmHg pressure, there exists a shift of the load-stretch curve after three cycles, with residual strain left in the tissue after unloading. Scott *et al.* (1972) hypothesized the main difference in mechanical properties between cerebral arterial and aneurysm tissue is due to elastin degradation during the aneurysm formation process. Monson (2001) did axial and inflation tests to investigate mechanical and failure properties of human cerebral arteries. He reported that after the preconditioning of cerebral arteries under a fixed inflation pressure of 150 mmHg and a fixed axial stretch of 1.04, there is large changes in the reference point and curvature of low strain associated with the preconditioning and burst curves. Monson (2001) attributed these to changes in the elastin structure of the vessels, and cited the finding of Scott *et al.* (1972) to support his hypothesis.

We propose to model the elastin progressive disruption and arterial weakening using an inelastic damage model. It builds on the previously introduced structural multi-mechanism model for cerebral arteries that includes collagen recruitment and a failure criterion for the disruption of elastin. The current model includes subfailure damage of the elastin, ground matrix or collagen fibers, represented by changes in tissue mechanical properties and unloaded reference length (Sun, 2003; Provenzano *et al.*, 2002). An inelastic damage function is introduced to characterize the progressive degradation of elastin arising directly from mechanical loading and indirectly from hemodynamic loading. A structural model is used to characterize the progressive damage of anisotropic collagen fibers.

Continuum damage mechanics was introduced by Kachanov (1958) to describe the deterioration of materials before the initiation of macrocracks. In continuume damage models, a continuous damage variable is used to represents average degradation in material properties which results from initiation and growth of microcracks and defects. Continuum damage constitutive models has been used for solving practical engineering problems including creep, fatigue, creep-fatigue interaction and ductile plastic fracture phenomena (Krajcinovic and Selvaraj, 1984; Chaboche, 1988; Lemaitre, 1985).

Damage has previously been modeled in other biological tissues. For example, Slaughter and Sacks (2001) modeled the change of tissue properties under cyclic loading. Avolio *et al.* (1998) hypothesized that the number of repeated pulsations to which the arterial wall is subjected leads to progressive elastin damage. The theoretical framework of damage mechanics has previously been used for the elasto-damage behavior of fibrous tissue (Natali *et al.*, 2005; Calvo *et al.*, 2007).

3.2 DAMAGE MODEL FOR CEREBRAL ARTERIES

3.2.1 Background for damage models

In this section, we quickly summarize the relevant thermodynamic considerations. Because of the multiple reference configurations involved in the constitutive response of the material, we make use of the thermodynamic inequalities in Eulerian form. More details can be found in Truesdell and Noll (1965) (page 294-295, which is elaborated on in CFT, Chapter E). This approach is appealing because unlike the volume, the infinitesimal mass does not vary with configuration. There is no a priori need to select a reference configuration in which to define the volume. This is particularly important in the case of multi-mechanism materials when the reference configuration will vary with each mechanism.

3.2.1.1 Clausius-Duhem inequality The local form of the Clausius-Duhem inequality can be written as

$$-\rho(\dot{\psi} + \eta\dot{\theta}) + \mathrm{tr}(\underline{T} : \underline{D}) \; - \; \frac{1}{\theta}\underline{q} \cdot \theta \geq 0, \tag{3.1}$$

where ψ is the Helmholtz free energy per unit mass,

$$\psi \; = \; u \; - \; \eta\theta. \tag{3.2}$$

η is the entropy per unit mass, and u is the internal energy per unit mass.

It follows directly from (3.1) that for isothermal processes with no heat transfer (θ = constant and $\underline{q} = \underline{q}_0 = 0$), the Clausius-Duhem inequality reduces to,

Isothermal form of the Clausius-Duhem inequality

Eulerian

$$-\rho\,\dot{\psi} \;+\; \underline{T} : \underline{D} \geq 0,$$

Lagrangian

$$-\rho_0\,\dot{\psi} \;+\; \underline{P}^T : \dot{\underline{F}} \geq 0,$$

or, alternatively,

$$-\rho_0\,\dot{\psi} \;+\; \frac{1}{2}\underline{S} : \dot{\underline{C}} \geq 0. \tag{3.3}$$

3.2.1.2 Clausius-Planck inequality If we impose the condition that heat flow from warmer to the colder region of a body, we can obtain a stronger statement than the Clausius-Duhem inequality. In the case that the flow is isothermal we recover the Clausius-Duhem inequality.

3.2.2 Continuum damage models for multi-mechanism materials

Continuum Damage Models(CDMs) are an example of constitutive models with internal variables. Here we consider isothermal theories for damage to multi-mechanism materials.

In particular, we assumed the Helmholtz free energy per unit mass can be written in the following form,

$$\psi \;=\; \hat{\psi}^{(0)}(\underline{C}_0, \underline{\xi}^{(0)}) \;+\; \sum_{i=1}^{N} \hat{\psi}^{(i)}(\underline{C}_i, \underline{A}_{i,i}, \underline{\xi}^{(i)}), \tag{3.4}$$

where the internal variables $\underline{\xi}^{(0)}$ and $\underline{\xi}^{(i)}$ are tensors of some unspecified order associated with damage to each of the mechanisms. Recall that $\underline{C}_0$ and $\underline{C}_i$ are the right Cauchy Green strain tensors relative to configurations κ_0 and κ_i, respectively. Furthermore, $\underline{A}_{i,i} = \underline{a}_{i,i} \otimes \underline{a}_{i,i}$, where $\underline{a}_{i,i}$ is a unit vector representing the direction of fiber family i in configuration κ_i.

In these notes, we restrict attention to isotropic damage models, we will consider a zero order tensor (scalar) for each mechanism with

$$\underset{\sim}{\xi}^{(0)} \to d_0, \qquad \underset{\sim}{\xi}^{(i)} \to d_i. \tag{3.5}$$

The internal variables $d_0, d_i (i = 1, N) \in [0, 1]$ and are called the *damage variables*. This form was first proposed by Kachanov (1958) to model creep rupture of metals. We now consider a specific continuum damage model of the form,

$$\psi \;=\; (1 - d_0)\hat{\psi}_0(\underset{\sim}{C}_0) \;+\; \sum_{i=1}^{N}(1 - d_i)\hat{\psi}_i(\underset{\sim}{C}_i, \underset{\sim}{A}_{i,i}), \tag{3.6}$$

where, we have set

$$\hat{\psi}^{(0)}(\underset{\sim}{C}_0, d_0) = (1 - d_0)\hat{\psi}_0(\underset{\sim}{C}_0), \qquad \hat{\psi}^{(i)}(\underset{\sim}{C}_i, \underset{\sim}{A}_{i,i}, d_i) \;=\; (1 - d_i)\hat{\psi}_i(\underset{\sim}{C}_i, \underset{\sim}{A}_{i,i}). \tag{3.7}$$

The functions $\hat{\psi}_0$ and $\hat{\psi}_i$ are the effective strain energy functions of the undamaged material. In particular,

$$\begin{aligned} &\psi_0(\underset{\sim}{C}_0): && \text{Effective strain energy of the undamaged elastin mechanism,} \\ &\psi_i(\underset{\sim}{C}_i, \underset{\sim}{A}_{i,i}): && \text{Effective strain energy of the undamaged collagen mechanism,} \end{aligned} \tag{3.8}$$

and the effective strain energies are normalized in the usual way such that $\psi_0(\underset{\sim}{I}) = 0$ and $\psi_i(\underset{\sim}{I}, \underset{\sim}{A}_{i,i}) = 0$.

Thermodynamic restrictions on acceptable forms of (3.6) can be obtained from the Clausius-Planck inequality for isothermal processes, (3.3). Taking the material derivative of (3.6), we can then evaluate the Clausius-Planck inequality in the context of a purely mechanical theory,

$$\begin{aligned} \left[\frac{1}{\rho}T_{ab} \;-\; 2(1 - d_0)\frac{\partial \psi_0}{\partial C_{0_{AB}}}F_{0_{aA}}F_{0_{bB}} \;-\; 2\sum_{i=1}^{N}(1 - d_i)\frac{\partial \psi_i}{\partial C_{i_{AB}}}F_{i_{aA}}F_{i_{bB}}\right] D_{ab} \\ + \psi_0\dot{d}_0 \;+\; \sum_{i=1}^{N}\psi_i\dot{d}_i \geq 0. \end{aligned} \tag{3.9}$$

Following the usual procedures developed by Coleman-Noll, we can then deduce that

$$T_{ab} \;=\; 2\rho(1-d_0)\frac{\partial \psi_0}{\partial C_{0_{AB}}}\, F_{0_{aA}}\, F_{0_{bB}} \;+\; 2\rho\sum_{i=1}^{N}(1-d_i)\frac{\partial \psi_i}{\partial C_{i_{AB}}} F_{i_{aA}}\, F_{i_{bB}}, \tag{3.10}$$

and

$$\psi_0 \dot{d}_0 \geq 0, \qquad \psi_i \dot{d}_i \geq 0. \tag{3.11}$$

Alternatively, in index free form,

$$\underline{T} \;=\; 2\rho(1-d_0)\underline{F}_0 \cdot \frac{\partial \psi_0}{\partial \underline{C}_0} \cdot \underline{F}_0{}^T \;+\; 2\rho\sum_{i=1}^{N}(1-d_i)\underline{F}_i \cdot \frac{\partial \psi_i}{\partial \underline{C}_i} \cdot \underline{F}_i^T. \tag{3.12}$$

Note that if we would like to obtain the stress tensor relative to the reference configuration, we need to be clear which reference configuration we have in mind. For example, considering $\underline{S} \;=\; J_0 \underline{F}_0^{-1} \underline{T}\, \underline{F}_0^{-T}$ and using (3.12) we obtain,

$$\underline{S} \;=\; 2\rho_0(1-d_0)\frac{\partial \psi_0}{\partial \underline{C}_0} \;+\; 2\rho_0\sum_{i=1}^{N}(1-d_i)\underline{F}_0^{-1}(t_i) \cdot \frac{\partial \psi_i}{\partial \underline{C}_i} \cdot \underline{F}_0^{-T}(t_i). \tag{3.13}$$

where it should be understood that we have calculated $\underline{S}$ relative to κ_0. Alternatively, we could have calculated $\underline{S}$ relative to κ_i.

3.2.3 Isotropic damage model for the elastin mechanism

In this study, following the approach of continuum damage mechanics (Krajcinovic, 1996), we model the gradual degradation of elastin or ground matrix as a process of continuous growth and accumulation of microvoids or microcracks via the evolution of internal damage variable as a function of loading path, time, cycle numbers or hemodynamic stress. Here, we assume the degradation of elastin can happen in any direction, so an isotropic damage theory can be used. In this case, only a scalar d_0 is needed as the damage variable (Simo and Ju, 1987). Generalizing the discrete weighting function for elastin deactivation, here, the increase of d_0 from 0 (no damage) to 1 (failure) characterizes the progressive degradation of elastin and gradual change in the material elastic response.

Following Section 3.2.2, the degraded elastin mechanism can be characterized through the strain energy function using the damage variable d_0,

$$\psi_{iso}(I_0, d_0) = (1 - d_0)\psi_0(I_0). \tag{3.14}$$

Here, $\psi_0(I_0)$ is the undamaged strain energy function (Simo and Ju, 1987).

There have been many studies regarding the cause of elastin degeneration. Biomechanically, the focal weakening, increasing fragility and degeneration of elastin can result from wall tension under persistent hemodynamic loads such as hypertension or pulsatile pressures (Stehbens , 1989; Inci and Spetzler, 2000; Humphrey and Taylor, 2008). More recent biochemical research shows that enzymatic factors also play key roles in elastin degeneration, where increased hemodynamic stress activates endothelial cells and matrix metalloproteinases (MMPs), which degrade the IEL (Sho et al., 2002; Hashimoto, 2006). Based on current research, we model elastin degradation as a damage process with two damage mechanisms, mechanical damage and enzymatic damage, both contributing to elastin degradation in terms of damage variables,

$$(1 - d_0) = (1 - d_{01}[\nu_{01}(t)])(1 - d_{02}[\nu_{02}(t)])(1 - d_{03}[\nu_{03}(t)]), \tag{3.15}$$

in which d_{01} and d_{02} are mechanical strain-based damage variables depending on material strain history in the load path, such as cyclic stretch or fatigue. d_{03} is an enzymatic creep damage variable depending on elevated hemodynamic stresses, such as wall shear stress (WSS), wall shear stress gradient (WSSG) or transmural pressures (ΔP). The damage metrics which control the evolution of damage variables are defined as $\nu_{01}(t)$, $\nu_{02}(t)$ and $\nu_{03}(t)$ respectively.

For the constitutive model of inelastic material, it is necessary to define the evolution functions for internal variables (flow rules) and deformation criteria. Here, we need damage criteria and damage functions.

For the mechanical damage mechanism, in typical Mullins softening damage process for arterial tissue (Hokanson and Yazdani, 1997), the cyclic weakening (softening) of tissue depends on the load path. Assuming a strain-driven damage mechanism (Simo and Ju, 1987) for the elastin degradation, for the first mechanical damage variable d_{01}, we can define

a maximum equivalent strain at time t as,

$$\nu_{01}(t) = \max_{s\in[0,t]} \sqrt{2\psi_0(I_0(s))}. \tag{3.16}$$

The damage criterion based on the maximum equivalent strain can be defined as,

$$\phi_0(I_0, \nu_{01}(t)) = \sqrt{2\psi_0(I_0)} - \nu_{01}(t) \leq 0, \tag{3.17}$$

in which a damage surface $\phi_0 = 0$ is formulated in equivalent strain space. The normal on the damage surface is,

$$\underline{N}_0 = \frac{\partial \phi_0}{\partial \underline{C}_0}. \tag{3.18}$$

Using the terminology from strain space plasticity (Naghdi and Trapp , 1975), we can describe unloading, neutral loading and loading states on the damage surface,

$$\phi_0 \;=\; 0 \;\; and \begin{cases} \underline{N}_0 : \dot{\underline{C}}_0 < 0, & \text{unloading} \\ \underline{N}_0 : \dot{\underline{C}}_0 = 0, & \text{neutral loading} \\ \underline{N}_0 : \dot{\underline{C}}_0 > 0. & \text{loading} \end{cases} \tag{3.19}$$

The evolution of the damage surface only happens at the state of loading on the damage surface, namely,

$$\dot{\nu_{01}} \;=\; \begin{cases} \dfrac{1}{\sqrt{2\psi_0(I_0)}} \dfrac{\partial \psi_0(I_0)}{\partial \underline{C}_0} : \dot{\underline{C}}_0, & \text{when} \;\; \phi_0 = 0 \;\; \text{and} \;\; \underline{N}_0 : \dot{\underline{C}}_0 > 0 \\ 0. & \text{otherwise} \end{cases} \tag{3.20}$$

The second mechanical damage variable d_{02} is defined as a function of the accumulated equivalent strain of the material through $\nu_{02}(t)$,

$$\nu_{02}(t) = \int_0^t \left| d\sqrt{2\psi_0(I_0(s))}/ds \right| \, ds. \tag{3.21}$$

For flow induced damage process, the elastin degradation depends on elevated local hemodynamic stress such as wall shear stress (WSS) or wall shear stress gradient (WSSG). Assuming enzymatic damage mechanism, we can define $\nu_{03}(t)$ as a function of WSS and

WSSG at time t as,

$$\nu_{03}(t) = f(WSS, WSSG). \tag{3.22}$$

For example, one choice is,

$$\nu_{03}(t) = \frac{1}{T}\int_0^t a(\zeta + b\iota)\, ds \quad where \;\; \zeta = \frac{WSS - WSS_T}{WSS_T}, \;\; \iota = \frac{WSSG - WSSG_T}{WSSG_T}. \tag{3.23}$$

Here, $a = \hat{a}(\zeta, \iota)$ is one if ζ and ι are both positive and is otherwise zero. Material parameters b and T are constants.

The damage metrics $\nu_{01}(t)$, $\nu_{02}(t)$ are clearly invariant to superposed rigid body motions. The form of $\nu_{03}(t)$ defined in (3.22) is purposely left quite general, but will similarly be an invariant quantity (Zeng et al., 2009). The damage variables d_{01}, d_{02} and d_{03} evolve with loading path, cycles or time according to the following damage criteria,

$$d_{0j} \;=\; \begin{cases} 0, & \nu_{0j} < \nu_{0js}, \\ D_{0j}[\nu_{0j}(t)], & \nu_{0js} \le \nu_{0j} < \nu_{0jf}, \\ 1, & \nu_{0jf} \le \nu_{0j}, \end{cases} \tag{3.24}$$

in which ν_{0js} are the critical values of $\nu_{0j}(t)$ for the start of elastin degradation, ν_{0jf} are the critical values of $\nu_{0j}(t)$ for elastin to reach complete failure, and $j = 1, 2, 3$ depending on the mode of damage under consideration, which corresponds to the maximum equivalent strain, accumulated equivalent strain and hemodynamic loading respectively.

3.2.4 Anisotropic damage model for collagen fibers

In this section, we generalize the structural model introduced in Section 2.2.4 to include anisotropic damage features for collagen fibers. In Section 2.2.4, we study the recruitment of dispersed collagen fiber families by introducing a fiber strain based criteria under physiological loading. Here, we study the mechanical-induced damage mechanism of collagen fibers, the gradual disruption and damage accumulation of fibers as a function of mechanical loading. Partial collagen disruption at higher strain level is expected to be associated with collagen growth and remodeling in aneurysm development, shown in Fig. 4. Supra-physiological loads during clinical interventions such as angioplasty surgery can induce mechanical injury

to arterial tissues including damage, tear or plastic deformation of collagen fibers (Holzapfel *et al.*, 2000; Gasser and Holzapfel, 2002; Oktay *et al.*, 1991).

In Section 2.2.4, the recruitment variable d_α only takes the value of 1 (no recruitment) or 0 (recruitment) at low strain level. At higher load levels, we assume that the collagen damage accumulates as fiber strain increases for recruited fibers. Following Section 3.2.2, the collagen mechanism is characterized by the Helmholtz free energy,

$$\psi_{aniso} = \sum_{\alpha=1}^{2}(1 - d_\alpha[s_{\alpha,\alpha}(t)])\psi_\alpha(I_\alpha, IV_{\alpha,\alpha}), \tag{3.25}$$

in which $d_\alpha[s_{\alpha,\alpha}(t)]$ is a mechanical strain-based recruitment or damage variable here depending on fiber strain history in the load path. $s_{\alpha,\alpha}$ is the metric of deformation for collagen disruption after recruitment,

$$s_{\alpha,\alpha} = \hat{s}_{\alpha,\alpha}(I_\alpha, IV_{\alpha,\alpha}) = \underline{H}_{\alpha,\alpha} : \underline{C}_\alpha - 1 \qquad \alpha = 1, 2. \tag{3.26}$$

The damage metric which controls the evolution of the damage variable is $\nu_\alpha(t)$, chosen as the maximum fiber strain at time t,

$$\nu_\alpha(t) = \max_{s\in[0,t]}(s_{\alpha,\alpha}(s)). \tag{3.27}$$

The damage criterion is,

$$\phi_\alpha(I_{\alpha,\alpha}, IV_{\alpha,\alpha}, \nu_\alpha(t)) = s_{\alpha,\alpha} - \nu_\alpha(t) \leq 0. \tag{3.28}$$

The normal on the damage surface $\phi_\alpha = 0$ is,

$$\underline{N}_\alpha = \frac{\partial \phi_\alpha}{\partial \underline{C}_\alpha}. \tag{3.29}$$

The evolution of the damage surface only happens at the state of loading on the damage surface,

$$\dot{\nu_\alpha} = \begin{cases} \underline{H}_{\alpha,\alpha} : \dot{\underline{C}}_\alpha, & \text{when } \phi_\alpha = 0 \text{ and } \underline{N}_\alpha : \dot{\underline{C}}_\alpha > 0 \\ 0. & \text{otherwise} \end{cases} \tag{3.30}$$

The damage variable d_α evolves with load path according to the damage criterion,

$$d_\alpha = \begin{cases} 0, & s_{\alpha a} < s_\alpha \text{ and } \nu_{\alpha s} > \nu_\alpha, \\ d_\alpha[\nu_\alpha(t)], & s_{\alpha a} < s_\alpha \text{ and } \nu_{\alpha s} \leq \nu_\alpha < \nu_{\alpha f}, \\ 1, & s_{\alpha a} < s_\alpha \text{ and } \nu_{\alpha f} \leq \nu_\alpha, \end{cases} \tag{3.31}$$

in which $\nu_{\alpha s}$ is the critical value of ν_α for the start of collage damage, and $\nu_{\alpha f}$ is the critical value of ν_α for fiber disruption.

4.0 FINITE ELEMENT IMPLEMENTATION

In this work, we choose to use a commercial general purpose finite element package (ANSYS 11.0 here), so that we can use the pre and post-processing features and robust solvers of commercial codes. The structural multi-mechanism model is implemented in this code through user defined subroutines.

4.1 NUMERICAL SCHEME

Arterial tissues are usually modeled as incompressible (Holzapfel, 2006; Humphrey, 2002). The numerical simulation of incompressible and nearly incompressible material is recognized as a numerical difficulty which often leads to mesh locking, ill-conditioning of the stiffness matrix and large oscillations in stress calculation (Herrmann , 1965; Oden and Key, 1970). In this work, we used a penalty method to model cerebral arteries as slightly compressible material by using a large bulk modulus (Holzapfel, 2000), and as a result stabilize the numerical solution for the constitutive response. We formulate the structural constitutive model as a compressible material model using the standard decoupled representation of the strain energy function, in which a volumetric part is introduced into the strain energy function accounting for material volume change. Then an appropriate incompressibility parameter is chosen to approximate the incompressibility constraint. Our numerical scheme is based on the following points (i) a good approximation for incompressible material behavior can be reached using a small value of the incompressibility parameters, and (ii) the slightly compressible scheme is the commonly available approach for modeling purely incompressible material with user routines in general purpose finite element codes.

4.1.1 Slightly compressible structural multi-mechanism model

Here, the structural multi-mechanism model is formulated as a compressible material for the purpose of numerical implementation. Following (Ogden , 1978), we use the multiplicative decomposition of the deformation gradient $\underline{F}_0$ defined in Eqs. (2.2) into a dilatational part $(J_0^{1/3}\underline{I})$ and a distortional part $(\bar{\underline{F}}_0)$,

$$\underline{F}_0 = (J_0^{1/3}\underline{I})\bar{\underline{F}}_0, \qquad J_0 = det(\underline{F}_0), \tag{4.1}$$

where J_0 is the determinant of deformation gradient, and $\underline{I}$ is an second order identity tensor. Similarly, for the deformation gradients $\underline{F}_\alpha$, we have,

$$\underline{F}_\alpha = (J_\alpha^{1/3}\underline{I})\bar{\underline{F}}_\alpha, \qquad J_\alpha = det(\underline{F}_\alpha), \qquad (\alpha = 1, 2). \tag{4.2}$$

The associated isochoric parts of the left and right Cauchy Green strain tensors for the elastin and collagen mechanisms are defined as,

$$\bar{\underline{B}}_0 = \bar{\underline{F}}_0 \cdot \bar{\underline{F}}_0^T, \qquad \bar{\underline{B}}_\alpha = \bar{\underline{F}}_\alpha \cdot \bar{\underline{F}}_\alpha^T, \tag{4.3}$$

and

$$\bar{\underline{C}}_0 = \bar{\underline{F}}_0^T \cdot \bar{\underline{F}}_0, \qquad \bar{\underline{C}}_\alpha = \bar{\underline{F}}_\alpha^T \cdot \bar{\underline{F}}_\alpha. \tag{4.4}$$

From Eqs. (2.3) and (2.13), we have,

$$\underline{B}_0 = \underline{F}_0 \cdot \underline{F}_0^T = J_0^{2/3}\bar{\underline{B}}_0, \qquad \underline{B}_\alpha = \underline{F}_\alpha \cdot \underline{F}_\alpha^T = J_\alpha^{2/3}\bar{\underline{B}}_\alpha, \tag{4.5}$$

$$\underline{C}_0 = \underline{F}_0^T \cdot \underline{F}_0 = J_0^{2/3}\bar{\underline{C}}_0, \qquad \underline{C}_\alpha = \underline{F}_\alpha^T \cdot \underline{F}_\alpha^T = J_\alpha^{2/3}\bar{\underline{C}}_\alpha. \tag{4.6}$$

Following (2.47), we use a decoupled form of strain energy as in Holzapfel *et al.* (2000),

$$\psi \;=\; \psi_{vol}(J_0) \;+\; (1-d_0)\psi_0(\bar{I}_0) \;+\; \sum_{\alpha=1}^{2}(1-d_\alpha)\psi_\alpha(\bar{I}_\alpha, \bar{IV}_{\alpha,\alpha}), \tag{4.7}$$

in which ψ_{vol} is a purely volumetric contribution to the total strain energy. Here, $\bar{I}_0$, $\bar{I}_\alpha$ and $\bar{IV}_{\alpha,\alpha}$ are the invariants of the isochoric parts of Cauchy Green tensors,

$$\bar{I}_0 = tr(\bar{\underline{C}}_0) = tr(\bar{\underline{B}}_0), \qquad \bar{I}_\alpha = tr(\bar{\underline{C}}_\alpha) = tr(\bar{\underline{B}}_\alpha), \qquad \bar{IV}_{\alpha,\alpha} = \bar{\underline{C}}_\alpha : \underline{a}_{\alpha,\alpha} \otimes \underline{a}_{\alpha,\alpha}. \tag{4.8}$$

d_0 and d_α are weighting functions from Eqs. (2.29) and (2.46), or damage functions from Eqs. (3.15) and (3.31). Here, the elastin deactivation and mechanical damage criteria are dependent on $\bar{I}_0$,

$$s_0 = \hat{s}_0(\bar{I}_0), \qquad \nu_{01}(t) = \max_{s\in[0,t]} \sqrt{2\psi_0(\bar{I}_0(s))}, \qquad \nu_{02}(t) = \int_0^t \left| d\sqrt{2\psi_0(I_0(s))}/ds \right| \, ds. \tag{4.9}$$

The collagen recruitment and damage criteria are dependent on the strain $\bar{E}_\alpha$ in the mean direction $\underline{a}_{\alpha,0}$ of distributed fiber families,

$$s_\alpha = \hat{s}_\alpha(\bar{E}_\alpha), \qquad \bar{E}_\alpha = \underline{H}_{\alpha,0} : \underline{\bar{C}}_0 - 1. \tag{4.10}$$

Based on the constitutive model formulated before, we can derive the general constitutive response of the compressible structural multi-mechanism model. The Cauchy stress tensor for the model is,

$$\underline{T} = \underline{T}_{vol} + (1-d_0)\underline{T}_0 + \sum_{\alpha=1}^{2}(1-d_\alpha)\underline{T}_\alpha, \tag{4.11}$$

where $\underline{T}_{vol}$ is the Cauchy stress from the volumetric strain energy ψ_{vol}, and $\underline{T}_0$ and $\underline{T}_\alpha$ are the Cauchy stress for the elastin and collagen mechanisms respectively, which are specified below.

It follows from (4.7),

$$\begin{aligned}
\underline{T}_{vol} &= J_0^{-1}\underline{F}_0 \cdot (2\frac{\partial \psi_{vol}(J_0)}{\partial \underline{C}_0}) \cdot \underline{F}_0^T \\
&= J_0^{-1}\underline{F}_0 \cdot (2\frac{\partial \psi_{vol}(J_0)}{\partial J_0}\frac{\partial J_0}{\partial \underline{C}_0}) \cdot \underline{F}_0^T \\
&= J_0^{-1}\underline{F}_0 \cdot (2\frac{\partial \psi_{vol}(J_0)}{\partial J_0}\frac{1}{2}J_0 C_0^{-1}) \cdot \underline{F}_0^T \\
&= \frac{\partial \psi_{vol}}{\partial J_0}\underline{I} \\
&= p\underline{I},
\end{aligned} \tag{4.12}$$

where p is the mechanical pressure,

$$p = \frac{\partial \psi_{vol}}{\partial J_0}. \tag{4.13}$$

Furthermore,

$$\begin{aligned}
\underline{T}_0 &= J_0^{-1}\underline{F}_0\cdot(2\frac{\partial\psi_0(\bar{I}_0)}{\partial\underline{C}_0})\cdot\underline{F}_0^T \\
&= J_0^{-1}\underline{F}_0\cdot(2\frac{\partial\psi_0(\bar{I}_0)}{\partial\bar{I}_0}\frac{\partial\bar{I}_0}{\partial\bar{\underline{C}}_0}:\frac{\partial\bar{\underline{C}}_0}{\partial\underline{C}_0})\cdot\underline{F}_0^T \\
&= J_0^{-1}\underline{F}_0\cdot(2\frac{\partial\psi_0}{\partial\bar{I}_0}\underline{I}:J_0^{-2/3}\underline{\mathbb{P}}_0^T)\cdot\underline{F}_0^T \\
&= 2J_0^{-5/3}\underline{F}_0\cdot(\frac{\partial\psi_0}{\partial\bar{I}_0}\underline{I}:\underline{\mathbb{P}}_0^T)\cdot\underline{F}_0^T \\
&= 2J_0^{-5/3}\underline{F}_0\cdot(\underline{\mathbb{P}}_0:\frac{\partial\psi_0}{\partial\bar{I}_0}\underline{I})\cdot\underline{F}_0^T, \qquad (4.14)
\end{aligned}$$

where $\underline{\mathbb{P}}_0$ is the projection tensor with respect to reference configuration κ_0,

$$\underline{\mathbb{P}}_0^T = J^{2/3}\frac{\partial\bar{\underline{C}}_0}{\partial\underline{C}_0} = \underline{\mathbb{I}} - \frac{1}{3}\underline{C}_0\otimes\underline{C}_0^{-1}, \qquad \underline{\mathbb{P}}_0 = \underline{\mathbb{I}} - \frac{1}{3}\underline{C}_0^{-1}\otimes\underline{C}_0. \qquad (4.15)$$

$\underline{\mathbb{I}}$ is the fourth-order unit tensor here, $\mathbb{I}_{ijkl} = \delta_{ik}\delta_{jl}$. Similarly to (4.14), we obtain,

$$\begin{aligned}
\underline{T}_\alpha &= J_\alpha^{-1}\underline{F}_\alpha\cdot(2\frac{\partial\psi_\alpha(\bar{I}_\alpha, I\bar{V}_{\alpha,\alpha})}{\partial\underline{C}_\alpha})\cdot\underline{F}_\alpha^T \\
&= J_\alpha^{-1}\underline{F}_\alpha\cdot[2(\frac{\partial\psi_\alpha(\bar{I}_\alpha, I\bar{V}_{\alpha,\alpha})}{\partial\bar{I}_\alpha}\frac{\partial\bar{I}_\alpha}{\partial\bar{\underline{C}}_\alpha} + \frac{\partial\psi_\alpha(\bar{I}_\alpha, I\bar{V}_{\alpha,\alpha})}{\partial I\bar{V}_{\alpha,\alpha}}\frac{\partial I\bar{V}_{\alpha,\alpha}}{\partial\bar{\underline{C}}_\alpha}):\frac{\partial\bar{\underline{C}}_\alpha}{\partial\underline{C}_\alpha}]\cdot\underline{F}_\alpha^T \\
&= J_\alpha^{-1}\underline{F}_\alpha\cdot[2(\frac{\partial\psi_\alpha}{\partial\bar{I}_\alpha}\underline{I} + \frac{\partial\psi_\alpha}{\partial I\bar{V}_{\alpha,\alpha}}(\underline{a}_{\alpha,\alpha}\otimes\underline{a}_{\alpha,\alpha})):J_\alpha^{-2/3}\underline{\mathbb{P}}_\alpha^T]\cdot\underline{F}_\alpha^T \\
&= 2J_\alpha^{-5/3}\underline{F}_\alpha\cdot[(\frac{\partial\psi_\alpha}{\partial\bar{I}_\alpha}\underline{I} + \frac{\partial\psi_\alpha}{\partial I\bar{V}_{\alpha,\alpha}}(\underline{a}_{\alpha,\alpha}\otimes\underline{a}_{\alpha,\alpha})):\underline{\mathbb{P}}_\alpha^T]\cdot\underline{F}_\alpha^T \\
&= 2J_\alpha^{-5/3}\underline{F}_\alpha\cdot[\underline{\mathbb{P}}_\alpha:(\frac{\partial\psi_\alpha}{\partial\bar{I}_\alpha}\underline{I} + \frac{\partial\psi_\alpha}{\partial I\bar{V}_{\alpha,\alpha}}(\underline{a}_{\alpha,\alpha}\otimes\underline{a}_{\alpha,\alpha})]\cdot\underline{F}_\alpha^T, \qquad (4.16)
\end{aligned}$$

where $\underline{\mathbb{P}}_\alpha$ is the projection tensor with respect to κ_α,

$$\underline{\mathbb{P}}_\alpha = \underline{\mathbb{I}} - \frac{1}{3}\underline{C}_\alpha^{-1}\otimes\underline{C}_\alpha. \qquad (4.17)$$

By substituting Eqs. (4.12), (4.14) and (4.16) into (4.11), the Cauchy stress tensor for the structural multi-mechanism model is,

$$\begin{aligned}
\underline{T} &= \frac{\partial\psi_{vol}}{\partial J_0}\underline{I} + 2(1-d_0)J_0^{-5/3}\underline{F}_0\cdot(\underline{\mathbb{P}}_0:\frac{\partial\psi_0}{\partial\bar{I}_0}\underline{I})\cdot\underline{F}_0^T \\
&+ \sum_{\alpha=1}^{2}2(1-d_\alpha)J_\alpha^{-5/3}\underline{F}_\alpha\cdot[\underline{\mathbb{P}}_\alpha:(\frac{\partial\psi_\alpha}{\partial\bar{I}_\alpha}\underline{I} + \frac{\partial\psi_\alpha}{\partial I\bar{V}_{\alpha,\alpha}}(\underline{a}_{\alpha,\alpha}\otimes\underline{a}_{\alpha,\alpha})]\cdot\underline{F}_\alpha^T. \qquad (4.18)
\end{aligned}$$

4.1.2 Elasticity tensor

An efficient implementation of the structural multi-mechanism model in the finite element methods requires the derivation of the elasticity tensor, called consistent linearized tangent moduli (Holzapfel, 2000). The general spatial elasticity tensor in an Eulerian setting is,

$$c_{abcd} = c_{vol_{abcd}} + (1 - d_0)c_{0_{abcd}} + \sum_{\alpha=1}^{2}(1 - d_\alpha)c_{\alpha_{abcd}}, \tag{4.19}$$

which is related to the material elasticity tensor in a Lagrangian setting,

$$\begin{aligned} c_{abcd} &= J_0^{-1}F_{0_{aA}}F_{0_{bB}}F_{0_{cC}}F_{0_{dD}}(\mathbb{C}_{vol_{ABCD}} + (1 - d_0)\mathbb{C}_{0_{ABCD}}) \\ &+ \sum_{\alpha=1}^{2}J_\alpha^{-1}F_{\alpha_{aA}}F_{\alpha_{bB}}F_{\alpha_{cC}}F_{\alpha_{dD}}(1 - d_\alpha)\mathbb{C}_{\alpha_{ABCD}}, \end{aligned} \tag{4.20}$$

where $c_{vol_{abcd}}$ and $\mathbb{C}_{vol_{ABCD}}$ are the spatial and material elasticity tensors from the volumetric strain energy ψ_{vol},

$$\begin{aligned} \underline{\mathbb{C}}_{vol} &= 4\frac{\partial^2\psi_{vol}(J_0)}{\partial\underline{C}_0\partial\underline{C}_0} \\ &= 2\frac{\partial(pJ_0\underline{C}_0^{-1})}{\partial\underline{C}_0} \\ &= 2pJ_0\frac{\partial\underline{C}_0^{-1}}{\partial\underline{C}_0} + 2\underline{C}_0^{-1}\otimes(p\frac{\partial J_0}{\partial\underline{C}_0} + J_0\frac{\partial p}{\partial\underline{C}_0}) \\ &= -2pJ_0(\underline{C}_0^{-1}\odot\underline{C}_0^{-1}) + 2(p + J_0\frac{\partial p}{\partial J_0})\underline{C}_0^{-1}\otimes\frac{\partial J_0}{\partial\underline{C}_0} \\ &= -2pJ_0(\underline{C}_0^{-1}\odot\underline{C}_0^{-1}) + J_0(p + J_0\frac{\partial p}{\partial J_0})\underline{C}_0^{-1}\otimes\underline{C}_0^{-1}, \end{aligned} \tag{4.21}$$

in which

$$\frac{\partial C_{0_{AB}}^{-1}}{\partial C_{0_{CD}}} = -\frac{1}{2}(C_{0_{AC}}^{-1}C_{0_{BD}}^{-1} + C_{0_{AD}}^{-1}C_{0_{BC}}^{-1}) = -(\underline{C}_0^{-1}\odot\underline{C}_0^{-1})_{ABCD}. \tag{4.22}$$

$c_{0_{abcd}}$ and $\mathbb{C}_{0_{ABCD}}$ are the spatial and material elasticity tensors for the elastin mechanism respectively, and $c_{\alpha_{abcd}}$ and $\mathbb{C}_{\alpha_{ABCD}}$ for the collagen mechanism.

$$\begin{aligned}
\underline{\mathbb{C}}_0 &= 4\frac{\partial^2\psi_0(\bar{I}_0)}{\partial\underline{C}_0\partial\underline{C}_0} \\
&= 4\frac{\partial[J_0^{-2/3}(\underline{\mathbb{P}}_0 : \frac{\partial\psi_0}{\partial\bar{I}_0}\underline{I})]}{\partial\underline{C}_0} \\
&= 4(\underline{\mathbb{P}}_0 : \frac{\partial\psi_0}{\partial\bar{I}_0}\underline{I}) \otimes \frac{\partial J_0^{-2/3}}{\partial\underline{C}_0} + 4J_0^{-2/3}\frac{\partial(\underline{\mathbb{P}}_0 : \frac{\partial\psi_0}{\partial\bar{I}_0}\underline{I})}{\partial\underline{C}_0} \\
&= -\frac{4}{3}(J_0^{-2/3}\underline{\mathbb{P}}_0 : \frac{\partial\psi_0}{\partial\bar{I}_0}\underline{I}) \otimes \underline{C}_0^{-1} + 4J_0^{-2/3}\frac{\partial(\underline{\mathbb{P}}_0 : \frac{\partial\psi_0}{\partial\bar{I}_0}\underline{I})}{\partial\underline{C}_0}, \qquad (4.23)
\end{aligned}$$

in which the second term is,

$$\begin{aligned}
\underline{\mathbb{A}} &= 4J_0^{-2/3}\frac{\partial}{\partial\underline{C}_0}(\underline{\mathbb{P}}_0 : \frac{\partial\psi_0}{\partial\bar{I}_0}\underline{I}) \\
&= 4J_0^{-2/3}\frac{\partial}{\partial\underline{C}_0}[\frac{\partial\psi_0}{\partial\bar{I}_0}\underline{I} - \frac{1}{3}(\underline{C}_0^{-1} \otimes \underline{C}_0) : \frac{\partial\psi_0}{\partial\bar{I}_0}\underline{I}] \\
&= 4J_0^{-2/3}[\frac{\partial}{\partial\bar{\underline{C}}_0}(\frac{\partial\psi_0}{\partial\bar{I}_0}\underline{I}) - \frac{1}{3}\frac{\partial(\frac{\partial\psi_0}{\partial\bar{I}_0}\underline{I} : \underline{C}_0)\underline{C}_0^{-1}}{\partial\bar{\underline{C}}_0}] : \frac{\partial\bar{\underline{C}}_0}{\partial\underline{C}_0} \\
&= 4J_0^{-4/3}[\frac{\partial^2\psi_0}{\partial\bar{\underline{I}}_0\partial\bar{\underline{I}}_0}(\underline{I} \otimes \underline{I}) - \frac{1}{3}\frac{\partial(\frac{\partial\psi_0}{\partial\bar{I}_0}\underline{I} : \underline{C}_0)\underline{C}_0^{-1}}{\partial\bar{\underline{C}}_0}] : \underline{\mathbb{P}}_0^T, \qquad (4.24)
\end{aligned}$$

and the second term in brackets is,

$$\begin{aligned}
\underline{\mathbb{B}} &= \frac{\partial(\frac{\partial\psi_0}{\partial\bar{I}_0}\underline{I} : \underline{C}_0)\underline{C}_0^{-1}}{\partial\bar{\underline{C}}_0} \\
&= \underline{C}_0^{-1} \otimes \frac{\partial}{\partial\bar{\underline{C}}_0}(\frac{\partial\psi_0}{\partial\bar{I}_0}\underline{I} : \underline{C}_0) + (\frac{\partial\psi_0}{\partial\bar{I}_0}\underline{I} : \underline{C}_0)\frac{\partial\underline{C}_0^{-1}}{\partial\bar{\underline{C}}_0} \\
&= \underline{C}_0^{-1} \otimes [\underline{C}_0 : \frac{\partial}{\partial\bar{\underline{C}}_0}(\frac{\partial\psi_0}{\partial\bar{I}_0}\underline{I}) + (\frac{\partial\psi_0}{\partial\bar{I}_0}\underline{I}) : \frac{\partial\underline{C}_0}{\partial\bar{\underline{C}}_0}] + (\frac{\partial\psi_0}{\partial\bar{I}_0}\underline{I} : \underline{C}_0)\frac{\partial\underline{C}_0^{-1}}{\partial\underline{C}_0}\frac{\partial\underline{C}_0}{\partial\bar{\underline{C}}_0} \\
&= \underline{C}_0^{-1} \otimes [\underline{C}_0 : \frac{\partial}{\partial\bar{\underline{C}}_0}(\frac{\partial\psi_0}{\partial\bar{I}_0}\underline{I}) + J_0^{2/3}\frac{\partial\psi_0}{\partial\bar{I}_0}\underline{I}] - (\frac{\partial\psi_0}{\partial\bar{I}_0}\underline{I} : \underline{C}_0)J_0^{2/3}(\underline{C}_0^{-1} \odot \underline{C}_0^{-1}) \\
&= \underline{C}_0^{-1} \otimes [\underline{C}_0 : \frac{\partial^2\psi_0}{\partial\bar{\underline{I}}_0\partial\bar{\underline{I}}_0}(\underline{I} \otimes \underline{I}) + J_0^{2/3}\frac{\partial\psi_0}{\partial\bar{I}_0}\underline{I}] - J_0^{2/3}(\frac{\partial\psi_0}{\partial\bar{I}_0}\underline{I} : \underline{C}_0)(\underline{C}_0^{-1} \odot \underline{C}_0^{-1}). \qquad (4.25)
\end{aligned}$$

By substituting (4.25) into (4.24), we have,

$$\begin{aligned}
\underline{\mathbb{A}} &= 4J_0^{-4/3}[\frac{\partial^2\psi_0}{\partial\bar{\underline{I}}_0\partial\bar{\underline{I}}_0}(\underline{I}\otimes\underline{I}) - \frac{1}{3}(\underline{C}_0^{-1}\otimes\underline{C}_0 : \frac{\partial^2\psi_0}{\partial\bar{\underline{I}}_0\partial\bar{\underline{I}}_0}(\underline{I}\otimes\underline{I}) + J_0^{2/3}\frac{\partial\psi_0}{\partial\bar{\underline{I}}_0}(\underline{C}_0^{-1}\otimes\underline{I}) \\
&- J_0^{2/3}(\frac{\partial\psi_0}{\partial\bar{\underline{I}}_0}\underline{I} : \underline{C}_0)(\underline{C}_0^{-1}\odot\underline{C}_0^{-1}))] : \underline{\mathbb{P}}_0^T \\
&= 4J_0^{-4/3}[(\underline{\mathbb{I}} - \frac{1}{3}\underline{C}_0^{-1}\otimes\underline{C}_0) : \frac{\partial^2\psi_0}{\partial\bar{\underline{I}}_0\partial\bar{\underline{I}}_0}(\underline{I}\otimes\underline{I}) : \underline{\mathbb{P}}_0^T - \frac{1}{3}J_0^{2/3}\frac{\partial\psi_0}{\partial\bar{\underline{I}}_0}(\underline{C}_0^{-1}\otimes\underline{I}) : \underline{\mathbb{P}}_0^T \\
&+ \frac{1}{3}J_0^{2/3}(\frac{\partial\psi_0}{\partial\bar{\underline{I}}_0}\underline{I} : \underline{C}_0)(\underline{C}_0^{-1}\odot\underline{C}_0^{-1}) : \underline{\mathbb{P}}_0^T] \\
&= 4J_0^{-4/3}\frac{\partial^2\psi_0}{\partial\bar{\underline{I}}_0\partial\bar{\underline{I}}_0}\underline{\mathbb{P}}_0 : (\underline{I}\otimes\underline{I}) : \underline{\mathbb{P}}_0^T - \frac{4}{3}J_0^{-2/3}\frac{\partial\psi_0}{\partial\bar{\underline{I}}_0}(\underline{C}_0^{-1}\otimes\underline{I}) : \underline{\mathbb{P}}_0^T \\
&+ \frac{4}{3}J_0^{-2/3}(\frac{\partial\psi_0}{\partial\bar{\underline{I}}_0}\underline{I} : \underline{C}_0)(\underline{C}_0^{-1}\odot\underline{C}_0^{-1}) : \underline{\mathbb{P}}_0^T. \qquad (4.26)
\end{aligned}$$

By substituting (4.24) into (4.23), the material elasticity tensor for the elastin is,

$$\begin{aligned}
\underline{\mathbb{C}}_0 &= -\frac{4}{3}(J_0^{-2/3}\underline{\mathbb{P}}_0 : \frac{\partial\psi_0}{\partial\bar{\underline{I}}_0}\underline{I})\otimes\underline{C}_0^{-1} + 4J_0^{-4/3}\frac{\partial^2\psi_0}{\partial\bar{\underline{I}}_0\partial\bar{\underline{I}}_0}\underline{\mathbb{P}}_0 : (\underline{I}\otimes\underline{I}) : \underline{\mathbb{P}}_0^T \\
&- \frac{4}{3}J_0^{-2/3}\frac{\partial\psi_0}{\partial\bar{\underline{I}}_0}(\underline{C}_0^{-1}\otimes\underline{I}) : \underline{\mathbb{P}}_0^T + \frac{4}{3}J_0^{-2/3}(\frac{\partial\psi_0}{\partial\bar{\underline{I}}_0}\underline{I} : \underline{C}_0)(\underline{C}_0^{-1}\odot\underline{C}_0^{-1}) : \underline{\mathbb{P}}_0^T. \qquad (4.27)
\end{aligned}$$

Following the similar derivation for $\underline{\mathbb{C}}_0$, we can get the material elasticity tensor for the collagen mechanisms,

$$\begin{aligned}
\underline{\mathbb{C}}_\alpha &= 4\frac{\partial^2\psi_\alpha(\bar{I}_\alpha, \bar{I}V_{\alpha,\alpha,})}{\partial\underline{C}_\alpha\partial\underline{C}_\alpha} \\
&= -\frac{4}{3}[J_\alpha^{-2/3}\underline{\mathbb{P}}_\alpha : (\frac{\partial\psi_\alpha}{\partial\bar{\underline{I}}_\alpha}\underline{I} + \frac{\partial\psi_\alpha}{\partial\bar{I}V_{\alpha,\alpha}}\underline{A}_{\alpha,\alpha})]\otimes\underline{C}_\alpha^{-1} \\
&+ 4J_\alpha^{-4/3}\underline{\mathbb{P}}_\alpha : [\frac{\partial^2\psi_\alpha}{\partial\bar{\underline{I}}_\alpha\partial\bar{\underline{I}}_\alpha}(\underline{I}\otimes\underline{I}) + \frac{\partial^2\psi_\alpha}{\partial\bar{\underline{I}}_\alpha\partial\bar{\underline{I}V}_{\alpha,\alpha}}(\underline{A}_{\alpha,\alpha}\otimes\underline{I}) \\
&+ \frac{\partial^2\psi_\alpha}{\partial\bar{\underline{I}V}_{\alpha,\alpha}\partial\bar{\underline{I}}_\alpha}(\underline{I}\otimes\underline{A}_{\alpha,\alpha}) + \frac{\partial^2\psi_\alpha}{\partial\bar{\underline{I}V}_{\alpha,\alpha}\partial\bar{\underline{I}V}_{\alpha,\alpha}}(\underline{A}_{\alpha,\alpha}\otimes\underline{A}_{\alpha,\alpha})] : \underline{\mathbb{P}}_\alpha^T \\
&- \frac{4}{3}J_\alpha^{-2/3}[\frac{\partial\psi_\alpha}{\partial\bar{\underline{I}}_\alpha}(\underline{C}_\alpha^{-1}\otimes\underline{I}) + \frac{\partial\psi_\alpha}{\partial\bar{I}V_{\alpha,\alpha}}(\underline{C}_\alpha^{-1}\otimes\underline{A}_{\alpha,\alpha})] : \underline{\mathbb{P}}_\alpha^T \\
&+ \frac{4}{3}J_\alpha^{-2/3}(\frac{\partial\psi_\alpha}{\partial\bar{\underline{I}}_\alpha}\underline{I} : \underline{C}_\alpha + \frac{\partial\psi_\alpha}{\partial\bar{I}V_{\alpha,\alpha}}\underline{A}_{\alpha,\alpha} : \underline{C}_\alpha)(\underline{C}_\alpha^{-1}\odot\underline{C}_\alpha^{-1}) : \underline{\mathbb{P}}_\alpha^T, \qquad (4.28)
\end{aligned}$$

in which $\underline{A}_{\alpha,\alpha}$ are introduced as the structure tensors for fiber orientations as in Holzapfel *et al.* (2000),

$$\underline{A}_{\alpha,\alpha} = \underline{a}_{\alpha,\alpha}\otimes\underline{a}_{\alpha,\alpha}. \qquad (4.29)$$

4.1.3 Elastodamage modulus

The finite element implementation of the mechanical damage model requires an elastodamage modulus. Based on the decoupled strain energy, following (4.14), the second Piola-Kirchhoff stress tensor for the damaged elastin mechanism is,

$$\underline{S}_{iso} = (1-d_0)\underline{S}_0 = (1-d_0)(2\frac{\partial\psi_0(\bar{I}_0)}{\partial\underline{C}_0}) = (1-d_0)[2J_0^{-2/3}(\underline{\mathbb{P}}_0 : \frac{\partial\psi_0}{\partial\bar{I}_0}\underline{I})]. \tag{4.30}$$

The evolution of the second Piola-Kirchhoff stress is,

$$\begin{aligned}\dot{\underline{S}_{iso}} &= (1-d_0)\frac{\partial\underline{S}_0}{\partial\underline{C}_0} : \dot{\underline{C}}_0 - \frac{\partial d_0(\nu_{01})}{\partial\nu_{01}}\dot{\nu}_{01}\underline{S}_0 \\ &= \frac{1}{2}(1-d_0)(4\frac{\partial^2\psi_0(\bar{I}_0)}{\partial\underline{C}_0\partial\underline{C}_0} : \dot{\underline{C}}_0) - \frac{\partial d_0(\nu_{01})}{\partial\nu_{01}}\dot{\nu}_{01}(2\frac{\partial\psi_0(\bar{I}_0)}{\partial\underline{C}_0}).\end{aligned} \tag{4.31}$$

For the strain-based cyclic damage model, this evolution only happens at the state of loading,

$$\dot{\underline{S}_{iso}} = \begin{cases} \left\{(1-d_0)\underline{\mathbb{C}}_0 - \dfrac{1}{\sqrt{2\psi_0(\underline{C}_0)}}\dfrac{\partial d_0(\nu_{01})}{\partial\nu_{01}}[2J_0^{-2/3}(\underline{\mathbb{P}}_0 : \dfrac{\partial\psi_0}{\partial\bar{I}_0}\underline{I})] \otimes [2J_0^{-2/3}(\underline{\mathbb{P}}_0 : \dfrac{\partial\psi_0}{\partial\bar{I}_0}\underline{I})]\right\} : \dfrac{\dot{\underline{C}}_0}{2}, \\ \qquad\qquad \phi_0 = 0 \ \text{ and } \ \underline{N}_0 : \dot{\underline{C}}_0 > 0, \\ (1-d_0)\underline{\mathbb{C}}_0 : \dfrac{\dot{\underline{C}}_0}{2}, \ \text{ otherwise,} \end{cases} \tag{4.32}$$

so the corresponding material elastodamage modulus for the damaged elastin mechanism can be expressed as,

$$\underline{\mathbb{C}}_{iso} = \begin{cases} (1-d_0)\underline{\mathbb{C}}_0 - \dfrac{1}{\sqrt{2\psi_0(\underline{C}_0)}}\dfrac{\partial d_0(\nu_{01})}{\partial\nu_{01}}[2J_0^{-2/3}(\underline{\mathbb{P}}_0 : \dfrac{\partial\psi_0}{\partial\bar{I}_0}\underline{I})] \otimes [2J_0^{-2/3}(\underline{\mathbb{P}}_0 : \dfrac{\partial\psi_0}{\partial\bar{I}_0}\underline{I})], \\ \qquad\qquad \phi_0 = 0 \ \text{ and } \ \underline{N}_0 : \dot{\underline{C}}_0 > 0, \\ (1-d_0)\underline{\mathbb{C}}_0, \ \text{ otherwise.} \end{cases} \tag{4.33}$$

Following the similar derivation for $\underline{\mathbb{C}}_{iso}$, we get the material elastodamage modulus for the damage collagen mechanism,

$$\underline{\mathbb{C}}_{aniso} = \begin{cases} (1-d_\alpha)\underline{\mathbb{C}}_\alpha - \dfrac{\partial d_\alpha(\nu_\alpha)}{\partial\nu_\alpha}[2\underline{H}_{\alpha,\alpha}] \otimes [2J_\alpha^{-2/3}\underline{\mathbb{P}}_\alpha : (\dfrac{\partial\psi_\alpha}{\partial\bar{I}_\alpha}\underline{I} + \dfrac{\partial\psi_\alpha}{\partial I\bar{V}_{\alpha,\alpha}}(\underline{a}_{\alpha,\alpha} \otimes \underline{a}_{\alpha,\alpha})], \\ \qquad\qquad \phi_\alpha = 0 \ \text{ and } \ \underline{N}_\alpha : \dot{\underline{C}}_\alpha > 0, \\ (1-d_\alpha)\underline{\mathbb{C}}_\alpha, \ \text{ otherwise.} \end{cases} \tag{4.34}$$

4.2 NUMERICAL VALIDATION

The finite element implementation of the structural multi-mechanism damage model is validated using analytical solutions. The uniaxial cyclic damage behavior of arterial tissues is presented here for one-element validation. The biaxial inflation and tension of a straight thick-walled cylindrical tube with constant thickness is also considered here.

In the following sections, we first summarize the specific constitutive equations which are used for the numerical implementation and analytical analysis. Then we perform one-element uniaxial tension tests. The general analytical solution is formulated for biaxial cylindrical inflation-tension for a structural multi-mechanism damage material with fiber distribution given in Section 2.2.4.1. The numerical simulations are compared with the analytical ones using specific geometric and material properties for validation purpose.

4.2.1 Constitutive model for numerical implementation

In the numerical implementation and analytical analysis, specific material functions are used. To be consistent with the study in Section 2.3.2, we implement the isotropic strain energy functions for the elastin mechanism and structural anisotropic functions for the dispersed collagen mechanism in homogeneous, isochoric forms, shown in Table 4. A Neo-Hookean strain energy function is also implemented to represent ground substance if necessary.

Here, a volumetric strain energy function (VOL) is chosen, in which μ is the compressibility parameter. In the penalty method for modeling nearly incompressible materials, μ is a penalty parameter to control the degree of incompressibility and the numerical behavior of the material model. Following (4.12), the volumetric Cauchy stress is,

$$\underline{T}_{vol} = \frac{2}{\mu}(J_0 - 1)\underline{I}, \tag{4.35}$$

in which $J_0 - 1$ is the volumetric change of material during deformation, and $1/\mu$ is physically the bulk modulus for general compressible materials. For purely incompressible materials, $J_0 - 1$ is zero and theoretically $1/\mu$ is infinity. Numerically, the smallest μ for converged and stabilized solution is typically chosen.

Table 4: Representative forms of the constitutive functions implemented in numerical validation studies.

Volumetric Function	
VOL:	$\psi_{vol} = \frac{1}{\mu}(J_0 - 1)^2,$
Ground Substance Function	
Neo-Hookean (G-NH):	$\psi_g = \frac{\eta_g}{2}\left(\bar{I}_0 - 3\right),$
Elastin Mechanism	
Strain Energy Function	
First Order Exponential (E-EXP1):	$\psi_0 = \frac{\eta_0}{2\gamma_0}\left(e^{\gamma_0(\bar{I}_0-3)} - 1\right),$
Elastin Deactivation Criterion	
E-DC:	$s_0 = \max(\bar{I}_0 - 3),$
Elastin Damage Functions	
E-DFj:	$D_{0j}[\nu_{0j}(t)] = 1 - \frac{1 - e^{c_j(1-\nu_{0j}/\nu_{0jf})}}{1 - e^{c_j(1-\nu_{0js}/\nu_{0jf})}},$ where j=1,2,3,
Collagen Mechanism	
Strain Energy Function	
Exponential (C-EXP2-disp):	$\psi_\alpha = \frac{\eta}{2\gamma}\left(e^{\gamma(k\bar{I}_\alpha+(1-3k)I\bar{V}_{\alpha,\alpha}-1)^2} - 1\right), \quad \alpha = 1, 2,$
Collagen Activation Criterion	
C-AC:	$s_\alpha = k\bar{I}_0 + (1-3k)I\bar{V}_{\alpha,0} - 1,$
Collagen Damage Function	
C-DF:	$d_\alpha[\nu_\alpha(t)] = 1 - \frac{1 - e^{c_4(1-\nu_\alpha/\nu_{\alpha f})}}{1 - e^{c_4(1-\nu_{\alpha s}/\nu_{\alpha f})}}.$

The deformation criteria for elastin deactivation (E-DC) and collagen activation (C-AC) are from (2.7), (2.45), (4.9) and (4.10). Exponential damage functions (Calvo *et al.*, 2007) are used here for elastin and collagen damage (E-DF1, E-DF2, E-DF3 and C-DF), where c_1, c_2, c_3 and c_4 are material constants.

4.2.2 Uniaxial tension tests of one-element

Uniaxial tension tests were performed using one eight-node solid element. Analytical solutions for uniaxial stretch of an arterial strip are used to validate the numerical implementation of the multi-mechanism model. The mechanical response of the arterial strip is assumed to arise from an isotropic elastin mechanism and two families of dispersed collagen fibers as illustrated schematically in Fig. 10. It is assumed that the two families of collagen fibers are embedded symmetrically, with angle β relative to the axial direction, representing the mean orientations of the fiber families. The boundary conditions for the tensile tests are illustrated in Fig. 10. Uniaxial displacement loads are applied to the strip. A cyclic displacement load of increasing loading-unloading magnitude is used for the validation of mechanical elastin damage and collagen damage (controlled through damage variables d_{01}, d_{02} and d_{α}). A one-step displacement loading is used for the validation of elastin enzymatic damage, (controlled through damage variable d_{03}). As detailed below, validation deformations are chosen to separately evaluate the role of each of the four damage variables.

Analytic solutions for the axial component of Cauchy stress, σ, as a function of stretch can be directly obtained from (2.48) for uniaxial stretch. In these studies the material is modeled using the strain energy and damage functions given in Table 4 and material parameters shown in Table 4.2.2. For the current study, it should be emphasized that the material parameters in Table 4.2.2 and damage functions in Table 4 are chosen for the purposes of numerical validation and investigation. In particular, they are chosen to ensure a wide range of physical responses to provide a more stringent numerical validation. There is a great need for experiments to determine suitable function forms for these damage variables in order to provide a foundation applications to cerebral vascular disease and treatment. This theoretical foundation and numerical developments given here, will help guide these experiments.

Fig. 11, Fig. 12 and Fig. 13 show the comparisons of four analytical solutions for axial stress σ as a function of uniaxial stretch λ in cyclic uniaxial loading of increasing magnitude, Fig. 10. The red curve in all four figures corresponds to the progressive mechanical damage of elastin based on maximum equivalent material strain with $d_0 = d_{01}$ ($d_{02} = 0.0$, $d_{03} = 0.0$

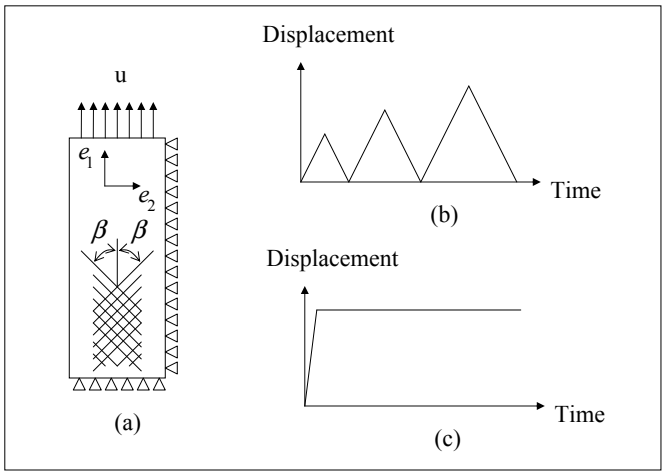

Figure 10: Boundary conditions used in the two validation tests. (a): Arterial tissue strip with uniaxial loading, (b): Cyclically increasing displacement boundary condition, (c): Step displacement boundary condition.

Table 5: Material parameters for an isotropic elastin mechanism (E-EXP1), dispersive anisotropic collagen mechanism (C-EXP2-disp), volumetric function (VOL) and damage functions (E-DC, E-DF1, E-DF2, E-DF3, C-AC and C-DF), as shown in Table 4.

Material parameters for strain energy functions

$\mu(\text{Pa}^{-1})$	η_0(KPa)	γ_0	η(KPa)	γ	$\beta_1 = -\beta_2$	k
1e-9	4.55	0.5651	125.0	1.88	56^o	0.201

Material parameters for damage functions

c_1	c_2	c_3	c_4	ν_{01s}(KPa)	ν_{01f}(KPa)	ν_{02s}(KPa)
0.25	2.1	10.0	0.002	100.0	250.0	100.0
ν_{02f}(KPa)	ν_{03s}	ν_{03f}	ν_{1s}	ν_{1f}	s_{1a}	s_{0b}
2100.0	0.0	1000.0	1.0	2.0	0.5435	3.48

and $d_\alpha = 0.0$) and eventual failure of elastin (point A). In contrast, the cyan curve in Fig. 11 corresponds to abrupt elastin failure (point B) without progressive damage (e.g. in Wulandana and Robertson (2005); Li and Robertson (2009)). The blue curve in Fig. 12 corresponds to progressive mechanical damage of elastin based on accumulated equivalent strain with $d_0 = d_{02}$ ($d_{01} = 0.0$, $d_{03} = 0.0$ and $d_\alpha = 0.0$) and eventual failure of elastin (point C). The green curve in Fig. 13 corresponds to the progressive mechanical damage of elastin and collagen based on maximum equivalent material strain and maximum fiber strain

respectively with $d_0 = d_{01}$ and $d_\alpha = d_1 = d_2$ ($d_{02} = 0.0$ and $d_{03} = 0.0$). The collagen damage starts at point D. Only collagen contributes to further loading after the elastin fails at point E. Eventually, collagen fails at point F. In all cases without collagen damage, after elastin failure, only collagen contributes to further loading and future loads follow the curve 1. In all cases, residual stretch is observed upon unloading after elastin failure. The analytical solutions for these three cases are used to validate the finite element solutions, Figs. 14, 15 and 17.

The finite element solutions for the uniaxial one-step load of the arterial strip with elastin enzymatic damage arising from hemodynamic loading with $d_0 = d_{03}$ ($d_{01} = 0.0$, $d_{02} = 0.0$ and $d_\alpha = 0.0$) are validated with the corresponding analytical solutions, Fig. 16. The solutions are represented as the axial stress as a function of time. For each curve, the values of WSS and WSSG are constant and above the threshold value. As expected from the functional form given in (3.23), the elastin degrades faster for higher levels of WSS and/or WSSG. As for the case of cyclic damage, Figs. 14, 15 and 17, after elastin failure only collagen contributes to further loading and future loads follow curve 2. In all cases, the numerical and analytical solutions match well with a maximum error less than 5%.

4.2.3 Cylindrical inflation and tension of a thick-walled artery

In this section, the analytical solution for the biaxial cylindrical inflation-tension of thick walled arteries using the structural multi-mechanism model with fiber distribution is formulated. The arterial wall is modeled as a straight wall with constant thickness, composed of a homogeneous structural multi-mechanism material. The deformation is assumed to be axisymmetric, quasi-static and uniform in the axial direction. To represent the loads on the arterial wall, pressures p_i, p_o and tension N are applied on the inner surface, outer surface and axial section of a straight cylinder respectively, Fig. 18. Residual stress is neglected in this analysis. We first looked for the stress response for a typical material point, and then the relationship between arterial wall stresses and transmural pressure. In the discussion of this section, we use the general form of the strain energy functions $\psi_0(I_0)$ and $\psi_\alpha(I_\alpha, IV_{\alpha,\alpha})$. The specific form of the functions can be found in Section 4.2.1.

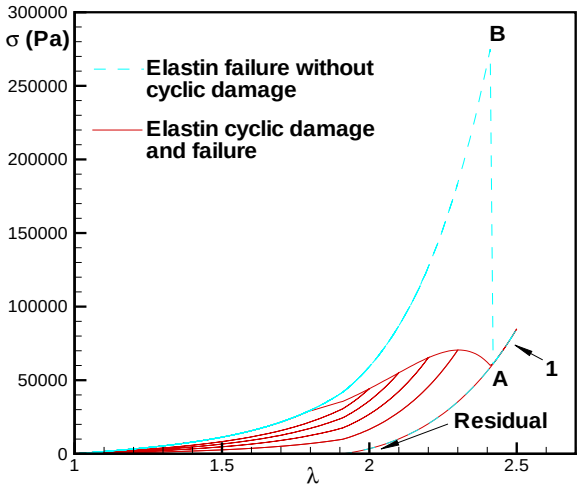

Figure 11: Comparison of two analytical solutions for elastin failure without damage and elastin cyclic damage d_{01}. Elastin failure at point B and A, respectively, with the remaining collagen mechanism following load curve 1.

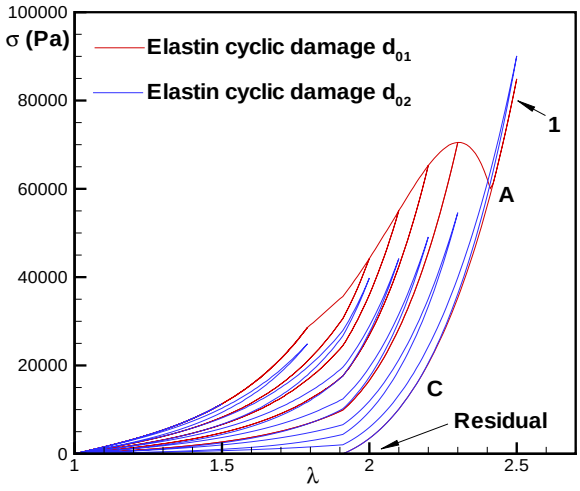

Figure 12: Comparison of two analytical solutions for elastin cyclic damage d_{01} and d_{02}. Elastin failure at point A and C, respectively, with the remaining collagen mechanism following load curve 1.

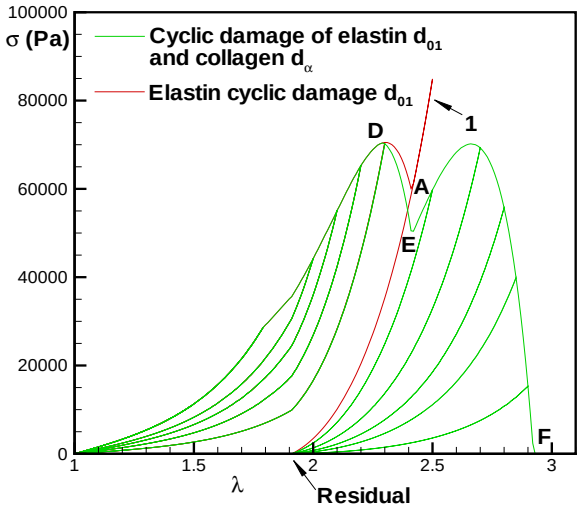

Figure 13: Comparison of two analytical solutions for elastin cyclic damage d_{01} and elastin cyclic damage d_{01} with collagen damage d_α. For elastin cyclic damage, elastin fails at point A with the remaining collagen following load curve 1. For elastin and collagen cyclic damage, elastin fails at point E; collagen starts to experience damage at point D and fails at point F.

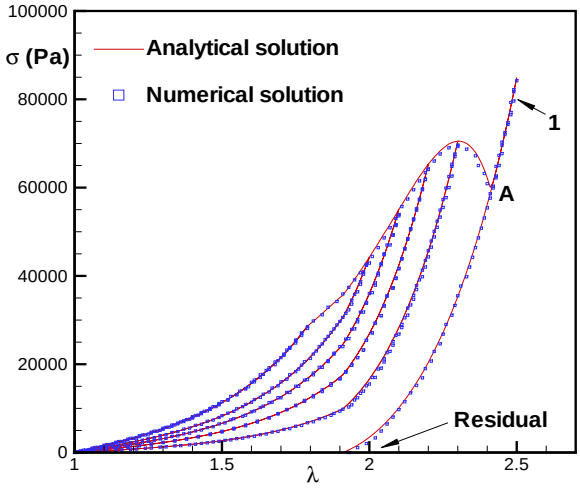

Figure 14: Comparison of the analytical and numerical solutions for elastin cyclic damage d_{01}. Elastin failure at point A with the remaining collagen following load curve 1.

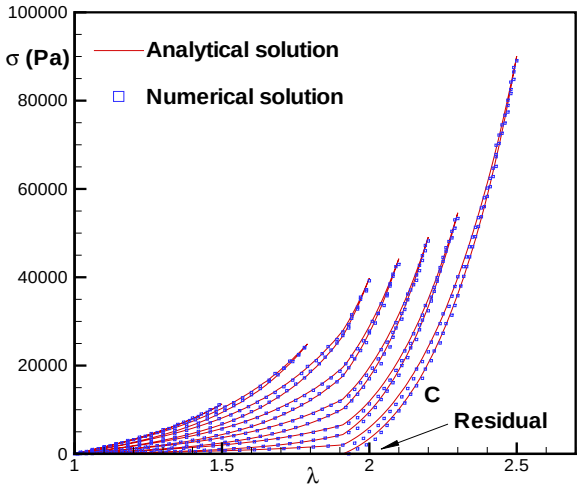

Figure 15: Comparison of the analytical and numerical solutions for elastin cyclic damage d_{02}. Elastin failure at point C.

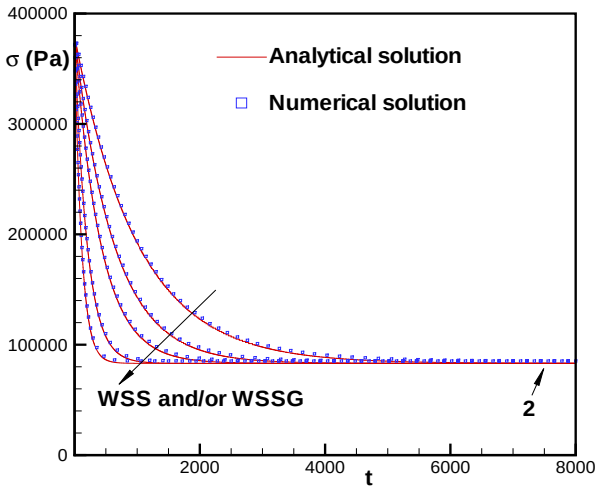

Figure 16: Comparison of the analytical and numerical solutions for elastin enzymatic damage d_{03} for different choices of WSS and/or WSSG. As these quantities are increased, the elastin degradation occurs more rapidly. The remaining collagen following load curve 2 after elastin failure.

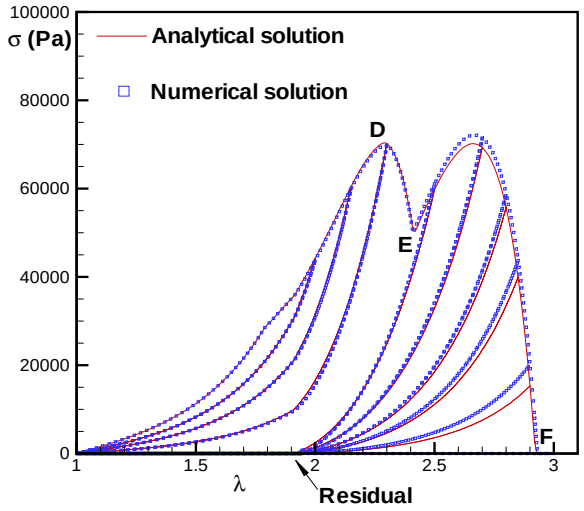

Figure 17: Comparison of the analytical and numerical solutions for elastin cyclic damage d_{01} with collagen damage d_α. Elastin fails at point E; collagen starts to experience damage at point D and fails at point F.

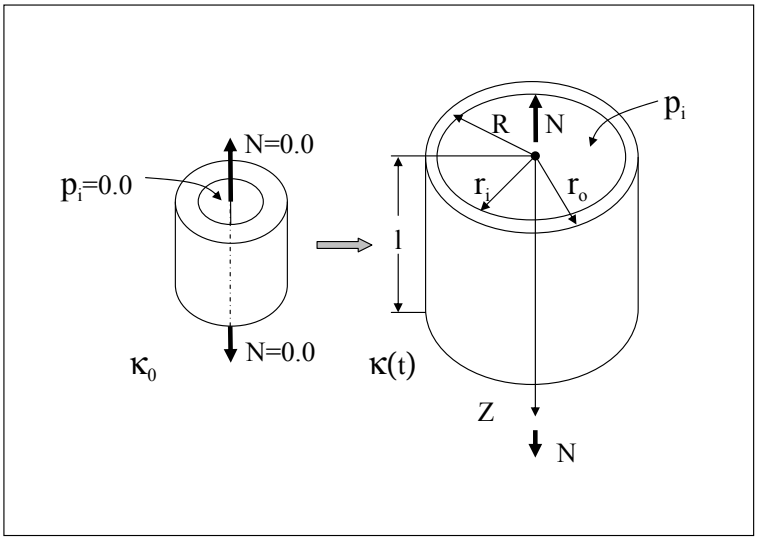

Figure 18: Cylinder in unloaded configuration κ_0 and loaded configuration $\kappa(t)$.

4.2.3.1 Kinematics and constitutive response During this biaxial deformation as shown in Fig. 18, the cylindrical arterial wall is inflated and extended. In term of cylindrical coordinate basis $\underline{e}_r$, $\underline{e}_\theta$, $\underline{e}_z$, a typical material point at position $\underline{X}_0 = R_0\underline{e}_r + Z_0\underline{e}_z$ in κ_0 is mapped to position $\underline{x} = R(R_0, Z)\underline{e}_r + Z(Z_0)\underline{e}_z$ in $\kappa(t)$. The geometry of the cylinder before and after deformation is defined as,

$$R_i \leq R_0 \leq R_o, \qquad 0 \leq Z_0 \leq L, \qquad r_i \leq R \leq r_o, \qquad 0 \leq Z \leq l, \tag{4.36}$$

in which R_i, R_o, and L denote the undeformed inner radius, outer radius and length respectively, and r_i, r_o, and l are the corresponding deformed geometrical parameters. It follows from the incompressibility constraint that,

$$Z(R^2 - r_i^2) = Z_0(R_0^2 - R_i^2). \tag{4.37}$$

The deformation gradient relative to the reference configuration κ_0 is,

$$[\underline{F}_0] = \begin{bmatrix} \dfrac{1}{\lambda_\Theta \lambda_Z} & 0 & 0 \\ 0 & \lambda_\Theta & 0 \\ 0 & 0 & \lambda_Z \end{bmatrix} = \begin{bmatrix} \dfrac{\partial R}{\partial R_0} & 0 & 0 \\ 0 & \dfrac{R}{R_0} & 0 \\ 0 & 0 & \dfrac{Z}{Z_0} \end{bmatrix}, \tag{4.38}$$

where $\lambda_\Theta = R/R_0$ is the circumferential stretch, and $\lambda_Z = Z/Z_0$ is the axial stretch. Applying (4.37),

$$[\underline{F}_0] = \begin{bmatrix} \dfrac{R_0}{R\lambda_Z} & 0 & 0 \\ 0 & \dfrac{R}{R_0} & 0 \\ 0 & 0 & \dfrac{Z}{Z_0} \end{bmatrix}. \tag{4.39}$$

The corresponding Cauchy-Green deformation tensors are,

$$[\underline{B}_0] = [\underline{C}_0] = \begin{bmatrix} \dfrac{1}{\lambda_\Theta^2 \lambda_Z^2} & 0 & 0 \\ 0 & \lambda_\Theta^2 & 0 \\ 0 & 0 & \lambda_Z^2 \end{bmatrix}, \tag{4.40}$$

with invariants,

$$I_0 = \frac{1}{\lambda_\Theta^2 \lambda_Z^2} + \lambda_\Theta^2 + \lambda_Z^2, \quad IV_{1,0} = IV_{2,0} = \lambda_\Theta^2 \cos^2\beta + \lambda_Z^2 \sin^2\beta. \tag{4.41}$$

Following (2.7) and (2.45), the deformation for elastin deactivation is,

$$s_0 = \max(\frac{1}{\lambda_\Theta^2 \lambda_Z^2} + \lambda_\Theta^2 + \lambda_Z^2 - 3), \tag{4.42}$$

and the measure for collagen activation is,

$$s_1 \;=\; s_2 \;=\; k(\frac{1}{\lambda_\Theta^2 \lambda_Z^2} + \frac{1}{\lambda_\Theta^2} + \lambda_Z^2) + (1-3k)(\lambda_\Theta^2 \cos^2\beta \;+\; \lambda_Z^2 \sin^2\beta) - 1. \tag{4.43}$$

We denote $\lambda_{\Theta a}$ and λ_{Za} as the circumferential and axial stretches at which $s_1 = s_2 = s_a$,

$$s_a \;=\; k(\frac{1}{\lambda_{\Theta a}^2 \lambda_{Za}^2} + \frac{1}{\lambda_{\Theta a}^2} + \lambda_{Za}^2) + (1-3k)(\lambda_{\Theta a}^2 \cos^2\beta \;+\; \lambda_{Za}^2 \sin^2\beta) - 1, \tag{4.44}$$

so that from Eq. (4.41),

$$IV_{1a,0} \;=\; IV_{2a,0} \;=\; \lambda_{\Theta a}^2 \cos^2\beta \;+\; \lambda_{Za}^2 \sin^2\beta. \tag{4.45}$$

Similarly, we denote $\lambda_{\Theta b}$ and λ_{Zb} as the circumferential and axial stretches at which $s_0 = s_b$, so that

$$s_b \;=\; \frac{1}{\lambda_{\Theta b}^2 \lambda_{Zb}^2} + \lambda_{\Theta b}^2 + \lambda_{Zb}^2 - 3. \tag{4.46}$$

The kinematic variables relative to reference configuration κ_α are,

$$[\underline{F}_\alpha] \;=\; \begin{bmatrix} \dfrac{\lambda_{\Theta a}\lambda_{Za}}{\lambda_\Theta \lambda_Z} & 0 & 0 \\ 0 & \dfrac{\lambda_\Theta}{\lambda_{\Theta a}} & 0 \\ 0 & 0 & \dfrac{\lambda_Z}{\lambda_{Za}} \end{bmatrix}, \tag{4.47}$$

$$[\underline{B}_\alpha] \;=\; [\underline{C}_\alpha] \;=\; \begin{bmatrix} \dfrac{\lambda_{\Theta a}^2 \lambda_{Za}^2}{\lambda_\Theta^2 \lambda_Z^2} & 0 & 0 \\ 0 & \dfrac{\lambda_\Theta^2}{\lambda_{\Theta a}^2} & 0 \\ 0 & 0 & \dfrac{\lambda_Z^2}{\lambda_{Za}^2} \end{bmatrix}, \tag{4.48}$$

with the following invariants,

$$I_\alpha = \frac{\lambda_{\Theta a}^2 \lambda_{Za}^2}{\lambda_\Theta^2 \lambda_Z^2} + \frac{\lambda_\Theta^2}{\lambda_{\Theta a}^2} + \frac{\lambda_Z^2}{\lambda_{Za}^2}, \qquad IV_{\alpha,\alpha} \;=\; \frac{\lambda_\Theta^2 \cos^2\beta + \lambda_Z^2 \sin^2\beta}{\lambda_{\Theta a}^2 \cos^2\beta + \lambda_{Za}^2 \sin^2\beta}. \tag{4.49}$$

Following (3.26), the measure for collagen damage is,

$$s_{\alpha,\alpha} \;=\; k(\frac{\lambda_{\Theta a}^2\lambda_{Za}^2}{\lambda_{\Theta}^2\lambda_{Z}^2}+\frac{\lambda_{\Theta}^2}{\lambda_{\Theta a}^2}+\frac{\lambda_{Z}^2}{\lambda_{Za}^2})+(1-3k)(\frac{\lambda_{\Theta}^2\cos^2\beta+\lambda_{Z}^2\sin^2\beta}{\lambda_{\Theta a}^2\cos^2\beta+\lambda_{Za}^2\sin^2\beta})-1. \tag{4.50}$$

The Cauchy stresses can be expressed as in (2.48).

4.2.3.2 Analytical solution for pressure and axial force

In the absence of body forces, the equilibrium equations for the biaxial deformation are,

$$div\underline{t}=0, \tag{4.51}$$

with boundary conditions,

$$\underline{t} \;=\; p_i\underline{e}_r \;\; at \;\; R=r_i, \qquad \underline{t} \;=\; -p_o\underline{e}_r \;\; at \;\; R=r_o,$$

$$\underline{t} \;=\; -N\underline{e}_z \;\; at \;\; Z=0, \qquad \underline{t} \;=\; N\underline{e}_z \;\; at \;\; Z=l. \tag{4.52}$$

Due to the geometrical and constitutive symmetry, the radial componenent of the equilibrium equations is,

$$\frac{\partial t_{RR}}{\partial R}+\frac{t_{RR}-t_{\Theta\Theta}}{R}=0. \tag{4.53}$$

By integrating Eq. (4.53) between r_i and r_o, we can obtain the transmural pressure,

$$\Delta p=p_i-p_o=\int_{r_i}^{r_o}\frac{1}{R}(t_{\Theta\Theta}-t_{RR})\,dR. \tag{4.54}$$

By definition, the axial force is,

$$N=\pi r_i^2p_i+F=2\pi\int_{r_i}^{r_o}t_{ZZ}R\,dR=2\pi[\int_{r_i}^{r_o}(t_{ZZ}-t_{RR})R\,dR+\int_{r_i}^{r_o}t_{RR}R\,dR], \tag{4.55}$$

in which F is the reduced axial force. By integrating by parts the last term of Eq. (4.55) and applying Eq. (4.53), we have,

$$\int_{r_i}^{r_o}t_{RR}R\,dR=\frac{r_i^2}{2}p_i-\frac{r_o^2}{2}p_o+\int_{r_i}^{r_o}(t_{RR}-t_{\Theta\Theta})\frac{R}{2}\,dR. \tag{4.56}$$

After substituting Eq. (4.56) into Eq. (4.55), the axial force can be expressed as,

$$N = \pi r_i^2 p_i + F = \pi r_i^2 p_i - \pi r_o^2 p_o + \pi \int_{r_i}^{r_o} (2t_{ZZ} - t_{RR} - t_{\Theta\Theta}) R \, dR. \tag{4.57}$$

From Eq. (2.48), the integrands in Eq. (4.54) and (4.57) are,

$$t_{\Theta\Theta} - t_{RR} = 2(1-d_0)\frac{\partial \psi_0}{\partial I_0}(\lambda_\Theta^2 - \frac{1}{\lambda_\Theta^2 \lambda_Z^2}) + \sum_{\alpha=1}^{2}(1-d_\alpha)\left[2\frac{\partial \psi_\alpha}{\partial I_\alpha}(\frac{\lambda_\Theta^2}{\lambda_{\Theta a}^2} - \frac{\lambda_{\Theta a}^2 \lambda_{Za}^2}{\lambda_\Theta^2 \lambda_Z^2}) + 2\frac{\partial \psi_\alpha}{\partial IV_{\alpha,\alpha}}\frac{\lambda_\Theta^2 \cos^2\beta}{IV_{\alpha a,0}}\right], \tag{4.58}$$

$$\begin{aligned} 2t_{ZZ} - t_{RR} - t_{\Theta\Theta} &= 2(1-d_0)\frac{\partial \psi_0}{\partial I_0}(2\lambda_Z^2 - \lambda_\Theta^2 - \frac{1}{\lambda_\Theta^2 \lambda_Z^2}) + \sum_{\alpha=1}^{2}(1-d_\alpha)[2\frac{\partial \psi_\alpha}{\partial I_\alpha}(\frac{2\lambda_Z^2}{\lambda_{Za}^2} - \frac{\lambda_\Theta^2}{\lambda_{\Theta a}^2} - \frac{\lambda_{\Theta a}^2 \lambda_{Za}^2}{\lambda_\Theta^2 \lambda_Z^2}) \\ &+ 2\frac{\partial \psi_\alpha}{\partial IV_{\alpha,\alpha}}\frac{(\lambda_Z^2 \sin^2\beta - \lambda_\Theta^2 \cos^2\beta)}{IV_{\alpha a,0}}]. \end{aligned} \tag{4.59}$$

Therefore, N can be evaluated for specific material functions using (4.57) and (4.59). Similarly, Δp can be determined from (4.54) and (4.58).

4.2.3.3 Comparison of numerical and analytical solutions

Using the implemented structural multi-mechanism model, a three dimensional finite element model was constructed to obtain the numerical solution for inflation and tension of a cylindrical artery. Due to the axisymmetric geometry, material and loads, a symmetric cylinder model was used to reduce the computational cost, Fig. 19. Eight-node solid elements were used for meshing.

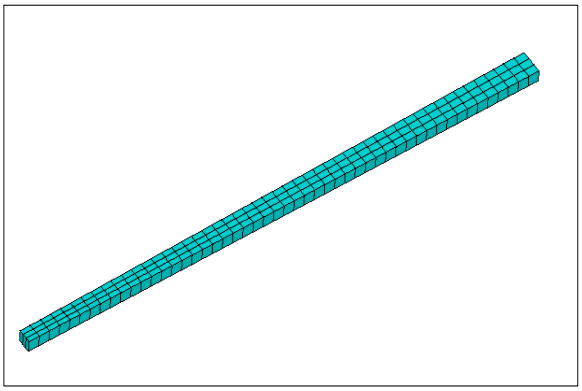

Figure 19: Symmetric finite element model for the inflation and tension of cylinder.

First, we look at the case in which a monotonic increased biaxial loads are applied. Constitutive model for elastin failure (E-DC) without cyclic damage is used here. The geometry and constitutive properties used in these analytical and numerical analyses are shown in Table 6. Three representative arterial thickness values are considered here in the range of $100 - 200\mu m$, as reported in Scott *et al.* (1972). The constitutive parameters were obtained by nonlinear regression analysis of the data of Scott *et al.* (1972) as in Section 2.3.2.

Table 6: Geometry and material parameters of the validation models, with combinations of first order exponential (E-EXP1) strain energy function for the elastin mechanism, second order exponential function for the collagen mechanism (C-EXP2-disp), elastin deactivation criterion (E-DC) and collagen activation criterion (C-AC).

$Thickness(\mu m)$	$R_i(mm)$	$R_o(mm)$	$\eta_0(KPa)$	γ_0	$\eta(KPa)$	γ	k	$\beta_1 = -\beta_2$	s_{1a}	s_{0b}
100	0.28	0.38	9.09	0.5652	252.0	1.91	0.199	56.7	0.5377	3.48
150	0.28	0.43	6.06	0.5651	167.9	1.90	0.200	56.5	0.5401	3.48
200	0.28	0.48	4.55	0.5651	125.0	1.88	0.201	56.2	0.5435	3.48

Fig. 20 shows the analytical solution (4.54) for transmural pressure (Δp) as a function of inner circumferential stretch $\lambda_{\Theta i}$ during the biaxial inflation and tension of a 200 μm thick cylinder. Two solutions with different inner radial stretch were presented. The axial stretch is the same for both cases: $\lambda_Z = 1.2$. The start point for elastin degradation can be observed from the load curves, at which $\lambda_{\Theta i} = \lambda_{\Theta b}$, $\lambda_{Zi} = \lambda_{Zb}$. Numerical oscillation can be observed on the load curves after the material starts a continuous degradation of the elastin.

The comparison of analytical solution and finite element solution for this biaxial inflation-tension analysis is shown in Figs. 21 and 22. Fig. 21 shows the result of a mesh density study in the cylinder thickness direction. Three simulation cases are compared with the analytical solutions using different mesh size. It is found that 100 elements are needed to obtain an accurate solution compared with the analytical one for the error to be less than 5% in this case. Fig. 22 shows the impact of the material compressibility parameter on the finite element solution. Three compressibility parameters are used for different cases, in which the case using $\mu = 10^{-9} Pa^{-1}$ is shown to match the analytical solution well with the error less than 5%. It is shown that the compressibility parameter is critical for obtaining satisfactory numerical solution compared with analytical solution for the modeling of incompressible material.

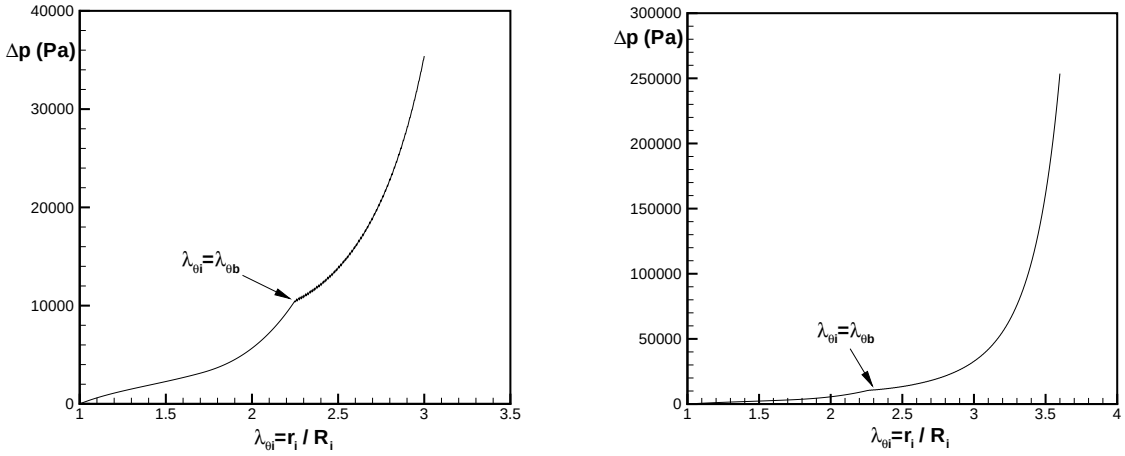

(a) (b)

Figure 20: Analytical solution for biaxial inflation-tension of 200 μm thick cylinder for two values of circumferential stretch: (a) $\lambda_{\Theta i} = 3.0$ and (b) $\lambda_{\Theta i} = 3.6$.

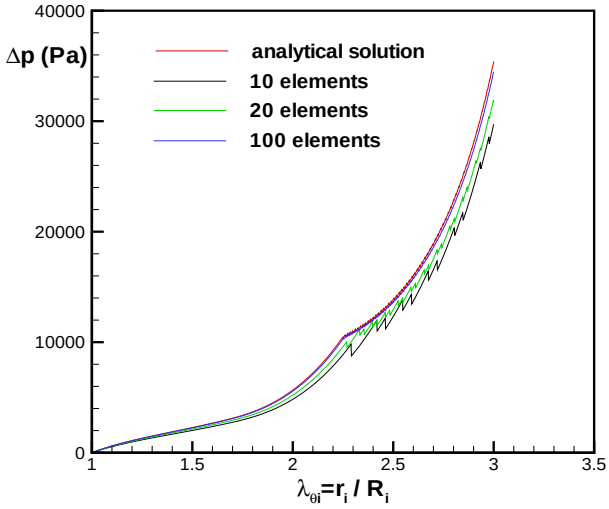

Figure 21: Comparison of analytical solution and numerical solution for biaxial inflation-tension of 200 μm thick cylinder with $\lambda_{\Theta i} = 3.0$ and $\lambda_Z = 1.2$. Study of mesh density.

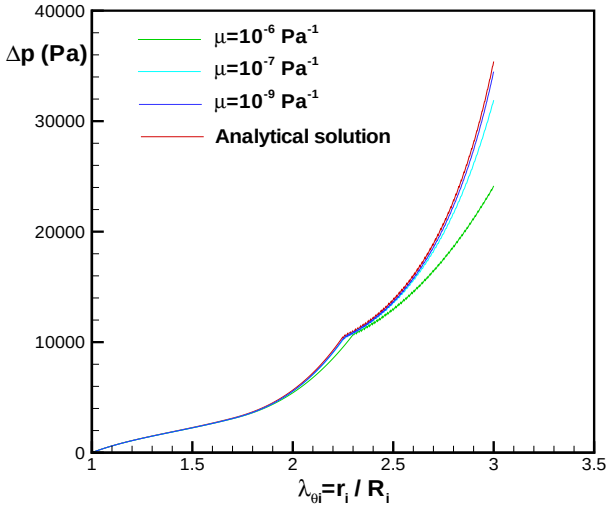

Figure 22: Comparison of analytical solution and numerical solution for biaxial inflation-tension of 200 μm thick cylinder with $\lambda_{\Theta i} = 3.0$ and $\lambda_Z = 1.2$. Study of incompressiblity.

Fig. 23 shows the comparison of finite element solution and analytical solution for the biaxial inflation-tension analysis with circumferential stretch $\lambda_{\Theta i} = 3.6$ and axial stretch $\lambda_Z = 1.2$. 100 elements are used through the cylinder thickness and a compressibility parameter $\mu = 10^{-12} Pa^{-1}$ is used in the analysis. The numerical solution converges to the analytical solution well.

Figs. 24-27 show some simulation results at one loading stage of the biaxial inflation-tension analysis. Fig. 24 shows the current collagen recruitment status through the cylinder thickness, in which a value of one corresponds to no collagen fiber recruitment and a value of zero represents recruited collagen fibers. Fig. 25 shows the current elastin degradation status through the cylinder thickness. Here, a value of one represents complete degradation or failure of elastin and a value of zero represents complete undegradated elastin. Fig. 26 visualizes the mean orientation distribution of the fiber families. The Cauchy stress in the radial direction is shown in Fig. 27.

Secondly, we investigate the case in which cyclically increasing biaxial loads are applied to the cylindrical model. Constitutive models for cyclic damage behavior of both elastin and

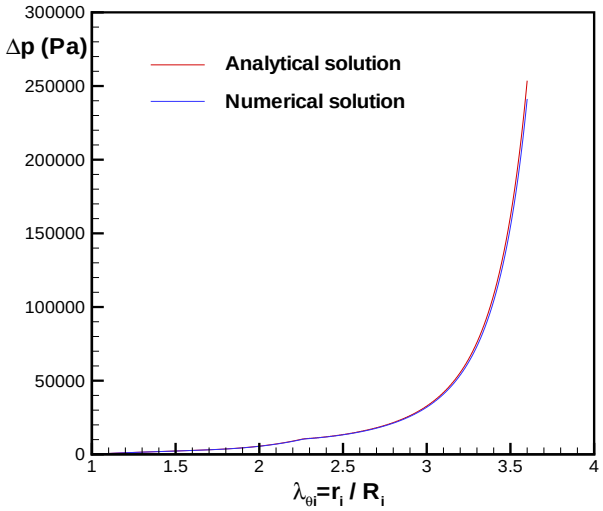

Figure 23: Comparison of analytical solution and numerical solution for biaxial inflation-tension of 200 μm thick cylinder with $\lambda_{\Theta i} = 3.6$ and $\lambda_Z = 1.2$.

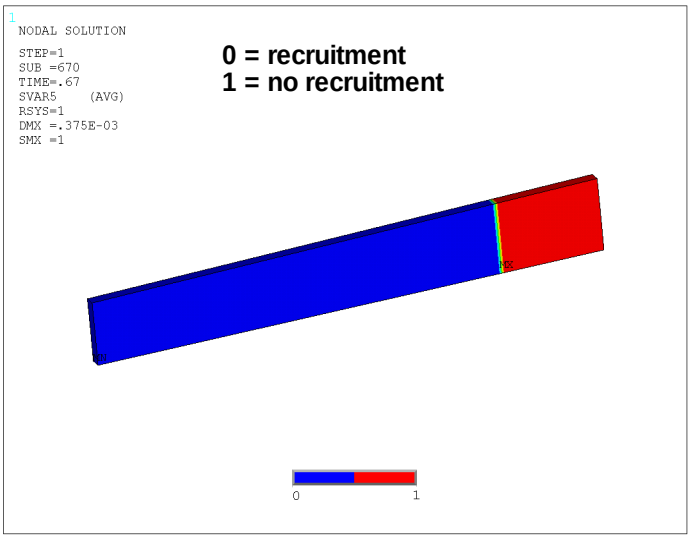

Figure 24: Collagen fiber recruitment status for biaxial inflation-tension of 200 μm thick cylinder with circumferential stretch $\lambda_{\Theta i} = 3.0$ and axial stretch $\lambda_Z = 1.2$.

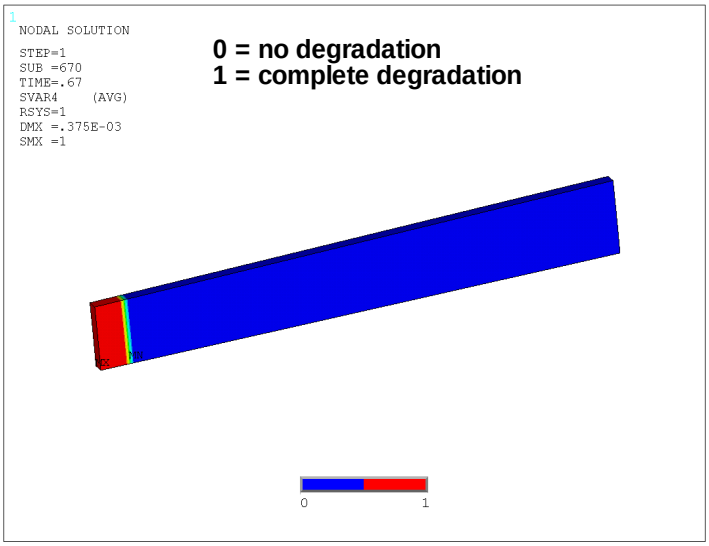

Figure 25: Elastin degradation status for biaxial inflation-tension.

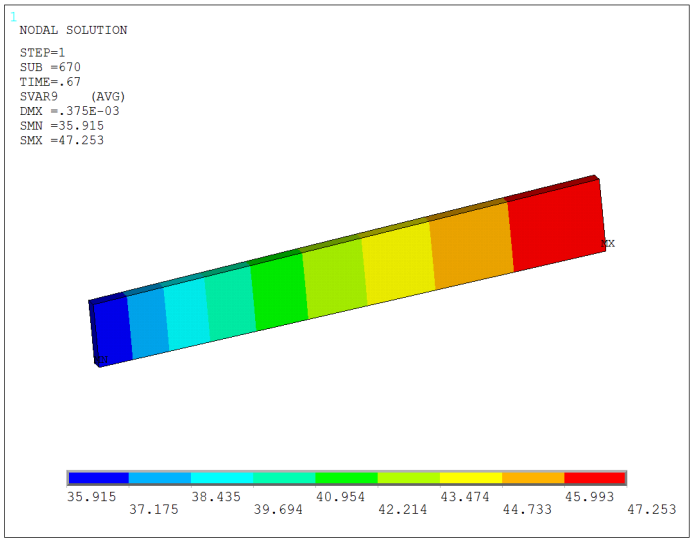

Figure 26: Mean orientation of collagen fiber family for biaxial inflation-tension.

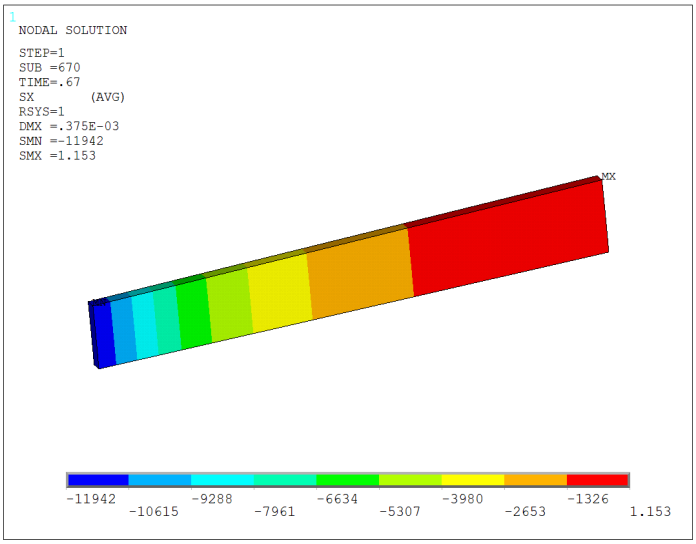

Figure 27: Cauchy stress in radial direction for biaxial inflation-tension.

collagen are utilized. Table 7 shows the geometrical and constitutive properties, in which the material parameters for $200\mu m$ thickness in Table 6 and damage parameters in Table 4.2.2 are used here.

Table 7: Geometric and material parameters of the validation models, with a first order exponential (E-EXP1) strain energy function for the elastin mechanism, second order exponential function for the collagen mechanism (C-EXP2-disp), Neo-Hookean function (G-NH)for ground substance, elastin damage criterion (E-DF1) and collagen activation criterion (C-DF).

$Thickness(\mu m)$	$R_i(mm)$	$R_o(mm)$	$\eta_g(KPa)$	$\eta_0(KPa)$	γ_0	$\eta(KPa)$	γ	k
200	2.8	3.0	1.0	4.55	0.5651	125.0	1.88	0.201
$\beta_1 = -\beta_2$	$\mu(\text{Pa}^{-1})$	s_{1a}	c_1	c_4	ν_{01s}(KPa)	ν_{01f}(KPa)	ν_{1s}	ν_{1f}
56.2	1e-9	0.5435	0.25	0.003	100.0	250.0	1.5	3.0

Figs. 28 and 29 show the comparison of analytical solutions and finite element solutions for the cyclic biaxial inflation-tension analysis. Biaxial displacement loads are applied in the circumferential and axial directions of the arterial model. The magnitudes of these loads increases cyclically in a linear way as shown in Fig. 10 (b). In Fig. 28, a maximum circumferential stretch $\lambda_{\Theta i} = 2.5$ and maximum axial stretch $\lambda_Z = 1.2$ are reached cyclically, and the elastin mechanial damage model (E-DF1) is used in the analysis with $d_0 = d_{01}$

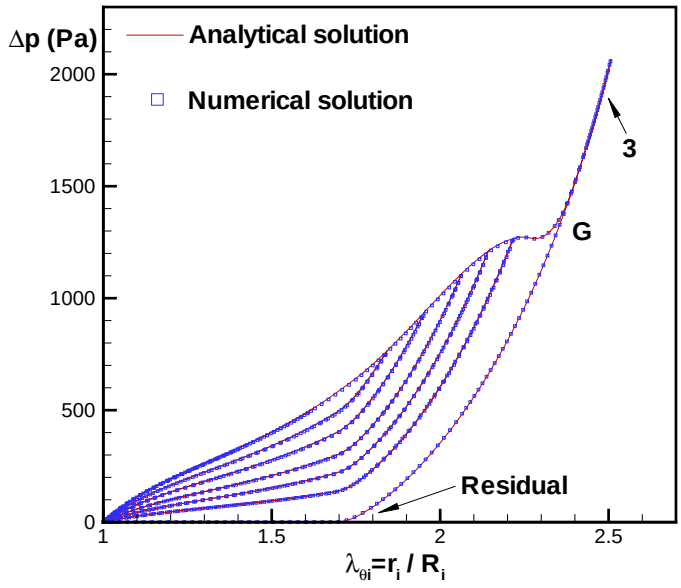

Figure 28: Comparison of analytical and numerical solutions for cyclic biaxial inflation-tension of a 200 μm thick cylinder with maximum stretches of $\lambda_{\Theta i} = 2.5$ and $\lambda_Z = 1.2$ for elastin cyclic damage d_{01}. All elastin fails after point G with collagen left following load curve 3.

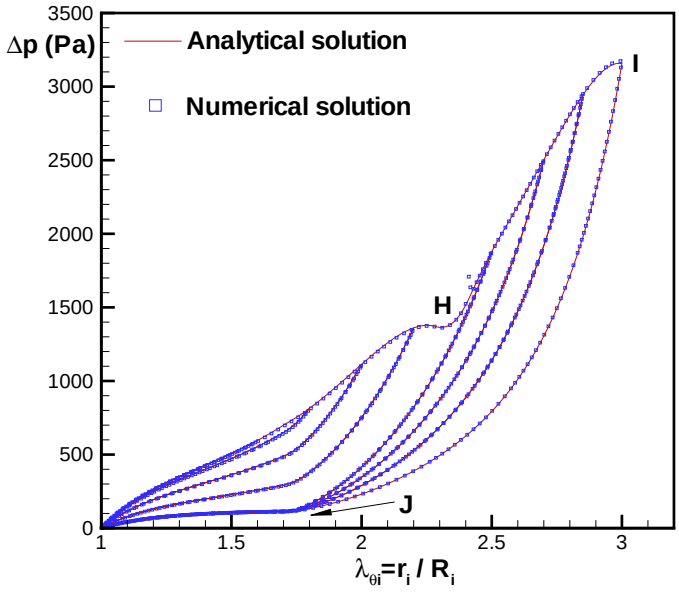

Figure 29: Comparison of analytical and numerical solutions for cyclic biaxial inflation-tension of a 200 μm thick cylinder with maximum stretches of $\lambda_{\Theta i} = 3.0$ and $\lambda_Z = 1.2$. Elastin cyclic damage d_{01} with collagen damage d_α. All elastin fails after point H, with collagen and ground substance loaded to point I. All collagen crimped after point J with ground substance left.

($d_{02} = 0.0$, $d_{03} = 0.0$ and $d_\alpha = 0.0$). Elastin is damaged progressively through the cylinder thickness. All elastin fails after point G and only collgen is left following load curve 3. Residual stretch is observed upon unloading.

In Fig. 29, maximum circumferential stretch is $\lambda_{\Theta i} = 3.0$, maximum axial stretch is $\lambda_Z = 1.2$, and the elastin mechanical damage model (E-DF1) is used together with the collagen damage model (C-DF), so $d_0 = d_{01}$ and $d_\alpha = d_1 = d_2$ ($d_{02} = 0.0$ and $d_{03} = 0.0$) here. For the purpose of numerical test, an undamaged ground substance is also utilized here as one material component to hold the cyclic loads especially when large damage of elastin and collagen happens. Both elastin and collagen are damaged progressively with complete elastin failure at point H. Collagen and ground substance are cyclically loaded until point I after elastin failure. During the unloading, all collagen is unrecruited after point J with only ground substance left. 100 solid elements are used through the cylinder thickness in both analyses. The numerical and analytical solutions match well with maximum errors less than 5%.

Figs. 30 and 31 show the current elastin (d_{01}) and collagen fiber (d_α) damage status respectively through the cylinder thickness at one loading stage of the cyclic biaxial inflation-tension analysis. Here, a value of one represents complete degradation or failure, a value of zero represents undamaged status, and a value between zero and one corresponds to the varying degrees of damage of elastin or collagen fibers.

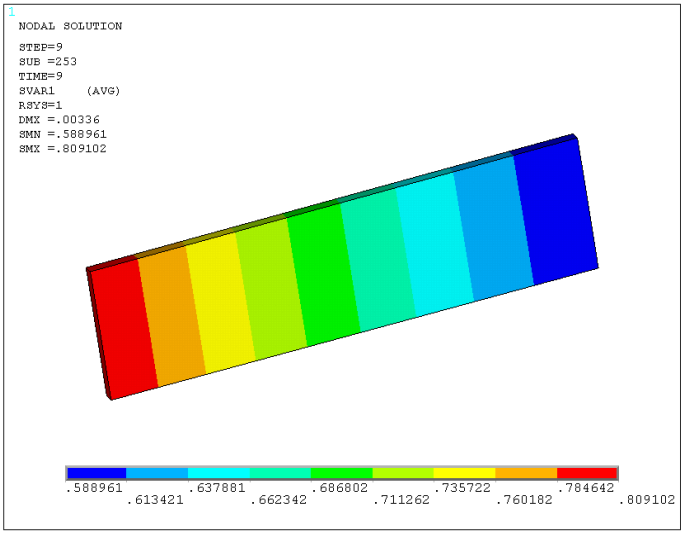

Figure 30: Elastin damage status (d_{01}) for cyclic biaxial inflation-tension of 200 μm thick cylinder with circumferential stretch $\lambda_{\Theta i} = 3.0$ and axial stretch $\lambda_Z = 1.2$.

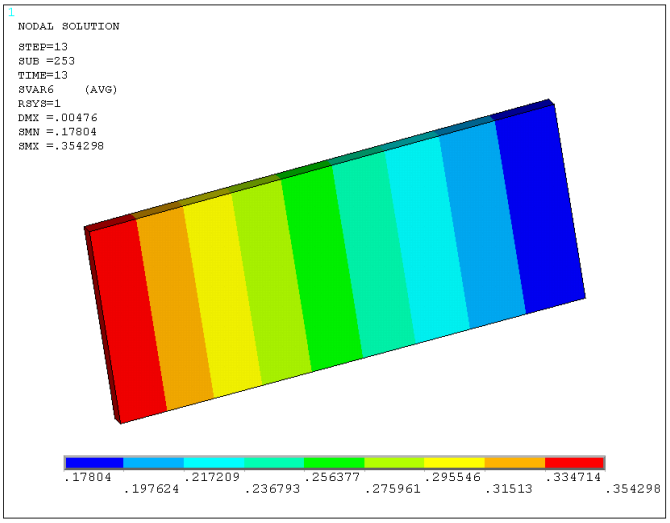

Figure 31: Collagen fiber damage status (d_α) for cyclic biaxial inflation-tension.

5.0 MODELING OF CEREBRAL ANGIOPLASTY

5.1 INTRODUCTION

Percutaneous transluminal angioplasty (PTA) is performed to treat atherosclerotic obstruction and vasospasm in cerebral vessels (Wojak *et al.*, 2006; Higashida *et al.*, 1992; Honma *et al.*, 1995), with the primary mechanical mechanism explained as the overstretching and widening of arterial wall layers: intima, media and adventitia (Castaneda-Zuniga *et al.*, 1980). PTA can introduce direct vascular damage by the deployment of balloon, stent and cerebral protection devices (Muller-Hulsbeck *et al.*, 2005). Transluminal dilatation of small and fragile intracranial arteries is more dangerous than that of extracranial arteries when overstretched. Visible vessel wall damage is observed at the site of PTA, characterized by intimal damage (endothelial damage, subendothelial destruction, fractured IEL) and medial changes (damaged myocytes, loss of dense bodies, gaps in the extracellular matrix, disorganized collagen fibers) (Castaneda-Zuniga *et al.*, 1981; Zollikofer *et al.*, 1984; Chavez *et al.*, 1990; Honma *et al.*, 1995; Connors and Wojak, 1999). These unusual morphological changes are usually absent in the distal arterial segments on which PTA has not been carried out.

Despite reparative processes including endothelial regeneration, damage of the internal elastic lamina (IEL) and media are grossly irreversible in the damaged region (Zollikofer *et al.*, 1984; Chavez *et al.*, 1990; Castaneda-Zuniga *et al.*, 1980). Intimal damage can lead to malignant thrombus/platelet aggregation progressing to total occlusion since intracranial vessels are relatively small and can be extremely thrombogenic (Connors and Wojak, 1999). In addition to such minor structural damages as areas of disruption and dissection throughout the vessel layers, major structural damage including partial tears of intima or media, splitting of atheromatous plaques and hemorrhages may result in stroke, and even a tear or rupture

of the vessel wall (Honma *et al.*, 1995; Connors and Wojak, 1999). However, the damage to the vessel wall following PTA has not been rigorously investigated.

In a controlled study of angioplasty in common carotid, iliac, and femoral arteries of mongrel dogs, changes to the arterial wall due to over inflation were studied at two dilation levels $(25\%, 50\%)$ (Zollikofer *et al.*, 1984). Damage to the wall was progressive increasing with inflation level. At 25% inflation, localized fractures and stretching of the IEL were observed. Damage to the media was limited to the inner one-third of the wall. At 50% inflation, further radial damage was seen including extensive damage to the IEL, dissection of the media, distorted SMC and disorganized collagen fibers through more than half the media. The changes were most pronounced in the inner layers and decreased towards the outer layers of the wall. At six months, the media exhibited signs of repair such as regeneration of smooth muscle cells and increased collagen contents in formerly dilated areas while the IEL showed no recovery, not even in places where it had been destroyed. For the long-lasting effects of PTA, the effects of growth and remodeling will be important such as intimal hyperplasia and fibrotic changes of the media in the dilated arterial wall (Zollikofer *et al.*, 1984; Honma *et al.*, 1995).

Arterial inelastic deformations including elastoplastic and damage mechanisms are important phenomena during supraphysiological loading such as mechanical treatments like PTA (Holzapfel *et al.*, 2000). From mechanical test of arteries (Holzapfel *et al.*, 2000; Oktay *et al.*, 1991), it was shown that mechanical damage results in significant changes in the mechanical behavior such as tissue softening (weakening) and non-recoverable deformation. The residual stretches are responsible for the luminal increase during PTA and are described as "controlled vessel injury" (Castaneda-Zuniga *et al.*, 1985).

Here, we simulate cerebral arterial angioplasty surgery using the structural damage model and use this simulation tool to analyze arterial tissue injury. A three-dimensional computational model of artery and balloon is built to simulate the artery-balloon interaction during an angioplasty procedure. A multi-step simulation scheme is utilized including the inflation-tension of artery, inflation of balloon and the contact between artery and balloon. Due to the extensive computational requirements for contact analysis with nonlinear materials, we use an axisymmetric model for the simulation. To characterize cerebral arteries, we build

a multi-layer artery model composed of the IEL, media and adventitia layers. Heterogeneous multi-mechanism materials including elastin, ground matrix and collagen are utilized for the arterial layers. A more rigid material model is used for balloon model. Related computational work can be found in Sidorov (2006); Gasser and Holzapfel (2007), in which Sidorov (2006) simulated angioplasty using a one-layer arterial model with isotropic multi-mechanism material (Wulandana and Robertson, 2005), and Gasser and Holzapfel (2007) analyzed angioplasty using an elastoplastic material formulation for arteries.

5.2 FINITE ELEMENT MODEL OF CEREBRAL ANGIOPLASTY

For the modeling of cerebral PTA, first we analyze the high pressure response of a multi-layer cerebral artery model. Then we use this artery model to simulate the artery-balloon interaction and tissue injury during cerebral PTA. The PTA pressure is estimated to be about 1.0 to 1.5 atm (Honma *et al.*, 1995). The balloon is usually undersized by 0.2 to 0.7 mm compared with the diameter of the vessel. Most lesions undergoing dilation are less than 10 mm long (usually 2 to 4 mm), and thus very short balloons are necessary. A typical intracerebral single-lumen angioplasty catheter is mostly 2 mm (diameter) by 10 mm (length) in size (Connors and Wojak, 1999).

5.2.1 High pressure response of a multi-layer arterial model

To represent the heterogeneous histological structure of cerebral arteries (Finlay *et al.*, 1995), we build a cylindrical arterial model with three layers: the IEL, media and adventitia, Fig. 32. The unloaded internal diameter is 2.3 mm with a total wall thickness of 125 μm. The IEL, media and adventitia occupy 1/10, 6/10 and 3/10 of the wall thickness respectively. For constitutive models, we use isotropic elastin material with damage for the IEL, and use the structural multi-mechanism model for ground matrix and collagen fibers in the media and adventitia. The fiber orientation for collagen families in the media is 7° here, representing nearly circumferential fiber families, while the mean fiber orientation for collagen families in

the adventitia is 56° to represent more dispersed fibers (Finlay *et al.*, 1995). Vessel injury is characterized by damage of elastin, ground matrix and collagen fibers in the IEL and media, representing intima and media damage. The adventitial collagen and ground matrix are assumed to be purely elastic since few acute vessel injury is observed in the adventitia (Zollikofer *et al.*, 1984; Honma *et al.*, 1995). The representative constitutive equations used in the following simulations are shown in Table 8, in which the mechanical strain-based damage mechanism is utilized for elasin/ground matrix and collagen damage.

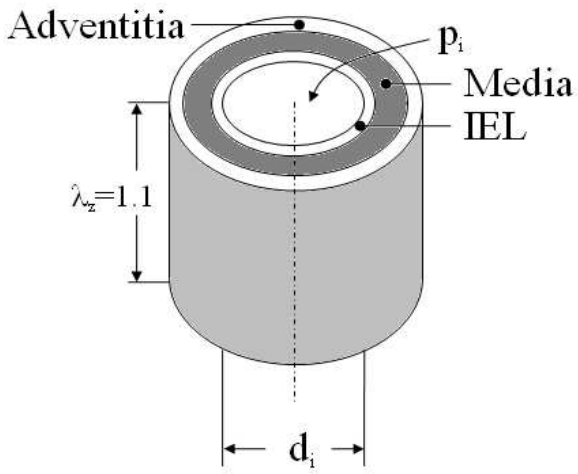

Figure 32: Cylindrical multi-layer artery model for biaxial inflation-tension.

We first simulate the high pressure response of the multi-later arterial wall. Material parameters used in this simulation are shown in Table 9. Since there is no experimental data available for individual layers of cerebral arteries, we choose the elastic parameters based on values from previous studies in Section 2.3.2 and Li and Robertson (2009); Li and Robertson (2009b). The damage parameters are chosen to ensure that large damage response happens in arterial layers during the typical PTA pressures and physically meaningful results are obtained. With a fixed axial stretch of 1.1, increased internal pressure is applied on the artery wall from zero to one bar, then unloaded to zero. Fig. 33 shows the loading and unloading curves for transmural pressure with change of arterial internal diameter. Vessel wall damage and weakening is clearly shown from the dissipation of loading-unloading curves, and also the wall diameter changes which is responsible for luminal increase after PTA. As shown in Fig. 33, the artery has a diameter of 3.480 mm at State A which is the physiological

Table 8: Representative forms of the constitutive functions used in angioplasty simulations.

Volumetric Function	
VOL:	$\psi_{vol} = \frac{1}{\mu}(J_0 - 1)^2,$
IEL Layer	
Elastin Strain Energy	
First Order Exponential (E-EXP1):	$\psi_{0E} = \frac{\eta_{0E}}{2\gamma_{0E}} \left(e^{\gamma_{0E}(\bar{I}_0 - 3)} - 1 \right),$
Elastin Damage	
E-DF1:	$d_{01E} = 1 - \frac{1 - e^{c_{1E}(1 - \nu_{01E}/\nu_{01fE})}}{1 - e^{c_{1E}(1 - \nu_{01sE}/\nu_{01fE})}},$
Media Layer	
Ground Matrix Strain Energy	
First Order Exponential (M-G-EXP1):	$\psi_{0M} = \frac{\eta_{0M}}{2\gamma_{0M}} \left(e^{\gamma_{0M}(\bar{I}_0 - 3)} - 1 \right),$
Collagen Strain Energy	
Exponential (M-C-EXP2-disp):	$\psi_{\alpha M} = \frac{\eta_M}{2\gamma_M} \left(e^{\gamma_M(k_M \bar{I}_\alpha + (1 - 3k_M)\bar{IV}_{\alpha,\alpha} - 1)^2} - 1 \right), \quad \alpha = 1, 2,$
Ground Matrix Damage	
M-G-DF1:	$d_{01M} = 1 - \frac{1 - e^{c_{1M}(1 - \nu_{01M}/\nu_{01fM})}}{1 - e^{c_{1M}(1 - \nu_{01sM}/\nu_{01fM})}},$
Collagen Damage	
M-C-DF:	$d_{\alpha M} = 1 - \frac{1 - e^{c_{4M}(1 - \nu_{\alpha M}/\nu_{\alpha fM})}}{1 - e^{c_{4M}(1 - \nu_{\alpha sM}/\nu_{\alpha fM})}},$
Adventitia Layer	
Ground Matrix Strain Energy	
First Order Exponential (A-G-EXP1):	$\psi_{0A} = \frac{\eta_{0A}}{2\gamma_{0A}} \left(e^{\gamma_{0A}(\bar{I}_0 - 3)} - 1 \right),$
Collagen Strain Energy	
Exponential (A-C-EXP2-disp):	$\psi_{\alpha A} = \frac{\eta_A}{2\gamma_A} \left(e^{\gamma_A(k_A \bar{I}_\alpha + (1 - 3k_A)\bar{IV}_{\alpha,\alpha} - 1)^2} - 1 \right), \quad \alpha = 1, 2.$

loading state, while the diameter increases to 3.631 mm at the physiological unloading state, State C. State B is the supraphysiological state, where wall diameter is 4.082 mm.

The distribution of circumferential Cauchy stress across the deformed wall thickness is shown in Figs. 34, 35 and 36 for States A, B and C respectively. It is shown that the IEL, media and adventitia layers have discontinuous stress distributions and stress gradients. The IEL stress level is the lowest for all three states. At State A, the highest wall stress is found in the media layer. This high stress shifts to the adventitia layer at States B and C, which is due to the inelastic damage in the media and stiffening of the adventitia from collagen recruitment during high pressure loading. The stress gradient in the media changes greatly from State A to States B and C, which is due to the nonhomogenerous damage accumulating across the media layer.

Table 9: Material parameters for three arterial layers in high-pressure response.

$\mu(\text{Pa}^{-1})$	$\eta_{0E}(KPa)$	γ_{0E}	c_{1E}	$\nu_{01sE}(KPa)$	$\nu_{01fE}(KPa)$	$\eta_{0M}(KPa)$	γ_{0M}	c_{1M}
1e-8	4.55	0.565	0.12	75.0	120.0	4.55	0.565	0.12
$\nu_{01sM}(KPa)$	$\nu_{01fM}(KPa)$	$\eta_M(KPa)$	γ_M	β_M	k_M	c_{4M}	$\nu_{\alpha sM}$	$\nu_{\alpha fM}$
75.0	120.0	125.0	1.88	7°	0.0	0.0025	1.3	2.5
$s_{\alpha aM}$	$\eta_{0A}(KPa)$	γ_{0A}	$\eta_A(KPa)$	γ_A	β_A	k_A	$s_{\alpha aA}$	
0.5435	0.51	5.086	125.0	1.88	56°	0.201	0.51	

5.2.2 Simulation of balloon-artery interaction during cerebral angioplasty

In this section, we simulate cerebral angioplasty using the multi-layer artery model and a balloon model, Fig. 37. We use a axisymmetric model with fore-aft symmetry so only part of the arterial segment and balloon are included in the computational model. The artery has an unloaded internal diameter of 2.5 mm (3.816 mm at the physiological loading state), a thickness of 125 μm and a length of 10 mm. The balloon has a external diameter of 1.8 mm and a length of 5 mm. The interaction between artery and balloon is simulated using a surface contact strategy. The model has 17000 3D solid elements, 2600 contact elements and four solid materials: balloon, IEL, media and adventitia. Material parameters used for arterial layers are shown in Table 10. Compared to the material parameters in Table 9, the elastic properties of the adventitia are modified to make the adventitia much stiffer than the media at high pressures, while keep the media stiffer at low pressures (Yu *et al.*, 1993; Holzapfel *et al.*, 2005). The damage properties of the IEL and media are also adjusted to

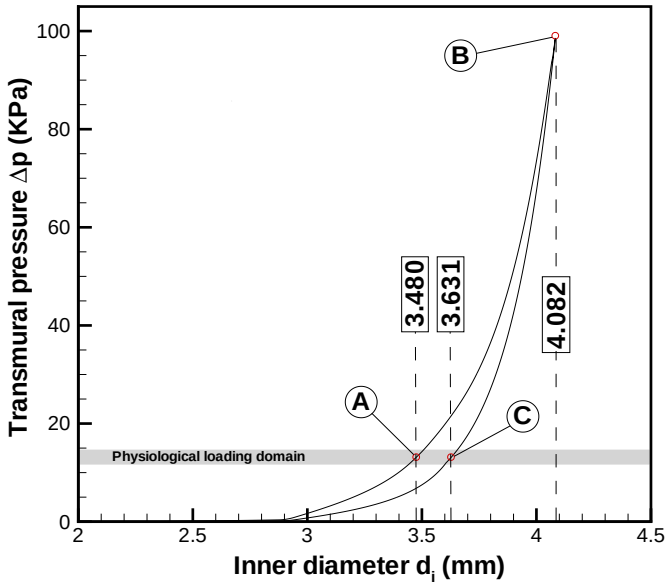

Figure 33: High pressure response of the multi-layer artery model for biaxial inflation-tension with axial stretch $\lambda_Z = 1.1$ and internal pressure increased from 0 to 1 bar (State B), then unloaded to 0.

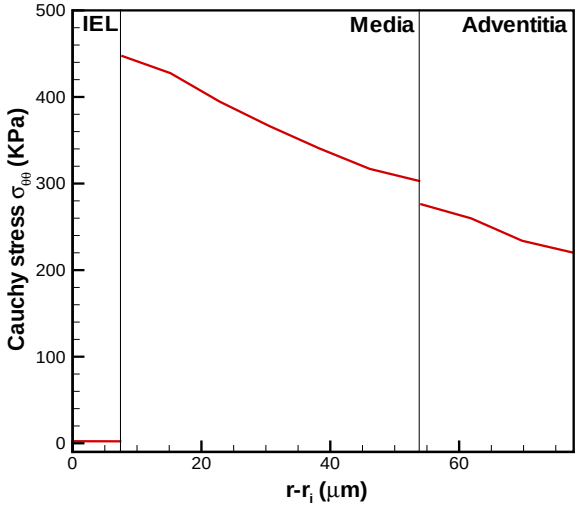

Figure 34: Circumferential Cauchy stress distribution across the deformed wall thickness at State A.

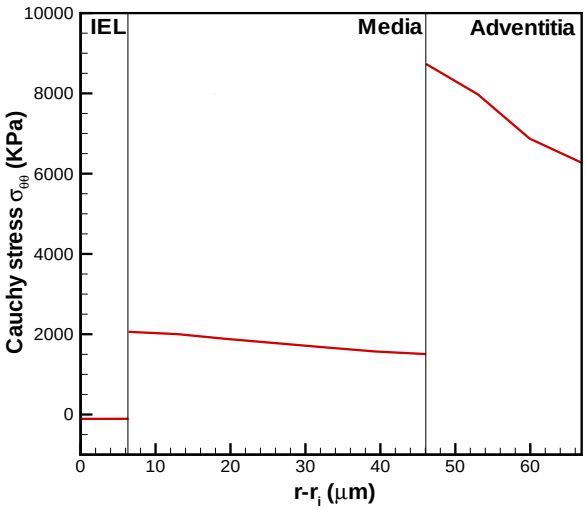

Figure 35: Circumferential Cauchy stress distribution across the deformed wall thickness at State B.

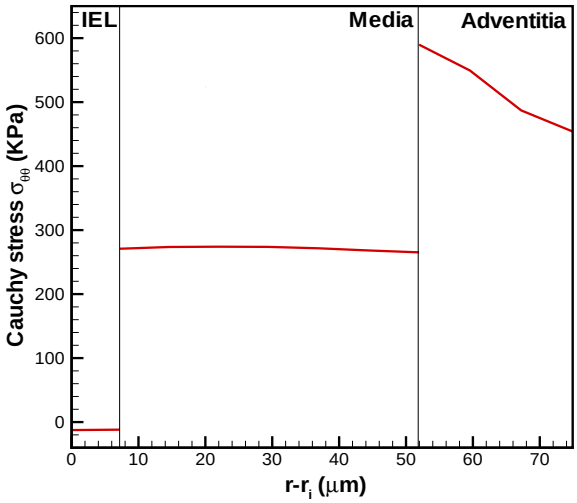

Figure 36: Circumferential Cauchy stress distribution across the deformed wall thickness at State C.

ensure a wider range of inelastic response during the more stringent angioplasty loads. A more rigid Neo-Hookean material is used for the balloon.

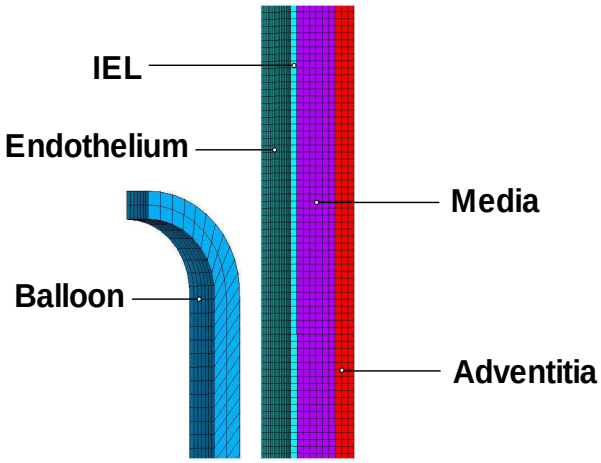

Figure 37: Balloon and artery model for cerebral angioplasty simulation.

Table 10: Material parameters for three arterial layers in balloon-artery interaction.

$\mu(\text{Pa}^{-1})$	$\eta_{0E}(KPa)$	γ_{0E}	c_{1E}	$\nu_{01sE}(KPa)$	$\nu_{01fE}(KPa)$	$\eta_{0M}(KPa)$	γ_{0M}	c_{1M}
1e-8	4.55	0.565	2.1	80.0	2100.0	4.55	0.565	1.8
$\nu_{01sM}(KPa)$	$\nu_{01fM}(KPa)$	$\eta_M(KPa)$	γ_M	β_M	k_M	c_{4M}	$\nu_{\alpha sM}$	$\nu_{\alpha fM}$
100.0	1800.0	125.0	1.88	7°	0.0	0.006	1.5	6.0
$s_{\alpha aM}$	$\eta_{0A}(KPa)$	γ_{0A}	$\eta_A(KPa)$	γ_A	β_A	k_A	$s_{\alpha aA}$	
0.5435	2.27	1.13	500.0	7.53	56°	0.201	0.51	

We use a multi-step loading procedure for the angioplasty simulation, with the four deformation states shown in Fig. 38. First, the artery is inflated to a transmural pressure $\Delta p = 13.33KPa$ with an axial stretch $\lambda_Z = 1.1$. This generates the arterial physiological deformation state before PTA (State A), which is associated with purely elastic response of arteries. Then, the balloon is deployed to contact and dilate the artery to 130% of its internal diameter by applying radial displacement loads on the balloon (States B-C). The inelastic damage and injury of arteries happen during this oversized dilatation process. Finally, the ballon is unloaded to bring the artery back to its physiological state after PTA (State D). At this final state, remaining deformation of the artery is found characterized by nonhomogenerous luminal increase, which is due to the nonrecoverable inelastic damage of the IEL and media induced by the supraphysiological loading.

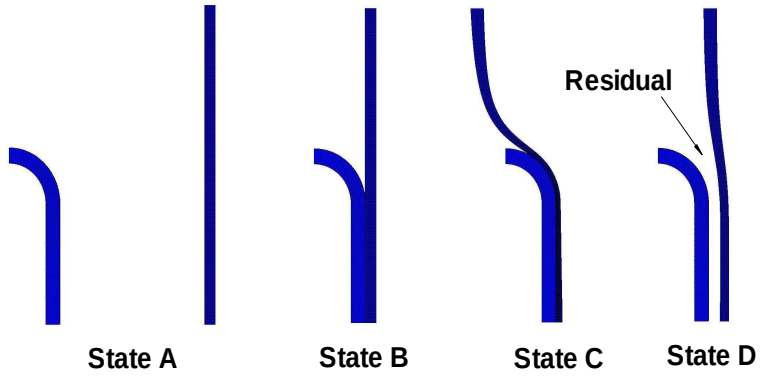

Figure 38: Deformation states of artery and balloon during multi-step cerebral angioplasty simulation. State A: arterial physiological state before angioplasty (transmural pressure $p_i = 13.33KPa$ and axial stretch $\lambda_Z = 1.1$); State B: initial contact of the balloon with the artery after balloon deploys; State C: maximum balloon inflation, arterial dilatation to 130% of its internal diameter; State D: arterial physiological state after angioplasty, balloon deflation with luminal increase left.

Figs. 39 and 40 show the distribution of major arterial damage in the IEL and media layers for two different balloon inflation levels: 120% oversized dilation state and 130% oversized dilation state. Maximum arterial damage is found near the tip of the balloon-artery contact region. At 120% oversized dilation level, the maximum elasin damage in the IEL is $d_{01E} = 0.27$, the maximum ground matrix damage in the media is $d_{01M} = 0.21$, and the maximum collagen damage in the media is $d_{\alpha M} = 0.16$. For further dilation to 130% oversized level when the balloon is fully inflated, arterial damage accumulates to higher levels with the following maximum values: $d_{01E} = 0.83$, $d_{01M} = 0.49$ and $d_{\alpha M} = 0.25$.

Figs. 41-44 show the distributions of the circumferential, axial, radial Cauchy stresses and von Mises stresses in the IEL, media and adventitia layers at the 120% oversized dilation level. The largest stresses are found in regions corresponding to highest IEL and media damage. Compressive radial Cauchy stresses are seen in highly damaged regions of the IEL and media, Fig. 44. The most dominate stresses in the arterial layers are the circumferential and axial Cauchy stresses, as shown in the figures.

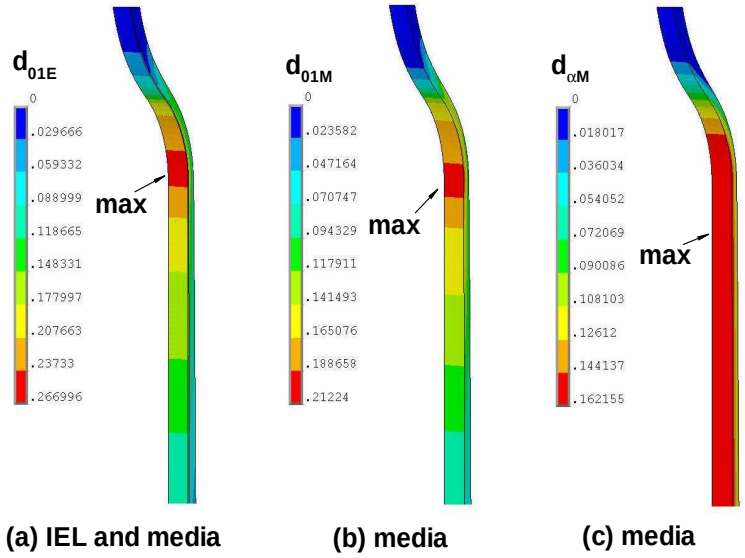

Figure 39: Damage distribution in the arterial layers at 120% oversized dilation state. The arrows indicate the locations of the maximum damage: (a) maximum elastin damage in the IEL $d_{01E} = 0.27$; (b) maximum ground matrix damage in the media $d_{01M} = 0.21$; (c) maximum collagen damage in the media $d_{\alpha M} = 0.16$.

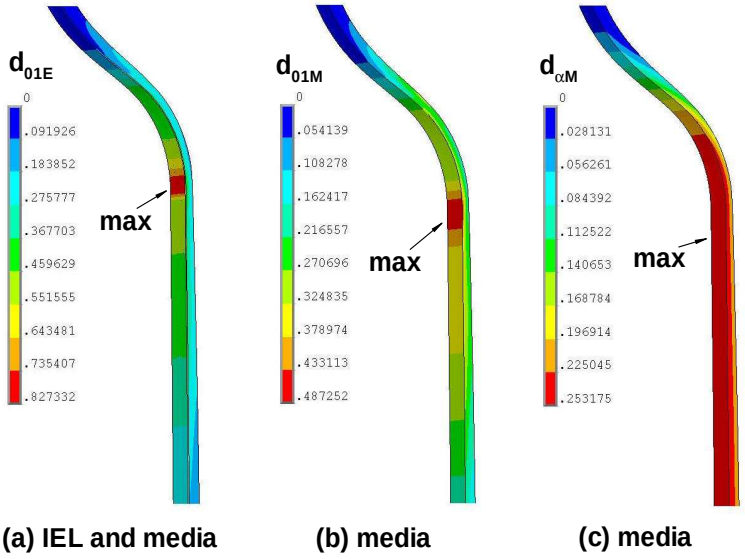

Figure 40: Damage distribution in the arterial layers at 130% oversized dilation state. The arrows indicate the locations of the maximum damage: (a) maximum elastin damage in the IEL $d_{01E} = 0.83$; (b) maximum ground matrix damage in the media $d_{01M} = 0.49$; (c) maximum collagen damage in the media $d_{\alpha M} = 0.25$.

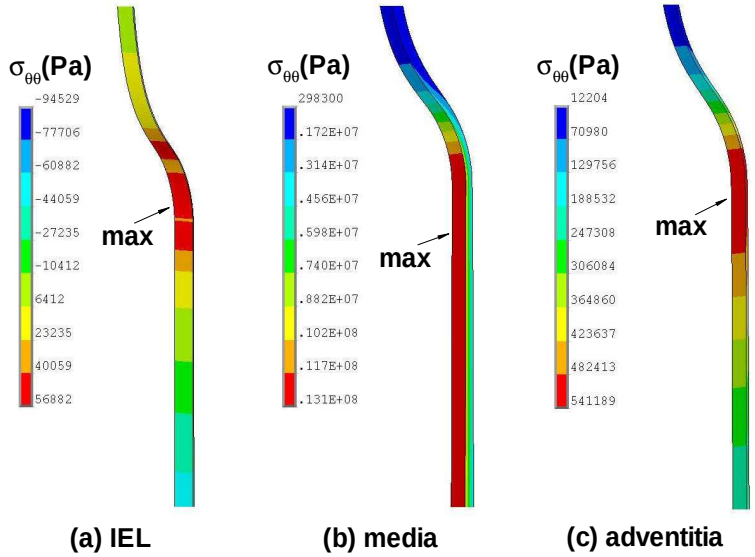

Figure 41: Distribution of the circumferential Cauchy stresses in the IEL, media and adventitia layers at 120% oversized dilation state. The arrows indicate the locations of the maximum values.

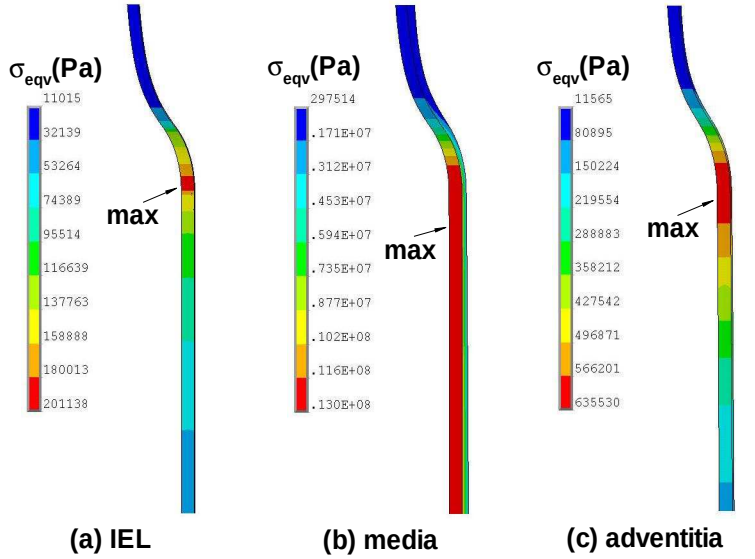

Figure 42: Distribution of the von Mises stresses in the IEL, media and adventitia layers at 120% oversized dilation state. The arrows indicate the locations of the maximum values.

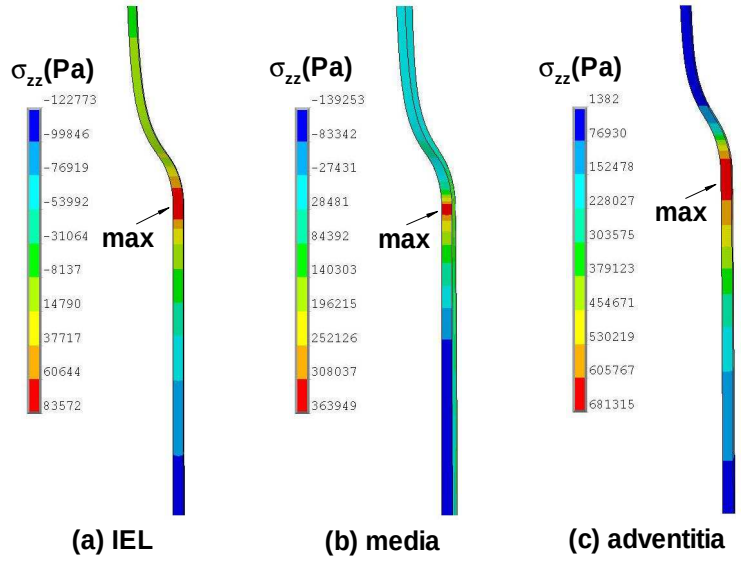

Figure 43: Distribution of the axial Cauchy stresses in the IEL, media and adventitia layers at 120% oversized dilation state. The arrows indicate the locations of the maximum values.

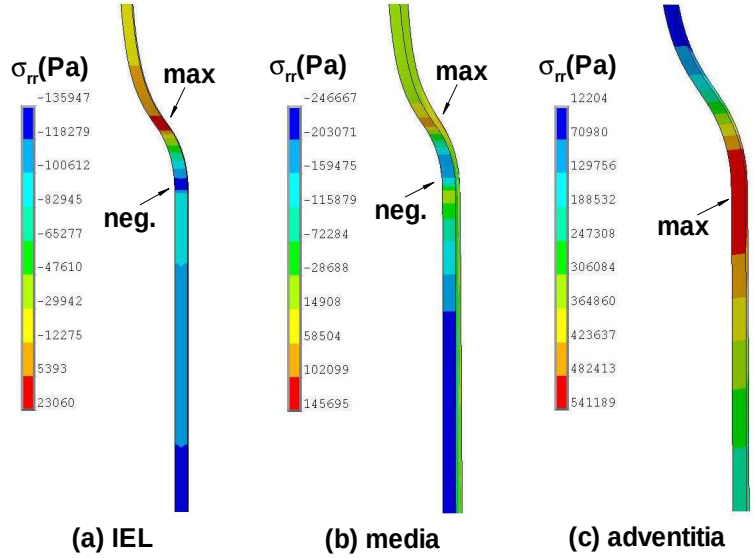

Figure 44: Distribution of the radial Cauchy stresses in the IEL, media and adventitia layers at 120% oversized dilation state. The arrows indicate the locations of the maximum values or negative stresses.

6.0 CONCLUSIONS AND DISCUSSIONS

A structural multi-mechanism damage model for cerebral arterial tissue (Li and Robertson, 2009b) has been developed that builds on a previous isotropic multi-mechanism model (Wulandana and Robertson, 2005) and a recent generalized anisotropic model (Li and Robertson, 2008, 2009). To characterize elastin failure and collagen in aneurysm formation, the cerebral arterial tissue is modeled as nonlinear, inelastic and incompressible with separate mechanisms for elastin and collagen in these models. Motivated by structural data on collagen fiber orientation in cerebral arteries (Finlay *et al.*, 1995), an anisotropic mechanism is represented by helical networks of crimped collagen fibers in the unloaded arterial wall. The collective response of fibers is modeled using a distribution function for fiber orientation (Spencer , 1984; Gasser *et al.*, 2006). The collagen fibers require a finite deformation to begin load bearing. The fiber activation criterion is a function of the local stretch of material elements tangent to the crimped fiber direction in the unloaded configuration.

As for most other mechanical models of the arterial wall, we take a continuum approach. It is assumed that the fibers can be approximated as continuously distributed throughout the material (or arterial layer) so that the fiber orientation vector and other quantities have meaning at each point in the material and are continuous functions of position. We do not account for microscopic effects in the composite such as interactions between the fibers and the matrix or coupling between the collagen fibers, or between the fiber families.

In the analysis here, all fiber families at each material point are assumed to have approximately the same level of waviness (s_a is a constant for all fibers at a point). In some soft tissue, the degree of fiber undulation can vary considerably with position (Sacks, 2003). If warranted by experimental data, it is straightforward to generalize the current model to account for this type of material inhomogeneity. This can be achieved by making s_a a func-

tion of position. Furthermore, it is assumed that collagen fibers are completely uncrimped at a discrete loading level $s = s_a$. This can be generalized by introducing an integral model for fiber recruitment.

It is assumed that all isotropic contributions of the wall are dependent on strain measured relative to κ_0. It is expected that this contribution will primarily come from elastin. The degradation of this mechanism, which we refer to as the elastin mechanism, is considered as arising from two possible modes of damage. In the first type, elastin degradation is dependent on two local measures of strain: a maximum equivalent strain as well as an accumulated equivalent strain. In the second mode of damage, elastin degradation arises indirectly from hemodynamic loading. We expect that pathological levels of the wall shear stress vector initiate a cascade of biochemical activities that lead to degradation of the wall, rather than directly damaging the elastin. For example, some aspects of the wall shear stress vector may lead to an imbalance in the production of MMPs and tissue inhibitor of metalloproteinases (TIMPs) which break down the elastin in the IEL. While at this point, the specific hemodynamic factors remain to be determined, preliminary studies suggest that elevated WSS and elevated (positive) WSSG can lead to IEL degradation in native and non-native bifurcations (Morimoto *et al.*, 2002; Meng *et al.*, 2006). We have given a representative functional form for the dependence of this second mode of damage on hemodynamic variables here.

In the proposed model, the two damage mechanisms are coupled in a multiplicative manner. An elastin layer previously weakened by biochemical factors will undergo larger deformations for the same physiological load. This can in turn lead to increased mechanical damage. Since cerebral aneurysms can form in the absence of hypertension, we anticipate the role of elevated hemodynamic pressures in aneurysm formation is to hasten mechanical damage of an IEL previously weakened by biochemical factors. For aneurysm formation, the coupled mechanical damage d_{02} and enzymatic damage d_{03} will be important damage mechanisms. The proposed damage model can be reduced to a purely mechanical damage model simply by setting the enzymatic damage variable d_{03} to zero. In addition, for the short term effects of angioplasty, only mechanical damage mechanism d_{01} is necessary.

The anisotropic structural multi-mechanism damage model was applied to the inelastic data of Scott *et al.* (1972) using a non-progressive failure criterion for the elastin mechanism. The mean fiber angle β, dispersion parameter k as well as the other material constants, were chosen based on a nonlinear regression analysis of the test data. If tissue specific histology data on fiber orientation and distribution in cerebral vessels becomes available, β and k can be directly estimated. First and second order exponential strain energy function were found to give excellent fits to the data for the elastin and collagen mechanisms. A second order exponential strain energy function was found to have the best fit to the data for both the elastin and collagen mechanisms, particularly in the regions of low tension. The current model has a slightly better fit with Scott et al.'s experimental results than the previous isotropic multi-mechanism model (Wulandana and Robertson, 2005). Although the data from Scott *et al.* (1972) are well fit to this multi-mechanism model, they are limited in their usefulness for evaluating anisotropic and damage material models.

The finite element implementation of the multi-mechanism model was shown to be accurate and robust based for numerical validations using representative material parameters and functional forms. This computational tool was used for the modeling of cerebral angioplasty in which arterial walls were featured multiple layers and material inhomogeneity (Li and Robertson, 2009c). To characterize tissue injury in cerebral angioplasty, the structural damage model was extended to include the isotropic damage of elastin, ground matrix and anisotropic damage of collagen. The qualitative features of PTA such as progressive damage, material softening and luminal increase were reproduced in the angioplasty simulation. In the future, this computational tool can also be used for more complex models of cerebral arteries that include features such as the progressive collagen recruitment and the contribution of smooth muscle. For the long lasting effects of PTA and the further development of aneurysms, arterial growth and remodeling will be important features to be modeled. In addition, more complex geometries such as arterial bifurcations can be considered, which are relevant to aneurysm formation.

In earlier work on angioplasty modeling, Gasser and Holzapfel (2007) used an anisotropic and elastoplastic material formulation for arteries (Holzapfel *et al.*, 2000; Gasser and Holzapfel, 2002), in which arterial injury was modeled using a plastic hardening variable. Here, we use

the multi-mechanism damage model which can capture balloon-induced mechanical damage of arterial components: elastin, ground matrix and collagen fibers, and related phenomena: softening (weakening) and residual stretches. To develop clinically relevant simulation tools for future studies, the current angioplasty model should be refined regarding several approximations. For example, we use a rigid walled balloon controlled by displacement loads. It is expected that the balloon material, its geometry including wall thickness, and the inflation pressure will be important in clinical operations. For simplicity, we have not included arterial plaque. For some applications, this idealization may also need to be relaxed. The current model does not incorporate arterial residual stresses, which may change wall stress distributions. Further, experimental data for the layer-specific responses of cerebral arteries are needed. Experimental data are required for a quantitative validation of the computational results, especially the relationship between loading and residual stretch. Due to the large number of material parameters utilized, a detailed sensitivity analysis should be carried out in future studies.

Computational cost is an important issue for the application of the multi-mechanism model in numerical simulations. The constitutive model includes anisotropic and inelastic damage features for nonlinear material under finite deformation, which are challenging computational tasks in finite element analysis. The current angioplasty study is based on an axisymmetric model with a rigid balloon, with a corresponding computational time of approximately five to six days using a 3.00GHz quad core workstation. Most of this computational time is used for the contact analysis of artery and balloon, in which a high degree of material distortion and damage is introduced. It is expected that the computational cost will be much more demanding for future angioplasty studies using more realistic balloon materials and loads. In addition, for future aneurysm studies with more complex geometries and coupled fluid-solid-growth models, the computational requirements will also be extremely important. We anticipate supercomputing facilities or other high performance computing facilities will be necessary for these future studies.

There remains a great need for in-vitro and in-vivo studies to further test and refine this model. For example, biaxial experiments coupled with evaluation of the corresponding IEL damage are needed to further develop the mechanical damage aspects of this model. Even

more challenging is the need to obtain data on hemodynamic driven elastin degradation that can be used to determine the functional form of ν_{03}. This includes further experimental work to confirm which hemodynamic factors should be included in this function. This is an area of active research involving animal studies of the kind described above as well as in-vitro studies. Robertson *et al.* introduced an in-vitro T-chamber which is able to reproduce the qualitative features of the WSS fields at arterial bifurcations (Chung and Robertson, 2003; Chung, 2004). This chamber has been extended (Larkin et al., 2007; Zeng et al., 2009) to expose cells to the specific WSS and WSSG fields identified by Meng and co-workers as directly associated with histological changes characteristic of aneurysm formation (Meng *et al.*, 2006; Meng et al., 2007). Recently, T-chambers have been used in preliminary studies to investigate the response of endothelial cells to elevated WSS and WSSG fields (Sakamoto et al., 2008; Szymanski et al., 2008). Continued work in this area will provide a strong basis for the further development and validation of the current damage model.

In summary, we feel, the next step to extend the current work is to develop more sophisticated models for tissue mechanobiology, including degeneration, repair, growth and remodeling. Such models can be used in future studies of hemodynamics-driven aneurysm formation and angioplasty-induced tissue injury. For studies of this kind, more complex, clinically relevant geometries are needed for the vessels and devices such as balloons and stents. Further mechanical characterization of balloons, stents and plaques as well as additional experimental data on load transfer mechanisms and long term tissue response to PTA are needed to develop more clinically relevant simulation tools.

BIBLIOGRAPHY

Atkinson, J. L. D., Sundt, T. M., Houser O. W., and Whisnant, J. P., 1989. Angiographic frequency of anterior circulation intracranial aneurysms. *J Neurosurg* 70, 551-555.

Avolio, A., Jones, D., and Tafazzoli-Shadpour, M., 1998. Quantification of alterations in structure and function of elastin in the arterial media. *Hypertension* 32, 170-175.

Billar, K. L., Sacks, M. S., 2000. Biaxial mechanical properties of the native and glutaraldehyde-treated aortic valve cusp: part II-a structural constitutive model. *J Biomech Eng* 122, 327–335.

Broderick, J. P., Brott, T. G., Duldner, J. E., Tomsick T., and Leach, A., 1994. Initial and recurrent bleeding are the major causes of death following subarachnoid hemorrhage. *Stroke* 25, 1342–1347.

Busby, D. E. and Burton, A. C., 1965. The effect of age on the elasticity of the major brain arteries. *Can J Physiol Pharm* 43, 185–202.

Calvo, B., Pena, E., Martinez M. A., and Doblare, M., 2007. An uncoupled directional damage model for fibred biological soft tissues. *Int J Numer Meth Eng* 69, 2036–2057.

Campbell, G. J. and Roach, M. R., 1981. Fenestrations in the internal elastic lamina at bifurcations of human cerebral arteries. *Stroke* 12, 489–496.

Camarata, P. J., Latchaw, R. E., R*ü*fenacht, D. A., and Heros, R. C., 1992. Intracranial aneurysms. *Investigative Radiology* 28, 373–382.

Canham, P. B., Ferguson, G. G., 1985. A mathematical model for the mechanics of saccular aneurysms. *Neurosurgery* 17, 291–295.

Canham, P. B., Finlay, H. M., Dixon, J. G., Boughner, D. R., and Chen, A., 1989. Measurements from light and polarised light microscopy of human coronary arteries fixed at distending pressure. *Cardiovasc Res* 23, 973–982.

Castaneda-Zuniga, W. R., Formanek, A., Tadavarthy, M., Vlodaver, Z., Edwards, J. E., Zollikofer, C., and Amplatz, K., 1980. The mechanism of balloon angioplasty. *Radiology* 135, 565–571.

Castaneda-Zuniga, W. R., Amplatz, K., Laerum, F., Formanek, A., Sibley, R., Edwards, J., and Vlodaver, Z., 1981. Mechanics of angioplasty: an experimental approach. *RadioGraphics* 1, 3, 1–14.

Castaneda-Zuniga, W. R., 1985. Pathophysiology of transluminal angioplasty. *In: Meyer, J., Erberl, R., Rupprecht, H. J. (eds) Improvement of myocardial perfusion* 138-141. Martinus Nijhoff Publisher, Boston.

Chaboche, J. L., 1988. Continuum damage mechanics: Part II-Damage growth, crack initiation, and crack growth. *J Appl Mech* 55, 65-72.

Chàvez, L., Takahashi, A., Yoshimoto, T., Su, C. C., Sugawara, T., and Fujii, Y., 1990. Morphological changes in normal canine basilar arteries after transluminal angioplasty. *Neurol Res* 12, 12–16.

Chuong, C. J., Fung, Y. C., 1986. On residual stresses in arteries. *J Biomech Eng* 108, 189–192.

Chung, B.-J., 2004. Studies of Blood Flow in Arterial Bifurcations: From Influence of Hemodynamics on Endothelial Cell Response to Vessel Wall Mechanics. *Doctoral Thesis* University of Pittsburgh, Pittsburgh, PA.

Chung, B.-J., and Robertson, A.M., 2003. A novel flow chamber to evaluate endothelial cell response to flow at arterial bifurcations. In: *Proceedings of the Biomedical Engineering Society (BMES)*, Nashville, Tennessee, 6P5.113.

Connors III, J. J. and Wojak, J. C., 1999. Percutaneous transluminal angioplasty for intracranial atherosclerotic lesions: evolution of technique and short-term results. *J Neurosurg* 91, 415–423.

Cope, D. A. and Roach, M. R., 1975. A scanning electron microscope study of human cerebral arteries. *Can J Physiol Pharm* 53, 651–659.

Crawford, T., 1959. Some observations on the pathogenesis and natural history of intracranial aneurysms. *J Neurol Neurosur Ps* 22, 259-266.

Cajander, S. and Hassler O., 1976. Enzymatic destruction of the elastic lamella at the mouth of the cerebral berry aneurysm? *Acta Neruol Scand* 53, 171-181.

Davis, E. C., 1993. Stability of elastin in the developing mouse aorta: a quantitative radioautographic study. *Histochemistry* 100, 17–26.

Davis, E. C., 1995. Elastic lamina growth in the developing mouse aorta. *J Histochem Cytochem* 43, 1115–1123.

De Vita, R., Slaughter, W. S., 2006. A structural constitutive model for the strain rate-dependent behavior of anterior cruciate ligaments. *Int J Solids Struct* 43, 1561–1570.

Debelle, L., Tamburro, A. M., 1999. Elastin: molecular description and function. *Int J Biochem Cell Biol* 31, 261–72.

Ferguson, G. G., 1970. Turbulence in human intracranial saccular aneurysms. *J Neurosurg* 33, 485–497.

Finlay, H. M., McCullough, L., Canham, P. B., 1995. Three-dimensional collagen organization of human brain arteries at different transmural pressures. *J Vasc Res* 32, 301–312.

Finlay, H. M., Whittaker, P., Canham, P. B., 1998. Collagen organization in the branching region of human brain arteries. *Stroke* 29, 1595–1601.

Forbus, W. D., 1930. On the origin of miliary aneurysms of the superficial cerebral arteries. *B Johns Hopkins Hosp* 47(5), 239–284.

Fonck, E., Prod′hom, G., Roy, S., Augsburger, L., Rüfenacht, D. A., and Stergiopulos, N., 2007. Effect of elastin degradation on carotid wall mechanics as assessed by a constituent-based biomechanical model. *Am J Physiol-Heart C* 292, H2754-H2763.

Fukuta, S., Hashimoto, N., and Naritomi, H. *et al.*, 2000. Prevention of rat cerebral aneurysm formation by inhibition of nitric oxide synthase. *Circulation* 101, 2532–2538.

Fung, Y. C., Fronek, K., and Patitucci, P., 1979. Pseudoelasticity of arteries and the choice of its mathematical expression. *Am J Physiol* 237, H620–H631.

Gasser, T.C., Holzapfel, G. A., 2002. A rate-independent elastoplastic constitutive model for biological fiber-reinforced composites at finite strains: continuum basis, algorithmic formulation and finite element implementation. *Comput Mech* 29, 340–360.

Gasser, T.C., Ogden, R. W., and Holzapfel, G. A., 2006. Hyperelastic modelling of arterial layers with distributed collagen fibre orientations. *J R Soc Interface* 3, 15–35.

Gasser, T.C., Holzapfel, G. A., 2007. Finite element modeling of balloon angioplasty by considering overstretch of remnant non-diseased tissues in lesions. *Comput Mech* 40, 47–60.

Hademenos, G. J., Massoud, T., Valentino, D. J., Duckwiler, G., Viñuela, F., 1994. A nonlinear mathematical model for the development and rupture of intracranial saccular aneurysms. *Neurol Res* 16, 376–384.

Hashimoto, N., Kim, C., Kikuchi, H., Kojima, M., Kang, Y.,Hazama, F., 1987. Experimental induction of cerebral aneurysms in monkeys. *J Neurosurg* 67(6), 903-905.

Hashimoto, T., Meng, H., and Young, W. L., 2006. Intracranial aneurysms: links among inflammation, hemodynamics and vascular remodeling. *Neurol Res* 28, 372–380.

Hazama, F., Kataoka, H., Yamada, E., Kayembe, K., Hashimoto, N., Kojima, M., and Kim C., 1986. Early changes of experimentally induced cerebral aneurysms in rats. *Am J Pathol* 124, 399–404.

Herrmann, L. R., 1965. Elasticity equations for incompressible and nearly incompressible materials by a variational theorem. *AIAA J* 3, 1896–1900.

Higashida, R. T., Halbach, V. V., Dowd, C. F., Dormandy. B., Bell, J., and Hieshima, G. B., 1992. Cerebral intravascular balloon dilatation therapy for intracranial arterial vasospasm: patient selection, technique, and clinical results. *Neurosurg Rev* 15, 2, 89–95.

Hoffman, A. S., Grande, L. A., and Park, J. B., 1977. Sequential enzymolysis of human aorta and resultant stress-strain behavior. *Biomater Med Devices Artif Organs* 5(2), 121–145.

Hokanson, J., and Yazdani, S., 1997. A constitutive model of the artery with damage. *Mech Res Commun* 24(2), 151–159.

Holzapfel, G. A., Gasser, T.C., and Ogden, R. W., 2000. A new constitutive framework for arterial wall mechanics and a comparative study of material models. *J Elasticity* 61, 1–48.

Holzapfel, G. A., Schulze-Bauer, C. A. J., Stadler, M., 2000. Mechanics of angioplasty:Wall, balloon and stent. *In: Casey, J. and Bao, G. (eds), Mechanics in Biology, AMD-Vol. 242/BED-Vol. 46* 141-156, The American Society of Mechanical Engineers, New York.

Holzapfel, G. A., 2000. *Nonlinear Solid Mechanics.* John Wiley & Sons Ltd., New York.

Holzapfel, G. A., Gasser, T.C., and Stadler, M., 2002. A structural model for the viscoelastic behavior of arterial walls: Continuum formulation and finite element analysis. *Eur J Mech A-Solid* 21, 441–463.

Holzapfel, G. A., Sommer, G., and Gasser, C. T., and Regitnig, P., 2005. Determination of the layer-specific mechanical properties of human coronary arteries with non-atherosclerotic intimal thickening, and related constitutive modeling. *Am J Physiol-Heart C* 289, H2048-H2058.

Holzapfel, G. A., and Ogden, R. W. (eds), 2006. *Mechanics of Biological Tissue.* Springer, Berlin Heidelberg New York.

Honma, Y., Fujiwara, T., Irie, K., Ohkawa, M., and Nagao, S., 1995. Morphological changes in human cerebral arteries after PTA for vasospasm caused by subarachnoid hemorrhage. *Neurosurgery* 36, 6, 1073–1081.

Humphrey, J. D., 1995. Mechanics of arterial wall: review and directions. *Crit Rev Biomed Eng* 23, 1–162.

Humphrey, J. D., Canham P. B., 2000. Structure, mechanical properties, and mechanics of intracranial saccular aneurysms. *J Elasticity* 61, 49–81.

Humphrey, J. D., Rajagopal K. R., 2002. A constrained mixture model for growth and remodeling of soft tissues. *Math Mod Meth Appl S* 12, 407–430.

Humphrey, J. D., 2002. *Cardiovascular Solid Mechanics: Cells, Tissues, and Organs.* Springer, Berlin Heidelberg New York.

Humphrey, J. D., Taylor, C. A., 2008. Intracranial and abdominal aortic aneurysms: similarities, differences, and need for a new class of computational models. *Annu Rev Biomed Eng* 10, 221–246.

Hung, E. J. and Botwin, M. R., 1975. Mechanics of rupture of cerebral saccular aneurysms. *J Biomech* 8, 385–392.

Ingall, T. J., Whisnant, J. P., Wiebers, D. O., O′Fallon, W. M., 1989. Has there been a decline in subarachnoid hemorrhage mortality? *Stroke* 20, 718–724.

Inagawa, T., and Hirano, A., 1990. Autopsy study of unruptured incidental intracranial aneurysms. *Surg Neurol* 34, 361-365.

Inci, S., and Spetzler, R. F., 2000. Intracranial aneurysms and arterial hypertension: a review and hypothesis. *Surg Neurol* 53, 530-542.

Kachanov, L. M., 1958. On the time to failure under creep conditions. *Izv AN SSSR, Otd Tekhn Nauk* 8, 26-31.

Keeley, F. W., 1979. The synthesis of soluble and insoluble elastin in chicken aorta as a function of development and age. Effect of a high cholesterol diet. *Can J Biochem* 57, 1273-1280.

Kim, C., Cervos-Navarro, J., Kikuchi, H., Hashimoto, N., and Hazama, F., 1992. Alterations in cerebral vessels in experimental animals and their possible relationship to the development of aneurysms. *Surg Neurol* 38, 331-337.

Kondo, S., Hashimoto, N., Kikuchi, H., Hazama, F., Nagata, I., and Kataoka, H., 1997. Cerebral aneurysms arising at nonbranching sites. An experimental study. *Stroke* 28(2), 398-404.

Kondo, S., Hashimoto, N., Kikuchi, H., Hazama, F., Nagata, I., Kataoka, H., Rosenblum, W.I., 1998. Apoptosis of medial smooth muscle cells in the development of saccular cerebral aneurysms in rats. *Stroke* 29, 181-189.

Krajcinovic, D., and Selvaraj, S., 1984. Creep rupture of metalsan analytical model. *J Eng Mater-T ASME* 160, 809-815.

Krajcinovic, D., 1996. *Damage Mechanics* Elsevier, New York.

Lanir, Y., 1983. Constitutive equations for fibrous connective tissues. *J Biomech* 16, 1–12.

Lanir, Y., Lichtenstein, O., and Imanuel, O., 1996. Optimal design of biaxial tests for structural material characterization of flat tissues. *J Biomech Eng* 118, 41–47.

Larkin, J., Barrow, J., Durka, M., Remic, D., Zeng, Z., Robertson, A.M., 2007. Design of a flow chamber to explore the initiation and development of cerebral aneurysms. In: *Proceedings of the 2007 Biomedical Engineering Society (BMES) Annual Fall Meeting*, Los Angeles, CA.

Lefevre, M., and Rucker, R. B., 1980. Aorta elastin turnover in normal and hypercholesterolemic Japanese quail. *Biochim Biophys Acta* 630, 519–529

Lemaitre, J., 1985. A continuous damage mechanics model for ductile fracture. *J Eng Mater-T ASME* 107, 83-89.

Li, D., and Robertson, A. M., 2008. A structural multi–mechanism damage model for cerebral arterial tissue and its finite element implementation. In: *Proceedings of the ASME 2008 Summer Bioengineering Conference (SBC-2008)*, Marco Island, Florida.

Li, D., and Robertson, A. M., 2009. A structural multi-mechanism constitutive equation for cerebral arterial tissue. *Int J Solids Struct* 46(14–15), 2920–2928.

Li, D., and Robertson, A. M., 2009. A structural multi-mechanism damage model for cerebral arterial tissue. *J Biomech Eng* 131(10), 101013–1–8.

Li, D., and Robertson, A. M., 2009. Finite element modeling of cerebral angioplasty using a multi-mechanism structural damage model. In: *Proceedings of the ASME 2009 Summer Bioengineering Conference (SBC-2009)*, Lake Tahoe, CA.

Liu, S. Q., Fung, Y. C., 1988. Zero-Stress states of arteries. *J Biomech Eng* 110, 82–84.

Longstreth, W. T., Nelson, L. M., Koepsell T. D., and Belle, G. V., 1993. Clinical course of spontaneous subarachnoid hemorrhage: A population-based study in king county, washington. *Neurology* 43, 712-718.

Mariencheck, M. C., Davis, E. C., Zhang, H., Ramirez, F., and Rosenbloom, J. *et al.*, 1995. Fibrillin-1 and fibrillin-2 show temporal and tissue-specific regulation of expression in developing elastic tissues. 31: 87-97 *Connect Tissue Res* 31, 87–97.

Meng, H., Swartz, D. D., and Wang, Z. *et al.*, 2006. A model system for mapping vascular responses to complex hemodynamics at arterial bifurcations in vivo. *Neurosurgery* 59(5), 1094–1101.

Meng, H.,Wang, Z., Hoi, Y., Gao, L., Metaxa, E., Swartz, D.D., Kolega, J., 2007. Complex hemodynamics at the apex of an arterial bifurcation induces vascular remodeling resembling cerebral aneurysm initiation. *Stroke* 38, 1924–1931.

McCormick, W. F., and Acosta-Rua, G. J., 1970. The size of intracranial saccular aneurysms: An autopsy study. *Neurosurgery* 33, 422-427.

Miskolczi, L., Guterman, L. R., Flaherty, J. D., and Hopkins, L. N., 1998. Saccular aneurysm induction by elastase digestion of the arterial wall: a new animal model. *Neurosurgery* 43, 595-601.

Morimoto, M., Miyamoto, S., and Mizoguchi, A., Kume, N., Kita, T., and Hashimoto, N., 2002. Mouse model of cerebral aneurysm: experimental induction by renal hypertension and local hemodynamic changes. *Stroke* 33, 1911–1915.

Monson, K. L., 2001. Mechanical and Failure Properties of Human Cerebral Blood Vessels. *Ph.D. Dissertation* University of California, Berkeley, CA.

Monson, K. L., Goldsmith, W, Barbaro, N. M., and Manley, G. T., 2003. Axial mechanical properties of fresh human cerebral blood vessels. *J Biomech Eng* 125(2), 288–294.

Monson, K. L., Barbaro, N. M., and Manley, G. T., 2006. Multiaxial response of human cerebral arteries. *Proceedings of the American Society of Biomechanics Annual Meeting* Blacksburg, VA.

Müller-Hülsbeck, S., Stolzmann, P., Liess, C., Hedderich, J., Paulsen, F., Jahnke, T., and Heller, M., 2005. Vessel wall damage caused by cerebral protection devices: ex vivo evaluation in porcine carotid arteries. *Radiology* 235, 454–460.

Naghdi, P. M., Trapp, J. A., 1975. The significance of formulating plasticity theory with reference to loading surfaces in strain space. *Int J Eng Sci* 13, 785–797.

Natali, A. N., Pavan, P. G., Carniel, E. L., and Dorow, C., 2004. Viscoelastic response of the periodontal ligament: an experimental-numerical analysis. *Connect Tissue Res* 45, 222–230.

Natali, A. N., Pavan, P. G., Carniel, E. L., Lucisano, M. E., and Taglialavoro, G., 2005. Anisotropic elasto-damage constitutive model for the biomechanical analysis of tendons. *Med Eng Phys* 27, 209–214.

Nyström, S. H. M., 1963. Development of intracranial aneurysms as revealed by electron microscopy. *Neurosurgery* 20, 329–337.

Oden, J. T., Key, J. E., 1970. Numerical analysis of finite axisymmetric deformations of incompressible elastic solids of revolution. *Int J Solids Struct* 6, 497–518.

Ogden, R. W., 1978. *Non-Linear Elastic Deformations* New York, Dover.

Oktay, H. S., Kang, T., Humphrey, J. D., and Bishop, G. G., 1991. Changes in the mechanical behavior of arteries following balloon angioplasty. In: *ASME 1991 Biomechanics Symposium* AMD-Vol. 120, American Society of Mechanical Engineers.

Pentimalli, L., Modesti, A., Vignati, A., Marchese, E., Albanese, A., Di Rocco, F., Coletti, A., Di Nardo, P., Fantini, C., Tirpakova, B., and Maira, G., 2004. Role of apoptosis in intracranial aneurysm rupture. *J Neurosurg* 101, 1018-1025.

Peters, M. W., Canham, P. B., Finlay, H. M., 1983. Circumferential alignment of muscle cells in the tunica media of the human brain artery. *Blood Vessels* 20, 221–233.

Provenzano, P. P., Heisey, D., Hayashi, K., Lakes, R., and Vanderby, R. Jr., 2002. Subfailure damage in ligament: a structural and cellular evaluation. *J Appl Physiol* 92, 362–371.

Ratechenson, R. A., and Wirth, F. P., 1995. *Ruptured Cerebral Aneurysm: Perioperative Management. Vol 6: Concepts in Neurosurgery.* Williams and Wilkins, Baltimore.

Rhodin, J. A. G., 1979. Architecture of the vessel wall. In: *Berne, R. M., Sperelakis, N. (eds) Vascular Smooth Muscle, Vol 2 of Handbook of Physiology, Section 2: The Cardiovascular System.* APS, Baltimore, pp. 1–31.

Roach, M. R., Burton, A. C., 1957. The reason for the shape of the distensibility curves of arteries. *Can J Biochem Physiol* 35, 681–690.

Roach, M. R., 1963. Changes in arterial distensibility as a cause of poststenotic dilatation. *Am J Cardiol* 12, 802–815.

Robertson, A. M., Li, D., Wulandana, R., 2007. The biomechanics of cerebral aneurysm initiation and development. In: *Proceedings of the 9th International Symposium on Future Medical Engineering Based on Bio-nanotechnology* Tohoku U, Sendai, Japan, 18–21.

Rowe, A. J., Finlay, H. M., Canham., P. B., 2003. Collagen biomechanics in cerebral arteries and bifurcations assessed by polarizing microscopy. *Can J Vasc Res* 40, 406–415.

Ryan, J. M. and Humphrey, J. D., 1999. Finite element based predictions of preferred material symmetries in saccular aneurysms. *Ann Biomed Eng* 27, 641–647.

Sacks, M. S., 2000. Biaxial mechanical evaluation of planar biological materials. *J Elasticity* 61, 199–246.

Sacks, M. S., 2000. A structural constitutive model for chemically treated planar tissues under biaxial loading. *Comput Mech* 26, 243–249.

Sacks, M. S., 2003. Incorporation of experimentally-derived fiber orientation into a structural constitutive model for planar collagenous tissues. *J Biomech Eng* 125, 280–287.

Sahs, A. L., 1966. Observations on the pathology of saccular aneurysms. *J Neurosurg* 24, 792–806.

Sakamoto, N., Ohashi,T., and Sato, M., 2008. High Shear Stress Induces Production of Matrix Metalloproteinase in Endothelial Cells. In: *Proceedings of the ASME 2008 Summer Bioengineering Conference (SBC2008),* Marco Island, Florida.

Samila, Z. J. and Carter, S. A., 1981. The effect of age on the unfolding of elastin lamellae and collagen fibers with stretch in human carotid arteries. *Can J Physiol Pharm* 59, 1050–1057.

Scott, S., Ferguson, G. G., and Roach, M. R., 1972. Comparison of the elastic properties of human intracranial arteries and aneurysms. *Can J Physiol Pharm* 50, 328–332.

Scanarini, M., Mingrino, S., Giordano, R., and Baroni, A., 1978. Hisotological and ultrastructural study of intracranial saccular aneurysmal wall. *Acta Neurochir* 43, 171–182.

Sekhar, L. N. and Heros, R. C., 1981. Origin, growth, and rupture of saccular aneurysms: a review. *Neurosurgery* 8, 248–260.

Sho, E., Sho, M., Singh, T. M., Nanjo, H., Komatsu, M., Xu, C., Masuda, H., and Zarins, C. K., 2002. Arterial enlargement in response to high flow requires early expression of matrix metalloproteinases to degrade extracellular matrix. *Exp Mol Pathol* 73, 142–153.

Sidorov, S., 2006. Finite Element Modeling of Human Artery Tissue with a Nonlinear Multi-Mechanism Inelastic Material. *Doctoral Thesis* University of Pittsburgh, Pittsburgh, PA.

Simo, J. C., and Ju, J. W., 1987. Strain- and stress-based continuum damage models-I. formulation. *Int J Solids Struct* 23, 821–840.

Slaughter, W. S., and Sacks, M. S., 2001. Modeling fatigue damage in chemically treated soft tissues. *Key Eng Mat* 198-199, 255–260.

Spencer, A.J. M., 1984. Constitutive Theory for Strongly Anisotropic Solids. In: *Continuum Theory of the Mechanics of Fibre-Reinforced Composites* (ed. A. J. M. Spencer), CISM Courses and Lectures No. 282, 1–32. Springer, Wien.

Stehbens, W. E., 1963. Histopathology of cerebral aneurysms. *Arch Neurol* 8, 272–285.

Stehbens, W. E., 1972. *Pathology of the Cerebral Blood Vessels. Structure and Pathophysiology.* C.V. Mosby.

Stehbens, W. E., 1989. Etiology of intracranial berry aneurysms. *J Neurosurg* 70, 823-831.

Stehbens, W. E., 1990. Pathology and pathogenesis of intracranial berry aneurysms. *Neurol Res* 12, 29-34.

Sugai, M., and Shoji, M., 1968. Pathogenesis of so-called congenital aneurysms of the brain. *Acta Pathol Japon* 18(2), 139–160.

Sun, W., 2003. Biomechanical Simulations of Heart Valve Biomaterials. *Doctoral Thesis* University of Pittsburgh, Pittsburgh, PA.

Szymanski, M. P., Metaxa, E., Meng, H., and Kolega, J.,2008. Endothelial cell layer subjected to impinging flow mimicking the apex of an arterial bifurcation. *Ann Biomed Eng* 36(10), 1681–1689.

Truesdell, C., and Noll, W., 1965. The Non-Linear Field Theories of Mechanics. In: *Handbuch der Physik* (ed. S. Flügge), Volume III/3. Springer–Verlag.

Vaishnav, R. N., Vossoughi, J., 1983. Estimation of residual strains in aortic segments. In: *Biomedical Engineering II: Recent Developments, C. W. Hall (Ed.).* Pergamon Press, New York, pp. 330–333.

Wojak, J. C., Dunlap D. C., Hargrave, K. R., Dealvare, L. A., Culbertson, H. S., and Connors III, J. J., 2006. Intracranial angioplasty and stenting: long-term results from a single center. *AJNR* 27, 1882–1892.

Wulandana, R., 2003. Applications of a nonlinear and inelastic constitutive equation for human cerebral arterial and aneurysm walls. *Doctoral Thesis* University of Pittsburgh, Pittsburgh, PA.

Wulandana, R. and Robertson, A. M., 2005. An inelastic multi-mechanism constitutive equation for cerebral arterial tissue. *Biomech Model Mechan* 4, 235–248.

Wulandana, R. and Robertson, A. M., 2005. A multi-mechanism constitutive equations for modeling aneurysm development including: collagen recruitment, elastin failure, collagen degradation and collagen synthesis. In: *Proceedings of the 2005 Summer Bioengineering Conference* ASME, Vail.

Yu, Q., Zhou, J., and Fung, Y. C., 1993. Neutral axis location in bending and Young's modulus of different layers of arterial wall. *Am J Physiol* 265, H52–H60.

Zeng, Z., Chung, B.-J., Durka M., and Robertson, A. M., 2009. An in vitro device for evaluation of cellular response to flows found at the apex of arterial bifurcations. In: *Advances in Mathematical Fluid Mechanics*, (ed. A. Sequeira and R. Rannacher), Springer Verlag, Wien, (in press).

Zollikofer, C. L., Salomonowitz, E., Sibley, R., Chain, J., Bruehlmann, W. F., Castaneda-Zuniga, W. R., and Amplatz, K., 1984. Transluminal angioplasty evaluated by electron microscopy. *Interv Radiology* 153, 369–374.

Zulliger, M. A., Fridez, P., Hayashi, K., Stergiopulos, N., 2004. A strain energy function for arteries accounting for wall composition and structure. *J Biomech* 37, 989–1000.